Universität Hamburg
DER FORSCHUNG | DER LEHRE | DER BILDUNG

Transcriptional regulation of male meiosis by the DREAM complex in *Arabidopsis thaliana*

Hasibe Tunçay

Dissertation with the aim of achieving a doctoral degree

at the Faculty of Mathematics, Informatics and Natural Sciences
Department of Biology

Universität Hamburg

Hamburg, July 2025

Transcriptional regulation of male meiosis by the DREAM complex in *Arabidopsis thaliana*

Hasibe Tunçay

Dissertation with the aim of achieving a doctoral degree

at the Faculty of Mathematics, Informatics and Natural Sciences
Department of Biology

Universität Hamburg

Supervisor: Prof. Dr. Arp Schnittger

Examiners: Prof. Dr. Arp Schnittger

Dr. Magdalena Weingartner

Date of oral defense: 21.10.2025

Table of Content

Table of Content I

List of Abbreviations IV

List of Figures and Tables VIII

List of Publications and Presentations XI

Declaration of contributions XIII

Abstract XV

Zusammenfassung XVI

INTRODUCTION 1

CHAPTER I. Transcriptional control of meiotic recombination by the DREAM complex 27

Abstract 29

Main 30

Methods 39

Figures & table 45

Suplemental data 52

CHAPTER II. Dissecting the multifaceted roles of the DREAM complex in meiosis 69

1. INTRODUCTION TO CHAPER II 71

2. RESULTS 74

2.1. DREAM mutants display defects in DSB repair 74

2.2. Impaired DREAM complex activity hinders meiotic progression 79

Durations of meiotic stages are altered in DREAM mutants 80

Meiosis progression is asynchronous in *tcx5/6* 83

Differential expression of meiotic cyclins, CDKs, and their regulators in DREAM Mutants 87

Aberrant meiotic microtubule organization observed in *tcx5/6* 90

2.3. Towards understanding the meiotic DREAM complex 92

The interplay between ALY1/2 and TCX5/6 92

Transcriptional up-regulation of DREAM Components in *aly1/2* and *tcx5/6* mutants 96

Initial functional characterization of MYB3Rs in meiosis 99

3. DISCUSSION 102

3.1. Regulation of DSB repair pathways by the DREAM complex 102

3.2. Progression and duration of meiosis in the absence of MuvB-core DREAM components 105

3.3. The functional interplay between ALYs and TCXs 109

3.4. The meiosis-specific DREAM complex 112

4. MATERIAL AND METHODS 115

4.1. Plant materials and growth conditions 115

4.2. Plasmids and plant transformation 115

4.3. Genotyping 116

4.4. Pollen and seed viability assessment 117

4.5. Cell spreads 117

4.6. Confocal microscopy 117

4.7. Live cell imaging and quantitative analysisof the meiotic phases 117

4.8. Transcriptome and CUT&Tag data anlaysis 118

4.9. Statistical analysis 118

5. SUPPLEMENTAL DATA 119

CHAPTER III. An outlook to regulation of meiosis by the DREAM complex through DNA methylation 127

1. INTRODUCTION 129

2. RESULTS 130

3. DISCUSSION 134

4. MATERIALS & METHODS 137

4.1. Plant materials and growth conditions 137
4.2. Genotyping 137
4.3. Cell spreads 137
4.4. Transcriptome and CUT&Tag data anlaysis 137
4.5. Statistical analysis 138
APPENDIX 139
REFERENCES 141
ACKNOWLEDGEMENT XIX
DECLERATION OF OATH XXV

List of Abbreviations

ALY	ALWAYS EARLY
ASY	ASYNAPTIC
AXR1	AUXIN RESISTANT 1
B-MYB	B-Myeloblastoma
BTE1	BARRIER OF TRANSCRIPTION ELONGATION1
BTL1	BTE1-LIKE1
Caf	Chromatin Assembly Factor
CDE	Cell-cycle dependent element
CDK	Cyclin-dependent kinase
CDKA;1	CYCLIN DEPENDENT KINASE A;1
CHR	Cell-cycle genes homology regions
CLE	CHR-like element
CMT	CHROMOMETHYLASE
CO	Crossover
Comr	Cookie Monster
CUT&Tag	Cleavage Under Targets and Tagmentation
D-loop	Displacement loop
DDM1	DECREASED DNA METHYLATION 1
dHJ	double Holiday Junction
DMC1	DISRUPTED MEIOTIC cDNA1
DNA	Deoxribonucleicacid
DP	DIMERIZATION PARTNER
DPL	DP-like
DRM	DOMAINS REARRANGED METHYLTRANSFERASE
DSB	Double strand break
E2F	E2 PROMOTER BINDING FACTOR
EFL	E2F-like
FANCD2	FANCONI ANEMIA D2
FANCM	FANCONI ANEMIA COMPLEMENTATION GROUP M
FC	Fold change
FIGL1	FIDGETIN-LIKE 1
FLAC	FLORAL ANTICIPATION CONTROLLER
FLIC	FLORAL INDUCTION CONTROLLER

FOXM	Forkhead Box Protein M
GFP	Green fluorescent protein
GO	Gene Ontology
H3K9me2	H3 lysine 9 dimethylation
HEI10	HUMAN ENHANCER INVASION 10
IBM1	INCREASE IN BONSAI METHYLATION 1
IHR	Inter-homolog recombination
JM	Joint molecule
JMJ14	JUMONJI 14
KYP	KRYPTONITE
LIN	ABNORMAL CELL LINEAGE PROTEIN
mEGFP	monomeric Enhanced Green Fluorescent Protein
MER3/RCK	MEIOTIC RECOMBINATION 3/ROCK-N-ROLLERS
MET1	METHYLTRANSFERASE1
MHF	MPH1-ASSOCIATED HISTONE-FOLD PROTEIN
Mip	Myb-interacting protein
MPS1	MULTIPOLAR SPINDLE 1
MRE11	MEIOTIC RECOMBINANT 11
MSA	M-specific activator
MSH	MUTS HOMOLOG
MSI	MULTICOPY SUPPRESSOR OF IRA
MT	Microtubule
MTL5	Metallothionein-Like 5
MTOPVIB	MEIOTIC TOPOISOMERASE VIB-LIKE
MuvB	Multi-vulva class B
Myb	Myeloblastoma
MYB3R	MYELOBLASTOMA 3R
NAC044	NAM, ATAF1, and CUC1/CUC2 (NAC) type protein 44
NBS1	NIJMEGEN BREAKAGE SYNDROME 1
NCO	non-Crossovers
NEB	Nuclear envelope breakdown
OSD1	OMISSION OF SECOND DIVISION 1
padj	Adjusted p-values
PDS5	PRECOCIOUS DISSOCIATION OF SISTERS 5
Plk1	Polo-like kinase 1

PMC	Pollen mother cell
PRO	Promoter
PTD	PARTING DANCERS
RAD50	RADIATION 50
RAD51	RADIATION 51
RB	Retinoblastoma
RBBP	RB-Binding Protein
RBR	RETINOBLASTOMA-RELATED
REC8	RECOMBINATION PROTEIN 8
RECQ4	RECQ HELICASE 4
RFP	Red fluorescent protein
RIN	RNA integrity number
RNA	Ribonucleicacid
RTR Complex	RMI1-TOP3α-RECQ4
SAC	Spindle assembly checkpoint
SC	Synaptonemal complex
SCC	Sister chromatid cohesion
SDS	SOLO DANCERS
SDSA	Synthesis-dependent strand annealing
SHOC1	SHORTAGE IN CHIASMATA 1
SMG7	SUPPRESSOR WITH MORPHOLOGICAL DEFECTS IN GENITALIA 7
SOG1	SUPPRESSOR OF GAMMA RESPONSE 1
SPO11-1	SPORULATION11-1
ssDNA	single-stranded DNA
SUVH	SUPPRESSOR OF VARIEGATION HOMOLOGUE
TAM	TARDY ASYNCHRONOUS MEIOSIS
TCX	TESMIN/TSO1-LIKE CXC
TDM/MS5	THREE-DIVISION MUTANT/ MALE STERILE 5
TE	Transposable element
TES	Transcription end site
TF	Transverse filament
tMAC	testis Meiotic Arrest Complex
Tomb	Tombala
Topi	Matotopetli

TSS	Transcription start site
TUA	TUBULIN ALPHA
VIM	VARIANT IN METHYLATION
WDR5A	HUMAN WD40-REPEAT 5 HOMOLOG A
WT	Wild-type
Wuc	Wake-Up-Call
ZYP1	ZIPPER 1

List of Figures and Tables

Figure 1. A general overview of meiosis. 2

Figure 2. Model of synapsis and meiotic recombination in plants....4

Figure 3. Meiotic recombination and DNA repair pathways. 6

Figure 4. Regulation of MuvB complex assembly and transcriptional control during the mammalian cell cycle. Figure taken from Hoareau *et al.*, 2024. 19

Figure 1.1. DREAM complex plays an important role in meiosis. 45

Figure 1.2. Transcriptome analysis of DREAM mutants and CUT&Tag with GFP-TCX5 reveals roles in cell cycle regulation and DNA repair....47

Figure 1.3. The DREAM complex activates *MER3* transcription. Overexpression of *MER3* in *aly1/2* and *tcx5/6* partially recovers CO loss. 49

Figure 1.4. A brief summary of DREAM complex regulating meiotic genes (A) in seedlings and (B) in anthers/meiocytes. 50

Figure 2.1. DREAM mutants display increased aberrant chromosome configurations at metaphase I in the absence of anti-CO factors....76

Figure 2.2. MUS81 expression and functional contribution to the meiotic recombination in DREAM mutants. 78

Figure 2.3. Duration of meiotic stages (in minutes) across WT, *aly1/2*, *lin37ab*, and *tcx5/6* genotypes. 82

Figure 2.4. Meiosis progression is asynchronous in *tcx5/6.* 85

Figure 2.5. Quantification of meiotic synchrony in WT and *tcx5/6* male meiocytes 86

Figure 2.6. Abnormal microtubule dynamics during meiosis in *tcx5/6* mutants revealed by live imaging. 91

Figure 2.7. Localization dependency and functional interplay between ALY1/2 and TCX5/6 during meiosis. 95

Figure 2.8. Reproductive and meiotic phenotypes of MYB3R mutants. 100

Figure 2.9. MYB3R3-mEGFP is expressed throughout meiosis and localizes to chromosomes. 101

Figure 3.1. Loss of *CMT3* in DREAM mutant background mostly recovers CO loss phenotype. 133

Supplementary Figure 1.1. DREAM mutants exhibit incomplete synapsis and form dyads and triads; however DSB formation occurs at WT level....52

Supplementary Figure 1.2. ALY1 and TCX5 are present throughout meiosis and localized to chromosomes. 53

Supplementary Figure 1.3. ALY1-GFP and GFP-TCX5 reporter lines rescue fertility defects in the respective double mutants. 54

Supplementary Figure 1.4. Integration of transcriptomic and CUT&Tag data reveals direct TCX5 targets among misregulated genes in *aly1/2* and *tcx5/6*. 55

Supplementary Figure 1.5. A *MER3-GFP* genomic reporter under the meiosis-specific *DMC1* promoter produces functional MER3 protein and rescues CO defects in *mer3*. 56

Supplementary Figure 1.6. Comparative analysis of TCX5 targets across tissues reveals shared regulatory roles in seedlings and anthers. 57

Supplementary Figure 1.7. The DREAM complex activates *SDS* transcription. 58

Supplementary Figure 2.1. DREAM mutants display chromosome fragmentation and entanglement in their combination with *fancm* and *recq4ab*. 119

Supplementary Figure 2.2. Loss of RECQ4A/B recovers CO loss phenotype in *mer3*. 120

Supplementary Figure 2.3. Combination of *aly1/2* and *tcx5/6* with *mus81* elevates CO loss phenotype in DREAM mutants and chromosome segregation defects. 120

Supplementary Figure 2.4. MT array states of meiotic phases.....121

Supplementary Figure 2.5. Meiosis is synchronous in *aly1/2* and *lin37ab*. 121

Supplementary Figure 2.6. Expression profiles of *ALY2, TCX5, TCX6* in male meiocytes. 122

Supplementary Figure 2.7. GFP-LIN37A and LIN37B-GFP expression and localization pattern in anthers at specific meiotic stages. 122

Supplementary Figure 2.8. Expression profiles of LIN52A and LIN52B in male meiocytes and TCX5 binding on their promoters in anther and seedlings. 123

Table 1. Comparative nomenclature of the DREAM complex proteins across different model organisms. 17

Table 1.1. Differential expression of genes in *aly1/2* and *tcx5/6* meiocytes, involved in recombination pathways. 51

Table 2.1. Differential expression of meiotic cyclins, CDKs, and their regulators in *tcx5/6* and *aly1/2* male meiocytes. 89

Table 2.2. DREAM complex components expression in *aly1/2* and *tcx5/6* mutants. 98

Table 2.3. PCR program using DreamTaq or Terra polymerase. * Annealing temperature can change depending on primer pairs used.....116

Table 3.1. Differential transcription levels of DNA methylation maintenance genes. 132

Supplementary Table 1.1. Transmission analysis of the *tcx6* allele in a *tcx5* mutant background indicates no gametophytic defect.....58

Supplementary Table 1.2. Sequencing quality metrics for RNA-seq of *aly1/2*, *tcx5/6*, and WT male meiocytes. 59

Supplementary Table 1.3. List of meiotic genes and their differential transcriptional levels in *aly1/2* and *tcx5/6* male meiocytes compared to WT. 60

Supplementary Table 3.1. Differential transcription levels of DREAM complex components, associated cell cycle regulators, plant-specific DREAM components and TCX5 binding to their promoter regions in somatic and reproductive tissues.....124

Appendix Table 1. Primer pairs used for genotyping each insertion line are listed. 139

List of Publications and Presentations

Publications

- **The DREAM Complex Represses Growth in Response to DNA Damage in Arabidopsis**. Lang, L., Pettkó-Szandtner A., Tunçay Elbaşı, H., Takatsuka H.,, Nomoto, Y., Zaki, A.,, Dorokhov, S., De Jaeger, G., Eeckhout, D., Ito, M., Magyar, Z., Bögre, L., Heese M., Schnittger, A. (2021) *Life Science Alliance 4(12).* http://doi.org/10.26508/lsa.202101141

- **The cohesin subunit RAD21.2 functions as a recombination silencer of ribosomal DNA arrays.** Kuttig, V., Sims, J., Hamamura, Y., Komaki S., Köhler, M., Stolze, S.C., De Jaeger-Braet, J., Tunçay Elbaşı, H., Nakagami, H., Virgilio Failla, A., Schlögelhofer, P., Schnittger, A. (Preprint - 2022) *bioRxiv* 2022.06.20.496767; https://doi.org/10.1101/2022.06.20.496767

- **ZYP1-mediated recruitment of PCH2 to the synaptonemal complex remodels the chromosome axis leading to crossover restriction.** Yang, C., Sofroni, K., Hamamura, Y., Hu, B., Tunçay Elbasi, H., Balboni, M., Chu, L., Stang, D., Heese, M., Schnittger, A. (2022) *Nucleic Acids Research*, 50 (22), 12924–12937. https://doi.org/10.1093/nar/gkac1160

- **The Two Plant-Specific DREAM Components FLIC and FLAC Repress Floral Transition in Arabidopsis.** Lucas, L., Böwer, F., Tunçay Elbaşı, H., Eeckhout, D., Marschlich, N., de Jaeger, G., Heese, M.,Schnittger, A. (Preprint-2023) *bioRxiv* 2023.08.07 https://doi.org/10.1101/2023.08.07.552284.

- **Seeding the Meiotic DNA Break Machinery and Initiating Recombination on Chromosome Axes.** Dereli, I., Telychko, V., Papanikos, F., Raveendran, K., Xu, J., Boekhout, M., Stanzione, M., Neuditschko, B., Sailaja Imjeti, N., Selezneva, E., Tuncay, H., Demir, S., Giannattasio, R., Gentzel, M., Bondarieva, A., Stevense, M., Barchi, M., Schnittger, A., Weir, J.R., Herzog, F., Keeney, S., Tóth, A. (2024) *Nature Communications* 15(1), 2941. https://doi.org/10.1038/s41467-024-47020-1.

Poster presentations

- Gordon Research Seminar on Meiosis, New London (USA), 2022 - **Control of Male Meiosis by the DREAM-complex**
- Gordon Research Conference on Meiosis, New London (USA), 2022 - **Control of Male Meiosis by the DREAM-complex**
- Gordon Research Seminar on Chromosome Dynamics, Lucca (Italy), 2023 - **Transcriptional regulation of male meiosis by the DREAM complex**
- Gordon Research Conference on Chromosome Dynamics, Lucca (Italy), 2023 - **Transcriptional regulation of male meiosis by the DREAM complex**
- 27th International Congress on Sexual Plant Reproduction, Rhode Island (USA), 2024, - **Transcriptional Control of Male Meiosis by the DREAM-complex in *Arabidopsis thaliana***
- Plant Meiosis Meeting, Poznan (Poland), 2024 – **DREAMing Meiosis: Transcriptional Control of Male Meiosis by the DREAM-complex in *Arabidopsis thaliana***

Oral Presentations

- Gordon Research Seminar on Chromosome Dynamics, Lucca (Italy), 2023 - **Transcriptional regulation of male meiosis by DREAM complex**
- Gordon Research Conference on Chromosome Dynamics, Lucca (Italy), 2023 - **Transcriptional regulation of male meiosis by DREAM complex**
- 27th International Congress on Sexual Plant Reproduction, Rhode Island (USA), 2024, - **Transcriptional Control of Male Meiosis by DREAM-complex in *Arabidopsis thaliana***
- Plant Meiosis Meeting, Poznan (Poland), 2024 – **DREAMing Meiosis: Transcriptional Control of Male Meiosis by the DREAM-complex in *Arabidopsis thaliana***
- MAYosis, (online meeting), 2025 - **DREAMing Meiosis: Transcriptional regulation of homologous recombination by the DREAM-complex in *Arabidopsis thaliana***

Declaration of contributions

I hereby declare that all results presented in this thesis were obtained by myself, except where explicitly stated otherwise. Below, I summarize the contributions made by collaborators:

- CUT&Tag data analysis, Gene Ontology (GO) enrichment analysis and differnetial gene expression analysis of transcriptome sequencing data were performed by Xing Ma, who is also listed as the second author of the manuscript included in Chapter I. Figure 1.2, Figure 1.3A, Supplementary Figure 1.4, Supplementary Figure 1.6, Supplementary Figure 1.7, Table 2.1, Table 2.2, Table 3.1, Supplementary Table 1.3, and Supplementary Table 2.1 assembled by me, contain analyses and visualizations conducted by Xing Ma, based on CUT&Tag and transcriptopme sequencing experiments carried out by myself.
- Figure 2.1 includes cytological data generated by Lovis Jahnecke (*aly1/2 recq4ab* acid spreads), a Master's rotation student in our lab, under my supervision.
- Live-cell imaging experiments were performed by Dr. Joke De Jaeger-Braet, and Dr. Yuki Hamamura using material I provided (REC8-GFP TagRFP- TUA5 *aly1/2*, REC8-GFP TagRFP- TUA5 *lin37ab* and REC8-GFP TagRFP- TUA5 *tcx5/6*, REC8-GFP TagRFP- TUA5 WT, respecitvely). The subsequent analysis of the live-cell imaging data and the preparation of all figures containing these results (Figure 2.3, Figure 2.4, Figure 2.5, Figure 2.6, Supplementary Figure 2.4, and Supplementary Figure 2.5) were carried out by me.

Abstract

Meiosis ensures genomic stability and diversity in sexual reproduction, requiring precise gene expression regulation. Despite its importance, control of the plant meiotic transcriptome remains poorly understood due to technical challenges. This study investigates the DREAM complex as a transcriptional regulator of male meiosis in *Arabidopsis thaliana*. Originally described as a transcriptional repressor of cell cycle genes in quiescent animal cells, the DREAM complex is now known to have a broader role and has been described to also influence reproductive development in *C. elegans, D. melanogaster*, and mice. So far, the Arabidopsis DREAM complex has been associated with cell cycle regulation, DNA damage response, and DNA methylation maintenance in somatic context.

In my thesis, I focused on the putative DNA-binding subunits TCX and ALY, which localize to chromosomes during meiosis. The double mutants *aly1/2* and *tcx5/6* exhibits reduced seed and pollen viability, increased pollen size variability, and meiotic defects including impaired pairing, synapsis, and crossover formation, leading to unbalanced chromosome segregation. To elucidate the origin of these defects, the transcriptomes of wildtype and mutant male meiocytes are compared, which reveals differential regulation of genes involved in cross over (CO) formation, double strand break (DSB) repair, and chromosome organization. Notably, anti-CO factors are upregulated, while the Class I CO pathway member *MER3* is downregulated. CUT&Tag assays shows that TCX5 binds the *MER3* promoter, and *MER3* overexpression partially rescues recombination defects in DREAM mutants, indicating that the DREAM transcriptionally regulates meiotic recombination to some extend via *MER3* transcriptional activation.

Furthermore, DREAM mutants display increased reliance on alternative DSB repair pathways. Combinations with *mus81* and anti-CO mutants show that DREAM is essential for effective DSB repair and genome integrity. Live-cell imaging of DREAM mutants revealed delayed and asynchronous meiotic progression and disrupted microtubule architecture in *tcx5/6*. Testing DREAM associated components for involvement in meiosis, I found that MYB3R3 localizes to meiotic chromosomes and that repressive MYB3Rs are required for proper chromosome segregation in meiosis II. Finally, altered DNA methylation patterns in DREAM mutants suggest that hypermethylation contributes to meiotic defects. Combining DNA methylation mutants with *aly1/2* or *tcx5/6* partially rescues these defects, highlighting methylation as an additional layer in DREAM-mediated regulation during meiosis.

Collectively, these findings establish the plant DREAM complex as a key regulator of meiotic gene expression, indispensable for meiotic recombination, DSB repair, and progression through meiosis.

Zusammenfassung

Die Meiose gewährleistet genomische Stabilität und Vielfalt im Rahmen der sexuellen Fortpflanzung und erfordert eine präzise Regulation der Genexpression. Die Kontrolle des meiotischen Transkriptoms von Pflanzen ist aufgrund technischer Herausforderungen noch weitgehend unverstanden. Diese Studie untersucht den DREAM-Komplex als transkriptionellen Regulator der männlichen Meiose in *Arabidopsis thaliana*. Ursprünglich wurde der DREAM-Komplex als transkriptioneller Repressor von Zellzyklusgenen in ruhenden tierischen Zellen beschrieben. Inzwischen ist bekannt, dass er eine breitere Rolle spielt und auch die reproduktive Entwicklung in C. elegans, D. melanogaster und Mäusen beeinflusst. Ein homologer Komplex in Arabidopsis ist an der Zellzyklusregulation, der DNA-Schadensreaktion und der Aufrechterhaltung der DNA-Methylierung im somatischen Kontext beteiligt.

In meiner Arbeit habe ich vor allem die mutmaßlich DNA-bindenden Untereinheiten TCX und ALY untersucht, die während der Meiose an den Chromosomen lokalisiert sind. Die Doppelmutanten *aly1/2* und *tcx5/6* zeigten eine verminderte Anzahl lebender Samen und Pollen, eine erhöhte Variabilität der Pollengröße sowie Defekte in der Meiose, z.B. gestörte Chromosomenpaarung, -synapsis und Crossover-Bildung, was zu einer unausgewogenen Chromosomensegregation führte. Um der Ursache dieser Defekte auf die Spur zu kommen, habe ich die Transkriptome von wildtypischen und mutierten männlichen Meiozyten verglichen und eine unterschiedliche Regulation von Genen beobachtet, die an der Bildung von Crossovern (CO), der Reparatur von Doppelstrangbrüchen (DSB) und der Chromosomenorganisation beteiligt sind. Während Anti-CO-Faktoren hochreguliert waren, war *MER3*, eine Komponente des Klasse-I-CO-Weges, herunterreguliert. CUT&Tag-Assays zeigten, dass TCX5 an den *MER3*-Promotor bindet und eine Überexpression von *MER3* rettete zum Teil die Rekombinationsdefekte der DREAM-Mutanten, was darauf hindeutet, dass der DREAM Komplex die meiotische Rekombination unter anderem über die Transkriptionsaktivierung von MER3 reguliert.

Darüber hinaus wiesen DREAM-Mutanten eine erhöhte Abhängigkeit von alternativen DSB-Reparaturwegen auf. Die Kombination mit *mus81*- und Anti-CO-Mutanten zeigte, dass der DREAM für eine effektive DSB-Reparatur und die Genomintegrität essenziell ist. Lebendzellbeobachtungen von DREAM-Mutanten ergaben eine verzögerte, asynchrone Meiose und eine gestörte Mikrotubuli-Dynamik in *tcx5/6*. Im Rahmen der Untersuchung von DREAM-assoziierten Komponenten auf ihre Beteiligung an der Meiose stellte ich fest, dass MYB3R3 an meiotische Chromosomen lokalisiert ist und dass repressive MYB3Rs für eine ordnungsgemäße Chromosomentrennung in der Meiose II erforderlich sind.

Schließlich deuteten veränderte DNA-Methylierungsmuster in den DREAM-Mutanten darauf hin, dass Hypermethylierung zu den Meiose-Defekten beiträgt. Die Kombination von DNA-Methylierungsmutanten mit *aly1/2* oder *tcx5/6* rettete diese Defekte teilweise, was Methylierung als eine weitere regulatorische Ebene in der DREAM-vermittelten Regulation während der Meiose identifiziert.

Insgesamt belegen diese Ergebnisse, dass der pflanzliche DREAM-Komplex einen wichtigen Regulator der meiotischen Genexpression darstellt, der für die meiotische Rekombination, die DSB-Reparatur und den Fortschritt der Meiose unverzichtbar ist.

INTRODUCTION

1. The meiotic division

Meiosis is a specialized cell division during which a single round of DNA replication is followed by two successive chromosome segregation events in meiosis I and meiosis II. This process reduces the DNA content by half, a crucial prerequisite for the fusion of gametes and the restoration of the diploid genome. Moreover, meiosis is crucial to generate genetic diversity through recombination, which occurs via crossover (CO) formation. These COs not only create novel allelic combinations but also establish physical connections between homologous chromosomes (homologs), ensuring their accurate segregation (Ma, 2006; Mercier *et al.*, 2015).

Following DNA replication during the S phase, cells enter an extended prophase I, which is characterized by key events such as homologous chromosome pairing and meiotic recombination (Figure 1, bottom panel). Prophase I is further subdivided into five stages: leptotene, zygotene, pachytene, diplotene, and diakinesis, each defined by characteristic chromosomal morphology and activity (Ma, 2006).

During leptotene, chromosomes begin to condense, and their ends associate with the nuclear envelope in preparation for homolog pairing (Zickler and Kleckner, 2015). Recombination is initiated at this stage through the formation of programmed double-strand breaks (DSBs)(Keeney, Giroux and Kleckner, 1997). In the zygotene stage, homologous chromosomes begin to align and pair, accompanied by the initiation of synapsis mediated by the formation of the synaptonemal complex (SC) (Higgins *et al.*, 2005; Hesse *et al.*, 2019). Partially synapsed chromosomes appear as thicker, thread-like structures as they draw closer together. In pachytene, chromosomes reach a fully synapsed state, with homologs tightly aligned through a fully formed SC, and are visible as thick threads under the microscope (Ross *et al.,* 1996). At diplotene stage, SC disassembles and homologs begin to separate following the disassembly of the synaptonemal complex, but remain connected at chiasmata, the cytological manifestations of COs between non-sister chromatids. During diakinesis, chromosomes recondense into highly compacted structures. COs, visible

as chiasmata, ensure that each pair of homologs is connected by at least one CO (Li *et al.*, 2021), resulting in the formation of stable bivalent structures.

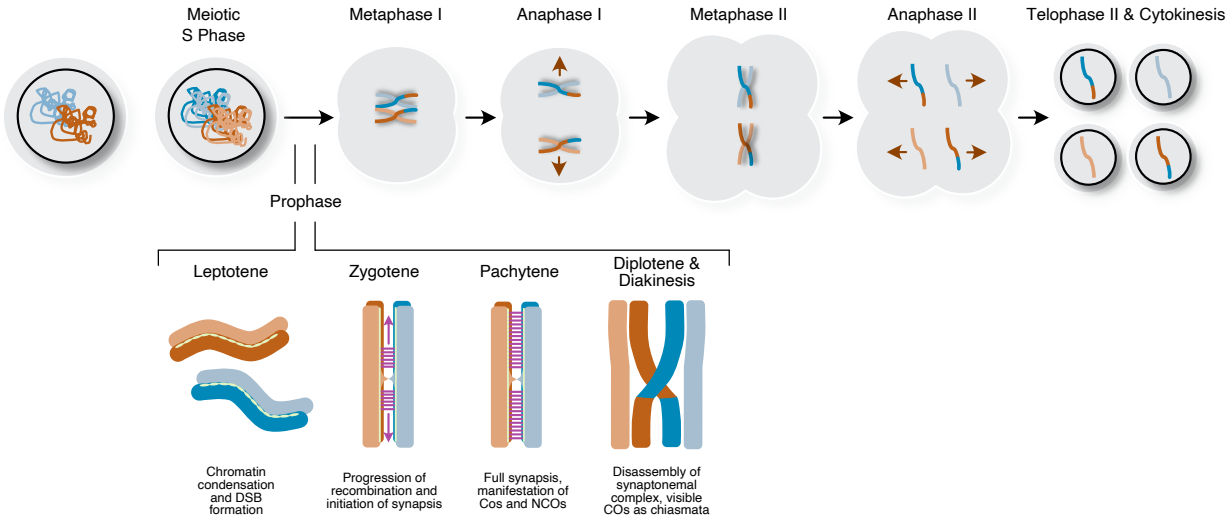


Figure 1. A general overview of meiosis.

DNA replication occurs during the S phase, resulting in duplicated sister chromatids. One pair of homologous chromosomes is depicted in blue (with sister chromatids in dark and light blue), and the other in orange (with sister chromatids in dark and light orange). The lower panel illustrates the sequential stages of meiotic prophase I: leptotene, zygotene, pachytene, diplotene, and diakinesis. In leptotene, chromosomes begin to condense and programmed double-strand breaks initiate recombination. During zygotene, homologous chromosomes undergo synapsis as recombination progresses. In pachytene, chromosomes are fully synapsed and appear as thick, thread-like structures. In diplotene, homologs begin to separate following the disassembly of the synaptonemal complex, but remain connected at chiasmata, the cytological manifestations of crossovers between non-sister chromatids. Finally, in diakinesis, further chromosome condensation leads to the formation of highly compacted bivalents. During metaphase I, homologous chromosomes align and are subsequently segregated to opposite poles during anaphase I. In metaphase II, recondensed chromosomes align once more, guided by two spindle apparatuses oriented perpendicularly. Anaphase II follows with the separation of sister chromatids, ultimately yielding four haploid gametes. Figure adapted from *Wijnker and Schnittger, 2013.*

Following prophase I (Figure 1), bivalents align at the metaphase plate during metaphase I, where microtubules emanating from opposite spindle poles form the first meiotic spindle (Brar and Amon, 2008; Miller *et al.*, 2012; Marston and Wassmann, 2017). To ensure accurate segregation, spindle microtubules must attach to the kinetochores, large protein structures assembled on the centromere of chromosomes that serve as anchoring sites for microtubule attachment, in a bi-oriented manner to

the sister chromatids of each homologous pair (Marston and Wassmann, 2017). This attachment process is monitored by the spindle assembly checkpoint (SAC), a kinetochore-associated surveillance mechanism that halts cell cycle progression until proper microtubule-kinetochore interactions are established (Watanabe, 2012; Gorbsky, 2015). Once all kinetochores are correctly connected to spindle microtubules, SAC is inactivated, permitting the segregation of homologous chromosomes to opposite poles during anaphase I. In telophase I, nuclei reform around the separated chromosome sets, and chromosomes temporarily decondense in the interkinesis phase.

During meiosis II, recondensed chromosomes align at the metaphase plate, facilitated by two spindle apparatuses oriented perpendicularly to each other during metaphase II. This perpendicular orientation is essential for the accurate separation of sister chromatids and the formation of four haploid cells. Unlike meiosis I, the kinetochores of sister chromatids in meiosis II attach to spindle microtubules emanating from opposite poles. Subsequently, during anaphase II, sister chromatids are segregated, and four nuclei reform during telophase II. Ultimately, four genetically distinct daughter cells are produced, each containing half the genetic material of the parent (De Storme and Geelen, 2013).

1.1. Meiotic recombination

Meiotic recombination is initiated by the formation of programmed DSBs catalyzed by the SPORULATION11-1 (SPO11-1)/SPO11-2 complex in association with the non-catalytic subunit MEIOTIC TOPOISOMERASE VIB-LIKE (MTOPVIB) at leptotene (Figure 2) (Keeney, Giroux and Kleckner, 1997; Grelon *et al.*, 2001; Osman *et al.*, 2011; Vrielynck *et al.*, 2016). Following their induction, DSBs are resected to produce 3′ single-stranded DNA (ssDNA) overhangs by the MRN complex, which comprises MEIOTIC RECOMBINANT 11 (MRE11), RADIATION 50 (RAD50) and NIJMEGEN BREAKAGE SYNDROME 1 (NBS1) (Lamarche, Orazio and Weitzman, 2010; Šamanić *et al.*, 2013). The resulting ssDNA is subsequently coated by the recombinases DMC1 and the RecA homolog RAD51 (Li *et al.*, 2004; Cloud *et al.*, 2012; Ines *et al.*, 2012, 2013), which mediate strand invasion into the homologous

chromosome which leads to the formation of a displacement loop (D-loop) structure to initiate homologous recombination (Figure 2).

In the absence of DMC1, DSBs are predominantly repaired via the sister chromatid, precluding CO formation and resulting in univalents. In contrast, *rad51* mutants fail to repair DSBs, leading to extensive chromosome fragmentation and complete sterility (Kurzbauer *et al.*, 2012; Chen *et al.*, 2021).

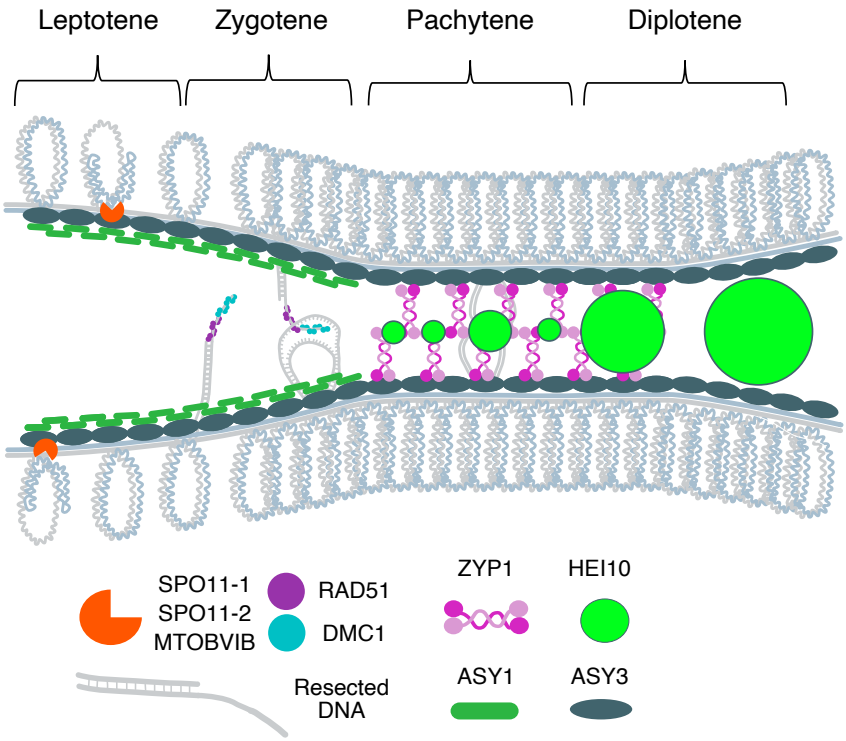


Figure 2. Model of synapsis and meiotic recombination in plants.

Meiosis initiates with the formation of a proteinaceous chromosome axis, composed primarily of ASY1 and ASY3, which provides a scaffold at the base of chromatin loops. Concurrently, programmed DSBs are introduced by the SPO11-1/SPO11-2 complex in association with the non-catalytic subunit MTOPVIB. These DSBs are then resected to generate 3′ single-stranded overhangs, which are bound by the recombinases DMC1 and RAD51. These recombinases mediate strand invasion into the homologous chromosome, forming a displacement loop (D-loop). As recombination progresses through pachytene, the transverse filament protein ZYP1 is progressively loaded onto the ASY1-labelled chromosome axes, initiating and completing synapsis along the entire length of homologous chromosomes. Simultaneously, HEI10 forms a hundred foci associated with the central element of the SC at zygotene and early pachytene, but many are later removed through HEI10 coarsening (Morgan *et al.* 2021), leaving only designated class I crossovers by late pachytene. Figure adapted from *Lloyd, 2022.*

Although hundreds of DSBs induced at the beginning of meiosis, only a small fraction are repaired as COs. In Arabidopsis, approximately 150 to 220 DSBs are generated during meiosis, yet only 9 to 11 of these are resolved as COs (Baudat and de Massy, 2007; Sanchez-Moran *et al.*, 2007). Following strand invasion and second end capture, a key recombination intermediate known as double Holliday Junction (dHJ) is formed (Brown and Bishop, 2015). The dHJs can be resolved into either CO or non-crossovers (NCOs) (Figure 3). A subset of these recombination intermediates enters the major recombination pathway, ZMM dependent pathway, which accounts for 85-90 % of COs in Arabidopsis (Bishop and Zickler, 2004; Mercier *et al.*, 2005).

In Arabidopsis, ZMM proteins include SHORTAGE IN CHIASMATA 1 (SHOC1), HUMAN ENHANCER INVASION 10 (HEI10), ZIPPER 4 (ZIP4), PARTING DANCERS (PTD), MEIOTIC RECOMBINATION 3/ROCK-N-ROLLERS (MER3/RCK), MUTS HOMOLOG 4 (MSH4) and MSH5. Within the ZMM-dependent CO pathway pathway, these proteins act synergistically to promote class I CO formation in an interference sensitive manner, which COs inhibit the formation of another CO nearby (Bishop and Zickler, 2004). MER3, a helicase, catalyzes D-loop extension and promotes dHJ formation (Mazina *et al.*, 2004; Chen *et al.*, 2005; Mercier *et al.*, 2005), functioning together with ZIP4 to coordinate chromatin dynamics (Chelysheva *et al.*, 2007). SHOC1 and PTD stabilize recombination intermediates and support dHJ maturation (Macaisne *et al.,* 2011; Ren *et al.*, 2019). The MSH4 and MSH5 complex further stabilizes dHJs and facilitates the recruitment of other ZMM components (Higgins *et al.*, 2008; Nandanan *et al.*, 2021). HEI10 serves as a dosage-sensitive regulator of CO formation (Chelysheva *et al.*, 2012; Morgan *et al.*, 2021; Wang *et al.*, 2023); it is initially observed as numerous small foci on synapsed chromosomes during early pachytene, but by late pachytene, it condenses into a limited number of large foci marking sites of designated class I COs (Figure 2).

The remaining 10-15 % of COs occur via class II COs or “non-interfering” COs. In Arabidopsis, these COs are generated through partially redundant pathways that rely on structure specific endonuclease MMS AND UV SENSITIVE 81 (MUS81) and DANCONI ANEMIA D2 (FANCD2) (Higgins *et al.*, 2008; Kurzbauer *et al.*, 2018) (Figure 3).

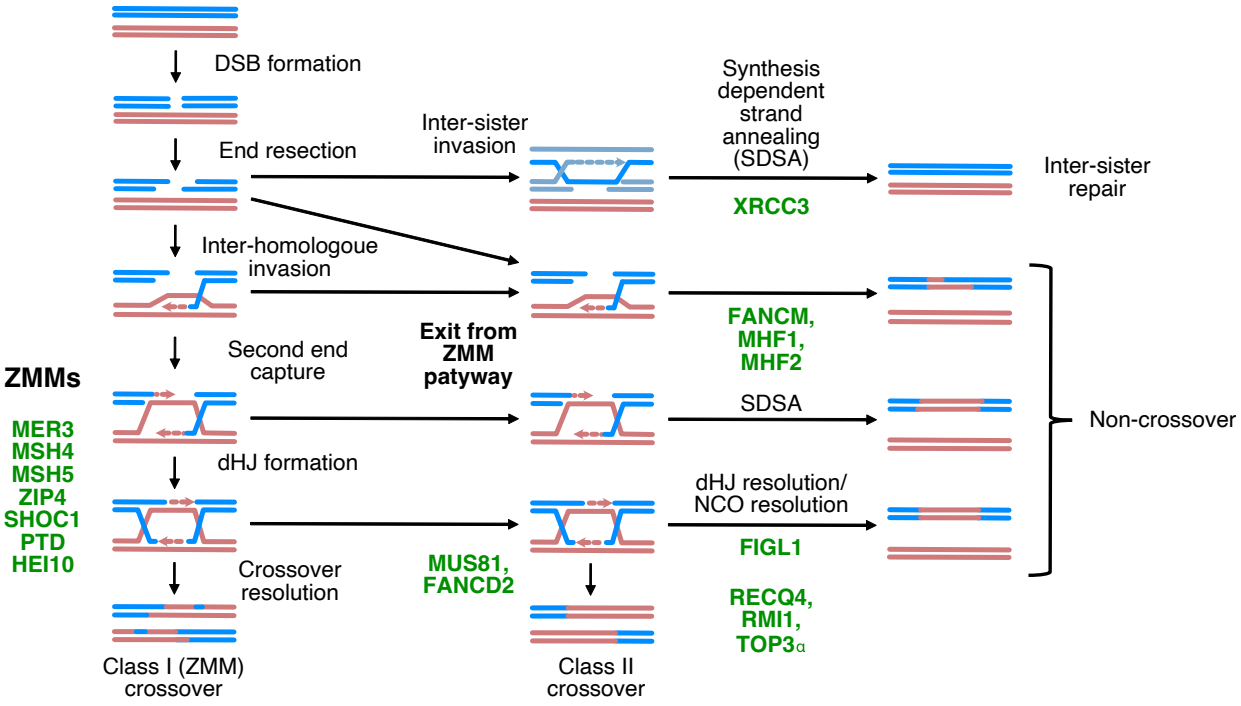


Figure 3. Meiotic recombination and DNA repair pathways.

Following DSB induction, DNA ends are resected to produce single-stranded DNA, which can invade a homologous chromosome and form D-loops or alternatively engage in inter-sister repair using the sister chromatid. D-loop extension and second-end capture give rise to dHJs, the hallmark recombination intermediates. These dHJs are resolved into class I COs via the ZMM-dependent pathway. Alternatively, a subset of recombination intermediates can be processed into class II COs through pathways involving MUS81 and FANCD2, which act in partially redundant roles. Recombination intermediates can be resolved as NCOs via SDSA or dHJ dissolution, a process mediated by helicases such as FANCM and RECQ4 along with their associated factors. Figure adapted from *Lloyd, 2022*.

The majority of DSBs are repaired as NCOs, primarly through the synthesis-dependent strand annealing (SDSA) pathway (Figure 3) (Sánchez-Rebato *et al.*, 2024), which is promoted by the DNA helicase FANCM and its cofactors MPH1-ASSOCIATED HISTONE-FOLD PROTEIN 1 (MHF1) and MHF2 (Crismani *et al.*, 2012; Girard *et al.*, 2014). Additionally, topoisomerase TOP3α, RECQ MEDIATED INSTABILITY 1 (RMI1) together with RECQ HELICASE 4A (RECQ4A) and RECQ4B, referred as RTR complex in Arabidopsis, mediates NCOs by dissolution of D-loops (Figure 3) (Hartung *et al.*, 2008; Séguéla-Arnaud *et al.*, 2015a). Mutants lacking TOP3α and RMI1 exhibit persistent chromosomal linkages at metaphase I and show extensive chromosome fragmentation during anaphase I.

These findings indicate a requirement for TOP3α-mediated single-strand decatenation in the completion of NCO repair (Séguéla-Arnaud *et al.*, 2017). The AAA-ATPase FIDGETIN-LIKE 1 (FIGL1) suppresses CO formation independently of FANCM by modulating DMC1- and RAD51-mediated early recombination events (Girard *et al.*, 2015; Kumar *et al.*, 2019; Emmenecker *et al.*, 2024).

Loss of FANCM results in a threefold increase in COs, whereas *recq4a recq4b* double mutants show up to a sixfold increase, with the additional COs derived exclusively from the class II pathway (Crismani *et al.*, 2012; Séguéla-Arnaud *et al.*, 2015a). Notably, combining mutations in these anti-crossover (anti-CO) factors with *zmm* mutants restores CO formation to near wild-type levels, thereby compensating for the CO defects typically observed in *zmm* mutants (Girard *et al.*, 2015; Séguéla-Arnaud *et al.*, 2015a; Serra *et al.*, 2017).

Together, these anti-CO factors constitute a regulatory network that limits CO formation and ensures that the majority of DSBs are resolved as NCOs. This restraint is critical for safeguarding genome integrity and promoting faithful meiotic chromosome segregation.

1.2. Synapsis formation via synaptonemal complex

One of the key processes in meiosis is the establishment of synapsis, which tightly connects aligned homologous chromosomes through the formation of the synaptonemal complex (SC). At early prophase, the chromosomes are organized as loop arrays by a proteinaceous structure called chromosome axis. This axis forms the structural foundation for SC assembly and its main components are the coiled-coil domain-containing ASYNAPTIC 3 (ASY3) and the HORMA domain-containing ASYNAPTIC 1 (ASY1) (Armstrong *et al.*, 2002; Wang *et al.*, 2011; Ferdous *et al.*, 2012). Mutants lacking these axis proteins exhibit severe meiotic defects, including impaired synapsis and defective DSB formation. In Arabidopsis, *asy1* mutants show a drastic reduction in CO formation, despite normal levels of DSBs and *asy3* mutants also exhibit reduced COs, to a lesser extent than *asy1* (Armstrong *et al.*, 2002; Ferdous *et al.*, 2012). In both *asy1* and *asy3* mutants, COs are predominantly located in more distal chromosomal regions, suggesting that the proper establishment of the

chromosome axis is essential for distributing COs along the chromosome length (Lambing *et al.*, 2020).

Additionally, ASY1 is essential for DISRUPTED MEIOTIC cDNA1 (DMC1) - dependent inter-homolog recombination (IHR), and its absence compromises the association of AtDMC1 with early recombination intermediates. Notably, ASY1 recruitment to the chromosome axis is dependent on ASY3 and is regulated through phosphorylation by CYCLIN DEPENDENT KINASE A;1 (CDKA;1) (Yang *et al.*, 2020).

Synapsis is initiated at zygotene and proceeds through the progressive installation of transverse filaments (TFs) perpendicular to chromosome axis, ultimately aligning them in close proximity along their entire length (Figure 2). Transverse filament protein, ZIPPER 1 (ZYP1), loads onto ASY1-decorated axial bridges, is integral to SC function. Functional studies using a *ZYP1* RNAi knockdown line revealed that loss of ZYP1 disrupts synapsis, leading to an increase in non-homologous recombination and the formation of multivalents (Higgins *et al.*, 2005). More recent work has demonstrated that ZYP1 is required for CO interference but is dispensable for the occurrence of recombination itself (Capilla-Pérez *et al.*, 2021; France *et al.*, 2021).

1.3. Cyclin-CDK mediated control of meiotic cell division

Progression through meiosis is tightly coordinated by cyclin-dependent kinase (CDK) – cyclin complexes, which orchestrate key cell cycle transitions. In both mammals and plants, multiple CDKs and cyclins exist, forming dynamic complexes that act in specific combinations to regulate distinct stages of meiosis. It is hypothesized that the activity of these CDK–cyclin complexes oscillates throughout meiotic division, with CDK activity declining to an intermediate level following meiosis I. This intermediate activity is thought to permit entry into meiosis II without an intervening S-phase. (Wijnker and Schnittger, 2013).

In plants, homologs for A- and B-type cyclins have been identified, along with a distinct class called D-type cyclins (Bulankova *et al.*, 2013). Several cyclins have defined roles in meiosis. The A-type cyclin TARDY ASYNCHRONOUS MEIOSIS

(TAM, CYCA1;2) is essential for proper progression through meiosis I and II. In *tam* mutants, premature cytokinesis occurs after meiosis I, producing diploid instead of haploid gametes (Wang *et al.*, 2004; Bulankova *et al.*, 2010; d'Erfurth *et al.*, 2010). SOLO DANCERS (SDS) is an atypical cyclin that promotes homolog pairing and CO formation during prophase I (Azumi *et al.*, 2002). Additionally, the B-type cyclin CYCB3;1 accumulates during metaphase I and II and contributes to spindle organization (Bulankova *et al.*, 2013).

In Arabidopsis, the mitotic CDK homolog CDKA;1 is expressed throughout meiosis and plays essential roles in chromosomal synapsis and recombination. Notably, CDKA;1 phosphorylates ASY1, a key component of the chromosome axis required for homolog pairing and synaptonemal complex formation (Dissmeyer *et al.*, 2007; Bulankova *et al.*, 2010; Yang *et al.*, 2019; Sofroni *et al.*, 2020). Additionally, CDKG1 is essential for synapsis and class I CO formation, particularly under high temperatures; loss of CDKG1 leads to univalent formation and pollen sterility (Zheng *et al.*, 2014; Nibau *et al.*, 2020).

2. Meiotic transcriptome

Proper execution of key meiotic events such homologous pairing, synapsis, recombination and chromosome segregation requires tightly regulated gene expression at the transcriptional level. A major challenge is that meiotic gene expression must occur in the context of highly condensed chromosomes, which restricts chromatin accessibility. Thus, the regulatory network governing meiosis must coordinate dynamic chromatin condensation and decondensation to both enable and restrict transcription, ensuring orderly meiotic progression. Despite its crucial role, the mechanisms underlying the regulation of gene expression during meiosis remain poorly understood.

2.1. The features of meiotic transcriptome across species

Understanding whether transcription remains active during meiosis is key to uncovering how gene expression supports critical meiotic events. Cross-species comparisons of meiotic transcriptomes can reveal conserved and divergent patterns, shedding light on the timing of expression switches and the regulatory logic that coordinates transcription with meiotic progression.

Notably, studies in yeast have shown that meiosis involves an unexpectedly dynamic transcriptome, including both coding and non-coding RNAs. These findings challenged earlier assumptions of widespread transcriptional silencing during meiosis and suggested that meiotic cells actively reshape their transcriptional landscape in a stage-specific manner (Vershon and Pierce, 2000; Mata *et al.*, 2002; Guisbert *et al.*, 2012).

Similarly, transcriptome analyses in *Caenorhabditis elegans* gonads, containing both germline and somatic cells, revealed highly dynamic gene expression patterns throughout germ cell development (Tzur *et al.*, 2018; Su *et al.*, 2024). Over 6,000 genes were identified as differentially expressed across meiotic stages, underscoring the complexity of the transcriptional program driving gametogenesis (Tzur *et al.*, 2018). Two major gene clusters with reciprocal expression changes were found to shift sharply at late pachytene, indicating a key transcriptional switch during

meiotic prophase I. These transitions were tightly correlated with developmental and cellular processes, reinforcing the idea that spatiotemporally restricted gene expression supports meiotic progression (Tzur *et al.*, 2018).

In mice, transcriptional activation of meiosis-related genes begins even in pre-meiotic cells, with many reaching peak expression during leptotene and zygotene. These genes, which are enriched for gene ontology (GO) terms such as “meiotic recombination,” “synaptonemal complex,” and “chromosome segregation,” become progressively downregulated as cells enter pachytene (Chen *et al.*, 2018). A global transcriptional switch occurs during the zygotene-to-pachytene transition, characterized by a sharp decline in meiotic gene expression and the concurrent upregulation of spermatogenesis-related programs. Genes involved in spermatid differentiation, fertilization, and flagellum assembly begin to be expressed already in pachytene, indicating that transcriptional priming for post-meiotic development starts well before meiosis is complete (Evans *et al.*, 2014; da Cruz *et al.*, 2016; Chen *et al.*, 2018).

In humans, oocytes are transcriptionally active during their growth phase, but transcription halts before maturation at the prophase-arrested germinal vesicle stage, with post-transcriptional regulation ensuring the timely use of stored maternal transcripts (Gao *et al.,* 2024; Zhang *et al.*, 2024; Caniçais *et al.*, 2025). In contrast, human testes exhibit active transcription during early meiotic prophase, with genes related to recombination, synapsis, and chromatin remodeling upregulated at leptotene and zygotene. While transcriptional programs shift markedly at meiotic entry and exit, changes within prophase I itself appear more gradual, suggesting a relatively stable transcriptional landscape during this stage (Jan *et al.*, 2017; Guo *et al.*, 2018; M. Wang *et al.*, 2018).

Although technical challenges in isolating pure meiocytes have long hindered precise meiotic transcriptome analyses in plants, advances over the past decade have begun to illuminate the dynamic landscape of meiotic gene expression in several species (Chen *et al.*, 2010; Yang *et al.*, 2011; Dukowic-Schulze *et al.*, 2014; Huang *et al.*, 2019; Barakate *et al.*, 2021; Barra *et al.*, 2021).

In wheat and maize, transcriptome analyses revealed that meiosis is accompanied by selective gene activation rather than global transcriptional silencing (Dukowic-Schulze *et al.*, 2014; Nelms and Walbot, 2019; Jiang *et al.*, 2023). Genes upregulated during prophase I include those involved in chromatin remodeling, DNA replication, translation, and microtubule organization, while genes related to photosynthesis and general metabolism are downregulated. Notably, gene expression patterns show a strong correlation with the functions of known meiotic regulators, many of which are specifically upregulated during distinct substages of meiosis (Jiang *et al.*, 2023).

In *Arabidopsis thaliana*, approximately 20,000 genes, around 60% of annotated genes, are expressed in male meiocytes, which is comparable with the transcriptional activity observed in maize (Chen *et al.*, 2010; Yang *et al.*, 2011; Dukowic-Schulze and Chen, 2014; Dukowic-Schulze *et al.*, 2014). Nearly half of the genes expressed in meiocytes are significantly enriched compared to vegetative tissues, highlighting the unique transcriptional identity of meiotic cells. Supporting this, the majority of 68 known meiotic genes, including *SPO11*, *DMC1*, *RAD51C*, *XRCC3*, *MSH4*, *MSH5*, *MER3/RCK*, *PTD*, *MUS81*, and *SDS*, were expressed at least two-fold higher in meiocytes or anthers compared to seedlings (Chen *et al.*, 2010; Yang *et al.*, 2011). Notably, meiotic transcriptomes also include transposable elements and mitochondrially encoded genes, indicating that meiotic gene expression extends beyond nuclear protein-coding genes (Chen *et al.*, 2010; Yang *et al.*, 2011; Dukowic-Schulze *et al.*, 2014).

These findings strongly indicate that, meiotic division is accompanied by broad and dynamic transcriptional activity, laying the foundation for investigating its regulatory control.

2.2. Methylation dynamics regulating meiotic transcription and recombination in *Arabidopsis*

DNA methylation is a key epigenetic modification involved in silencing transposable elements and regulating gene expression. In *Arabidopsis thaliana*, methylation occurs in three sequence contexts—CG, CHG, and CHH—each maintained by distinct sets of DNA methyltransferases (Du *et al.*, 2015). The ortholog of DNA methyltransferase1, METHYLTRANSFERASE1 (MET1) , along with VARIANT IN METHYLATION (VIM) proteins, preserves CG methylation (Kankel *et al.*, 2003; Saze, Scheid and Paszkowski, 2003; Woo *et al.*, 2007; Stroud *et al.*, 2013; Shook and Richards, 2014). CHG methylation is maintained by CHROMOMETHYLASE 3 (CMT3) and coupled with histone methylation through histone H3 lysine 9 dimethylation (H3K9me2), which is established by KRYPTONITE/ SUPPRESSOR OF VARIEGATION 3-9 HOMOLOGUE PROTEIN 4 (KYP/SUVH4), SUVH5, and SUVH6 (Bartee *et al.,* 2001; Lindroth *et al.*, 2001; Du *et al.*, 2012). CHH methylation is catalyzed either by CMT2 in heterochromatin or by DOMAINS REARRANGED METHYLTRANSFERASE 1/2 (DRM1/2) via the RNA-directed DNA methylation (RdDM) pathway in euchromatin (Law and Jacobsen, 2010; Zemach *et al.*, 2013; Stroud *et al.*, 2014).

Notably, RNA-directed DNA methylation (RdDM) is required for *de novo* methylation in all three sequence contexts (Matzke and Mosher, 2014; Erdmann and Picard, 2020). Together, MET1, DRM1/2, CMT2, and CMT3 maintain the genome-wide DNA methylation (L. He *et al.*, 2022). The chromatin remodeler DDM1 (DECREASED DNA METHYLATION 1) is also essential for heterochromatin accessibility and proper DNA methylation, particularly in transposon-rich regions (Zemach *et al.*, 2013; Lee *et al.*, 2023).

During male germline development, DNA methylation undergoes significant reprogramming. Compared to somatic cells, pollen mother cells (PMCs), male meiocytes, display elevated CG and CHG methylation but reduced CHH methylation, indicating enhanced CMT3 and reduced CMT2 activity (Hsieh *et al.*, 2016; Walker *et al.*, 2018). In addition, RdDM shifts its targeting from transposable elements in somatic tissues to protein-coding genes in the male germline, establishing ~400 germline-

specific methylated loci, called MetGenes (Walker *et al.*, 2018), many of which are protein-coding genes not methylated in somatic tissues. These MetGenes include regulators of meiosis such as *MULTIPOLAR SPINDLE 1* (*MPS1)*, where *de novo* methylation promotes correct splicing and gene expression, supporting meiotic progression.

Beyond its direct regulation, DNA methylation is modulated by chromatin context, particularly through histone modifications such as H3K9me2 (Du *et al.*, 2015). The H3K9 demethylase IBM1 (INCREASE IN BONSAI METHYLATION 1) prevents ectopic accumulation of H3K9me2 and CHG methylation within gene body accompanied by reduced gene expression (Saze *et al.*, 2008; Du *et al.*, 2015; Inagaki *et al.*, 2017). In *ibm1* mutants, this deregulation leads to genome-wide hypermethylation in gene bodies and results in reduced chiasma formation. These meiotic defects are associated with altered gene expression and misregulation of the cohesin cofactor PRECOCIOUS DISSOCIATION OF SISTERS 5 (PDS5), implicating IBM1 in the coordination of chromatin state and chromosome behavior during meiosis (C. He *et al.*, 2022; Cheng, 2022).

Epigenetic mutants reveal how DNA methylation pathways influence the meiotic recombination landscape (Chowdary, Saini and Singh, 2023). In *ddm1* mutants, CO frequency increases in euchromatic regions, while heterochromatic pericentromeric regions show no change (Melamed-Bessudo and Levy, 2012). Similarly, in *met1* mutants, COs are redistributed from pericentromeres to chromosome arms without altering overall DSB or CO frequency (Yelina *et al.*, 2012, 2015). In contrast, loss of *CMT3* or H3K9 methyltransferases (*SUVH4/5/6*) leads to increased DSB formation and elevated COs, including both class I and class II types, particularly in pericentromeric regions (Choi *et al.*, 2018; Underwood *et al.*, 2018). Furthermore, the DNA polymerase ε subunit POL2A interacts with *SUVH2/9* to repress transcription near meiotic DSB hotspots, modulating recombination independently of siRNA-directed pathways (C. Wang *et al.*, 2022).

Together, these findings show that DNA methylation in Arabidopsis male meiosis is not static but dynamically reconfigured to regulate transcription, maintain

chromatin structure, and fine-tune the spatial distribution of meiotic recombination, thereby ensuring the integrity and success of meiotic division.

3. DREAM complexes

The DREAM (Dimerization partner (DP), Retinoblastoma-like (RB-like), E2 Promoter Binding Factor (E2F), and Multi-vulva class B (MuvB)) complex is a highly conserved, multisubunit transcriptional regulator central to the control of cell cycle-dependent gene expression in eukaryotes (Fischer and Müller, 2017). Initially discovered in *Drosophila melanogaster* as the dREAM complex (Drosophila Rb, E2F, and Myeloblastoma (Myb)) (Beall *et al.*, 2002; Korenjak *et al.*, 2004; Lewis *et al.*, 2004) and later in *Caenorhabditis elegans* through identification of synthetic multivulval class B (synMuvB) genes (Harrison *et al.*, 2006), DREAM complexes have emerged as key players in orchestrating transcriptional programs associated with proliferation, quiescence, differentiation, reproduction and apoptosis (Beall *et al.*, 2007; Georlette *et al.*, 2007; Litovchick *et al.*, 2007; Schmit *et al.,* 2009; Litovchick *et al.*, 2011; Rovani *et al.*, 2012; Sadasivam and DeCaprio, 2013; Tabuchi *et al.*, 2013; Kobayashi *et al.*, 2015).

DREAM complexes are versatile in structure and function. Their modular architecture includes a conserved MuvB core, consisting of ABNORMAL CELL LINEAGE PROTEIN (LIN9), LIN37, LIN52, LIN54, and BB-BINDING PROTEIN 4 (RBBP4)/MULTICOPY SUPPRESSOR OF IRA (MSI) homologues, coupled with dynamically interacting partners such as RB-like proteins, E2F transcription factors, and Myb family regulators (Fischer and Müller, 2017; Walston, Iness and Litovchick, 2021). These interactions shift across developmental stages, environmental conditions, and cell-cycle phases, enabling the complex to selectively regulate diverse sets of target genes. Depending on their composition, DREAM complexes influence gene expression via multiple mechanisms, including chromatin remodeling, recruitment of transcriptional cofactors, and direct DNA binding at specific cis-regulatory elements (Blanchard *et al.*, 2014; Latorre *et al.*, 2015; Marceau *et al.*, 2016; Goetsch and Strome, 2022; Koliopoulos *et al.*, 2022).

While DREAM has been extensively characterized in animal systems, its presence and function in plants have only recently been discovered (Ning *et al.*, 2020; Lang *et al.*, 2021). In *Arabidopsis thaliana*, the MuvB core is composed of homologues

such as ALWAYS EARLY (ALY), LIN37, LIN52, TESMIN/TSO1-LIKE CXC (TCX), and MULTICOPY SUPPRESSOR OF IRA (MSI). This plant MuvB core associates with RETINOBLASTOMA-RELATED 1 (RBR1), DIMERIZATION PARTNER (DP), E2 PROMOTER BINDING FACTOR (E2F), and MYELOBLASTOMA 3R (MYB3R) to fine-tune transcriptional control. These interactions regulate critical processes including the cell cycle, DNA methylation, responses to genotoxic stress, and developmental transitions such as the initiation of flowering (Kobayashi *et al.*, 2015; Ning *et al.*, 2020; Lang *et al.*, 2021, 2023). Since the naming of DREAM components varies widely between organisms, an overview of their orthologous nomenclature across species is provided in Table 1 to aid clarity and comparison.

Table 1. Comparative nomenclature of the DREAM complex proteins across different model organisms.

ALWAYS EARLY (ALY); B-Myeloblastoma (B-MYB); BARRIER OF TRANSCRIPTION ELONGATION (BTE); BTE1-LIKE (BTL); Cookie Monster (Comr); Chromatin Assembly Factor (Caf); DIMERIZATION PARTNER (DP); DP-like (DPL); E2F-like (EFL); E2 PROMOTER BINDING FACTOR (E2F); FLORAL ANTICIPATION CONTROLLER (FLAC); FLORAL INDUCTION CONTROLLER (FLIC); Forkhead Box Protein M (FOXM); ABNORMAL CELL LINEAGE PROTEIN (LIN); Matotopetli (Topi); Myb-Interacting Protein (Mip); MULTICOPY SUPPRESSOR OF IRA (MSI); Myeloblastoma (MYB); MYELOBLASTOMA 3R (MYB3R); RB-Binding Protein (RBBP); Retinoblastoma Family (Rbf); RETINOBLASTOMA-RELATED (RBR); TESMIN/TSO1-LIKE CXC (TCX); Tombola (Tomb); Wake-Up-Call (Wuc).

A. thaliana **DREAM**	***C. elegans*** **DRM**	***D. melanogaster*** **dREAM**	***D. melanogaster*** **tMAC**	***H. sapiens*** **DREAM**
ALY	LIN-9	Mip130	Aly	LIN9
LIN37	LIN-37	Mip40	Mip40	LIN37
LIN52	LIN-52	Lin52	Wuc	LIN52
MSI	LIN-53	Caf1	p55	RBBP4
TCX	LIN-35	Mip120	Tomb	LIN54
DP	DPL-1	Dp	-	DP
E2F	EFL-1	E2f2	-	E2F
RBR1	LIN-35	Rbf	-	p107/p130
MYB3R	-	Myb	-	B-MYB
-	-	-	-	FOXM1
-	-	-	Topi	-
-	-	-	Comr	-
FLIC	-	-	-	-
FLAC	-	-	-	-
BTE1	-	-	-	-
BTL1	-	-	-	-

3.1. The DREAM as a master regulator of cell cycle

The canonical role of the DREAM complex is a transcriptional regulator of cell cycle, which is conserved among eukaryotes. The cell cycle, comprising the precise sequence of gap 1 (G1), synthesis (S), G2, and mitosis (M) phases, is a series of tightly regulated processes that ensure accurate DNA replication and division into daughter cells (Malumbres and Barbacid, 2009; Walston, Iness and Litovchick, 2021). Disruption of this regulation can lead to pathological conditions, such as the unchecked proliferation characteristic of cancer. While DREAM-like complexes have been identified in diverse eukaryotic systems, their mechanistic roles have been most thoroughly characterized in mammals. Accordingly, this subsection focuses on the mammalian DREAM complex in the context of cell cycle regulation, as schematically represented in Figure 4 (Hoareau *et al.*, 2024).

In mammals, DREAM predominantly binds promoters of early and late cell cycle genes, acting mainly as a transcriptional repressor during the G0 and G1 phases (Litovchick *et al.*, 2007; Sadasivam and DeCaprio, 2013). This repression is mediated through the assembly of p107/p130, E2F4/5, and the MuvB core, forming the canonical DREAM complex (Pilkinton *et al.,* 2007). The transition into the cell cycle is initiated by cyclin D–CDK4/6-mediated phosphorylation of p107/p130, which disrupts their interaction with LIN52 and E2F4/5, leading to disassembly of the DREAM complex and subsequent activation of target gene transcription (Guiley *et al.*, 2015; Schade *et al.*, 2019).

As human cells transition into S and G2/M phases, the DREAM complex is converted into the MMB (Myb–MuvB) and later into the MMB–FOXM1 complex through sequential recruitment of B-MYB and Forkhead box protein M1 (FOXM1) (Fischer, Grossmann, *et al.*, 2016). This transformation enhances the transcriptional activation of G2/M-specific genes (Schmit *et al.*, 2009; Marceau *et al.*, 2016). This shift is tightly regulated both transcriptionally, through repression of *MYBL2* and *FOXM1*, and post-translationally, via phosphorylation by CDKs and Polo-like kinase 1 (Plk1), which activates these transcription factors (Marceau *et al.*, 2019; Werwein *et al.*, 2019; Gallo *et al.*, 2022).

In humans, transcriptional specificity of DREAM is achieved via the recognition of conserved promoter motifs. LIN54 binds to cell cycle genes homology regions (CHRs) and CHR-like elements (CLEs), while E2F/DP proteins target cell cycle–dependent elements (CDEs). These motifs can occur independently or in tandem, providing a multi-layered mechanism for transcriptional regulation (Müller and Engeland, 2010; Fischer, *et al.*, 2016; Müller *et al.*, 2016).

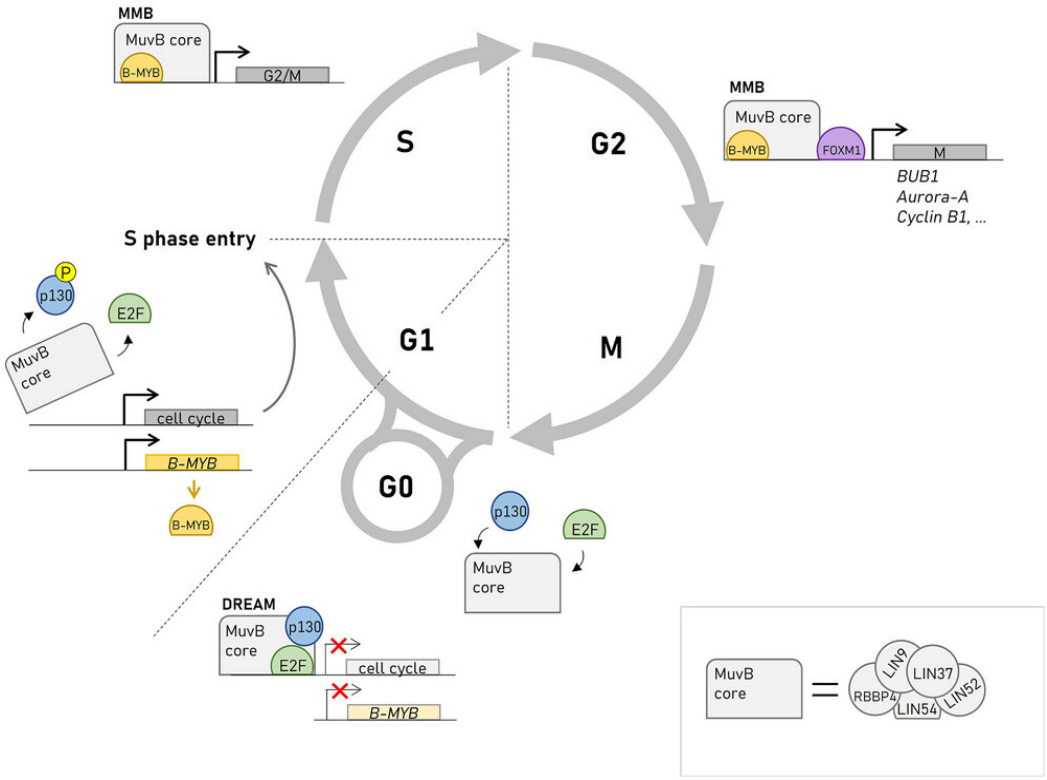


Figure 4. Regulation of MuvB complex assembly and transcriptional control during the mammalian cell cycle. Figure taken from Hoareau *et al.*, 2024.

This figure illustrates the dynamic association of MuvB-core subunits with different regulatory partners across cell-cycle phases. In G1 phase, phosphorylation of DREAM components by CDKs, including CDK2 and CDK4, initiates complex disassembly. Notably, phosphorylation of p130 disrupts its interaction with the MuvB core, leading to DREAM complex dissociation. Upon release of p130 and E2F4, the MuvB core—through LIN54's binding to CHRs—facilitates S-phase entry. Subsequently, newly synthesized B-MYB associates with the MuvB core to form the Myb–MuvB (MMB) complex, which no longer regulates E2F targets but instead activates genes required for the G2/M transition. During G2 and M phases, the MMB complex recruits additional factors, including FOXM1, to promote transcription of key mitotic genes such as *Cyclin B1*, *BUB1*, and *Aurora A* (Hoareau *et al.*, 2024).

While the function of mammalian DREAM/MuvB complexes is largely confined to the regulation of cell cycle–associated genes, studies in other model organisms have revealed broader regulatory roles. In *C. elegans*, the DRM complex represses not only cell cycle specific genes but also germline specific transcripts in somatic tissues. Loss of the pocket protein ortholog LIN-35 results in the upregulation of cell cycle genes and is accompanied by depletion of HTZ-1, the *C. elegans* ortholog of the histone variant H2A.Z, within gene bodies (Tabuchi *et al.*, 2011, 2013; Kudron *et al.*, 2013; Latorre *et al.*, 2015; Rechtsteiner *et al.*, 2019). Similarly, in *D.melanogaster*, the dREAM/MMB complex regulates a wider spectrum of genes beyond the cell cycle, including those involved in development (Lewis *et al.*, 2004; Georlette *et al.*, 2007), olfactory receptor gene expression (Sim *et al.*, 2012), and programmed cell death (Rovani *et al.*, 2012). These findings highlight both the conserved core functions of DREAM complexes as a cell cycle regulator across metazoans and their evolutionary adaptation to species-specific regulatory networks.

3.2. *Arabidopsis* DREAM complex

In *Arabidopsis thaliana*, MuvB-core components have only been recently discovered. Using pull-down and mass spectrometry experiments, interaction studies among RBR1, E2FB or E2FC, DPA or DPB, and homologs of the MuvB core proteins revealed the existence of DREAM-like repressor and activator complexes. At the time of initial characterization, no plant homologs were identified for LIN37 or LIN52. However, ALY and TCX proteins were recognized as functional counterparts of LIN9 and LIN54, respectively (Kobayashi and Suzuki, *et al.*, 2015).

While MYB3Rs in plants interact with a plant-specific cis-regulatory sequence known as the M-specific activator (MSA) element, their co-enrichment at E2F target sites hinted at the existence of a multiprotein regulatory complex (Haga *et al.*, 2011; Magyar *et al.*, 2012; Kobayashi and Suzuki, *et al.*, 2015). The identification of ALY2, ALY3 and TCX5, TCX6 in complex with RBR1 and MYB3Rs led to the proposal of two functionally distinct DREAM assemblies, one activating and one repressing, containing MYB3R1/4 and MYB3R1/3/5 respectively (Fischer and DeCaprio, 2015; Kobayashi *et al.*, 2015). A switch between repressor and activator MYB3Rs occurs in

the G2 phase, once G2/M genes are desired to be expressed. Notably, MYB3R1 in particular has been demonstrated to have a marked dual role, contributing significantly to both activating and repressive abilities (Kobayashi *et al.*, 2015; Magyar, Bögre and Ito, 2016). LIN37 and LIN52 orthologues could be detected in later studies, establishing a complete orthologous MuvB-core in plants (Ning *et al.*, 2020; Lang *et al.*, 2021).

TCX proteins (TESMIN/TSO1-like CXC domain-containing proteins) belong to the CHC (CXC–Hinge–CXC) protein family and are structurally defined by a conserved tandem repeat of CXC domains linked by a hinge region (Hauser *et al.*, 2000; Song *et al.*, 2000; Andersen *et al.*, 2007). Functional analyses have shown that TCX5 and TCX6 act redundantly to regulate DNA methylation homeostasis, primarily in quiescent cells (Ning *et al.*, 2020). Loss of both genes leads to global hypermethylation, ectopic cell proliferation, and enlarged organs, due to de-repression of methylation maintenance genes.

A defining feature of *Arabidopsis* ALY is the presence of an N-terminal MYB domain (Bhatt *et al.*, 2004), a motif absent in *Drosophila* ALY/LIN9 (White-Cooper *et al.*, 2000). This domain implies a potential for direct DNA binding, suggesting that plant ALY proteins may not solely function as scaffolds but could also participate in gene targeting via sequence-specific interactions. This structural innovation may reflect plant-specific adaptations to integrate transcriptional regulation more directly with chromatin architecture.

Together with TCX5/6, ALY1/2/3 form a critical part of the plant MuvB core. Their cooperative roles are evident in both epigenetic regulation and stress response. For instance, mutants of *aly2 aly3* show hypermethylation similar to *tcx5 tcx6*, and triple mutants of *aly1 aly2 aly3* are synthetically lethal, highlighting their essential and partially redundant roles in genome stability and development (Ning *et al.*, 2020).

Beyond DNA methylation and cell cycle regulation, the DREAM complex is also implicated in genotoxic stress responses. The full complex is recruited to the RBR1 interactome under DNA damage conditions and functions in coordination with the plant-specific NAM, ATAF1, and CUC1/CUC2 (NAC) type protein NAC044

transcription factor (Lang *et al.*, 2021). NAC044, a homolog of SOG1 (SUPPRESSOR OF GAMMA RESPONSE 1), binds RBR1 via a conserved LxCxE motif. NAC044 mutants, like *lin37ab* and *e2fb*, exhibit tolerance to DNA damage due to impaired growth arrest (Takahashi *et al.*, 2019; Lang *et al.*, 2021). These findings indicate the complex's pivotal role in modulating gene expression in response to genotoxic stress.

Additionally, recent research identified BTE1 and BTL1 as plant-specific DREAM-associated repressors. These factors inhibit transcription by blocking the COMPASS-like methyltransferase HUMAN WD40-REPEAT 5 HOMOLOG A (WDR5A) and impeding RNA Polymerase II elongation. BTE1 is recruited to chromatin in an E2F-dependent manner, and its mutation confers hypersensitivity to DNA damage, reinforcing the dual role of DREAM in transcriptional and chromatin-level repression (Wang *et al.*, 2022)

The DREAM complex also contributes to developmental transitions unique to plants, such as flowering. Mutations in TCX5/6 and other core components lead to alterations in flowering time (Ning *et al.*, 2020), while the newly characterized plant-specific components FLIC (FLORAL INITIATION CONTROLLER) and FLAC (FLORAL ANTICIPATION CONTROLLER) are required for proper floral timing and reproductive development. FLIC and FLAC physically interact with LIN37B and components of the JUMONJI 14 (JMJ14)-NAC050/052 module, possibly forming a specialized DREAM variant for flowering control (Lang *et al.*, 2023).

Interestingly, some canonical MuvB components diverge significantly in plants. Arabidopsis LIN52, for example, lacks the conserved phosphorylation and LxSxExL motifs necessary for RBR1 interaction in animals. Instead, TCX proteins likely mediate the RBR1 association in the plant DREAM complex. Interestingly, no stirking developmental defects have been reported yet for *lin52ab*, while *lin37ab* mutants exhibit both early flowering and stress tolerance (Lang *et al.*, 2021, 2023).

MSI1, a WD40 repeat protein, also contributes to DREAM complex function and epigenetic regulation. Homozygous *msi1* mutants are gametophytically lethal, and MSI1 depletion affects flowering, shoot development, and stress responses in a DNA

methylation dependent manner (Hennig *et al.*, 2003; Bouveret *et al.*, 2006; Xu *et al.*, 2022).

In summary, the plant DREAM complex integrates canonical cell-cycle control with plant-specific regulatory networks, including chromatin remodeling, DNA methylation, and floral transition. Structural divergence of components like ALY and TCX highlights how plants have adapted this conserved complex to their unique developmental and environmental demands.

3.3. A role in reproductive development for the DREAM homologs

Beyond its canonical role in cell cycle regulation, the DREAM complex and its evolutionary paralogs also participate in reproductive development across multiple species. In *Drosophila melanogaster*, a testis-specific DREAM paralog known as the testis Meiotic Arrest Complex (tMAC) plays a critical role in spermatocyte differentiation and meiotic progression (Beall *et al.*, 2007; Beattie, 2016). tMAC is composed of several dREAM components, such as Mip40 and Caf1/p55, as well as homologs of Mip130 (Aly) and Mip120 (Tomb), and additional testis-specific factors including Topi and Comr (Jiang and White-Cooper, 2003; Jiang *et al.*, 2007; Doggett *et al.*, 2011a; Laktionov *et al.*, 2014). Functional studies have shown that tMAC activates a broad set of genes essential for the G2/meiosis transition and spermatid differentiation, while the canonical dREAM complex represses genes not expressed in spermatocytes (Laktionov *et al.*, 2018). DNA adenine methyltransferase identification (DamID) analyses further support the model that dREAM and tMAC bind distinct sets of promoters in the testis, suggesting a division of labor between repression and activation of testis-specific transcriptional programs. Moreover, loss of Mip120 leads to arrest of oogenesis and chromosomal defects, although the mechanisms, particularly whether they involve regulation of meiotic genes, remain to be fully elucidated (Cheng *et al.*, 2017).

In *C.elegans*, the DRM complex, a functional analog of DREAM, also regulates germline development. LIN-54, a component of this complex, is essential for the activation of germline-specific transcriptional programs, and its loss results in sterility (Tabuchi *et al.*, 2011, 2013). Furthermore, mutations in DRM components in *C.elegans*

induce germline-like expression of DNA repair genes in somatic cells, indicating a broader role in restricting the ectopic expression of germline genes (Bujarrabal-Dueso *et al.*, 2023).

In mice, the LIN54 paralog TESMIN (also known as Metallothionein-Like 5, MTL5) is essential for spermatogenesis. TESMIN translocates from the cytoplasm to the nucleus during meiosis in a LIN9-dependent manner and interacts with A-MYB and all MuvB core components except LIN54, forming a testis-specific DREAM-like complex (Oji *et al.*, 2020; Zhang *et al.*, 2021). Loss of TESMIN results in meiotic arrest at the pachytene stage and consequent male infertility.

These findings suggest that, while the canonical DREAM complex is associated primarily with mitotic cell cycle control, its specialized paralogs have evolved distinct functions critical for gametogenesis and reproductive tissue-specific gene regulation across species.

4. Research aim

For my dissertation, I investigated the transcriptional regulation of male meiosis in *Arabidopsis thaliana* by the DREAM complex. Loss of DREAM function resulted in a broad spectrum of meiotic defects. Using transcriptomic, genomic, and genetic approaches, I explored the underlying mechanisms responsible for these phenotypes.

Chapter I, entitled *"Transcriptional Control of Meiotic Recombination by the DREAM Complex"*, presents a manuscript prepared for submission to *Nature Genetics* in Letter format. This chapter focuses on the role of the DREAM complex in regulating the transcription of key components in the CO formation pathway.

Chapter II, *"Dissecting the Multifaceted Roles of the DREAM Complex in Meiosis"*, expands on additional functions of the complex in meiotic progression and provides an initial characterization of the composition of the meiotic DREAM complex.

Finally, Chapter III, *"An Outlook on the Regulation of Meiosis by the DREAM Complex through DNA Methylation"*, examines how DNA methylation influences DREAM-mediated transcriptional control during meiosis.

CHAPTER I. Transcriptional control of meiotic recombination by the DREAM complex

Chapter I – Transcriptional conrol of meiotic recombination by the DREAM complex

The following chapter is presented in the manuscript format intended for submission as a Letter to *Nature Genetics*.

The formatting has been adapted to align with the style of this thesis; however, the content remains unchanged. Figure numbering has been adjusted to conform to the thesis's identifier style. References are included in the consolidated reference list at the end of this thesis.

Transcriptional control of meiotic recombination by the DREAM complex

Hasibe Tunçay [1], Xing Ma [2], Lucas Lang [1], Franziska Böwer [1], Maren Köhler [1], David Latrasse [2], Moussa Benhamed [2], and Arp Schnittger [1]

[1] Department of Developmental Biology, University of Hamburg, 22609 Hamburg, Germany

[2] Institute of Plant Sciences-Paris-Saclay, Gif-sur-Yvette, France

Abstract

The meiotic processes of chromosome segregation and recombination, crucial for sexual reproduction and evolution, require a specialized gene set. However, the mechanisms governing the expression of these genes remain largely elusive in multicellular eukaryotes. Here, we identify the DREAM complex as a transcriptional regulator of meiotic recombination in *Arabidopsis*. We find that the DREAM complex localizes to meiotic chromosomes and reducing DREAM function leads to defects in meiotic recombination causing sterility. Meiocyte-specific transcriptomics together with genome-wide analysis of DREAM-bound genes revealed recombination-associated genes, including the crossover-promoting helicase MER3, as direct targets of the DREAM complex. Bypassing DREAM regulation of MER3 partially restored recombination defects in plants with reduced DREAM activity. Consequently, our data unravel the DREAM complex as a major regulator of meiosis. Given that reduction of the DREAM function is associated with reproductive defects in other species, such as Drosophila and mice, this function might be conserved among multicellular eukaryotes.

Main

The DREAM complex is an ancient transcriptional regulator across eukaryotes, with conserved core components spanning from humans to flowering plants (Litovchick *et al.*, 2007; Sadasivam and DeCaprio, 2013; Fischer and Müller, 2017; Ning *et al.*, 2020; Lang *et al.*, 2021; Koliopoulos *et al.*, 2022). Pioneering studies in *C. elegans, Drosophila*, mice, and human cells revealed a crucial role of the DREAM complex (named after Dimerization partner, RB-like, E2F, and MuvB) in controlling cell cycle and developmental genes (Fischer *et al.*, 2022), while reduced DREAM activity leads to developmental defects and maladies such as cancer (Hwang and Kim, 2025).

Recently, the full complement of the animal DREAM complex has been identified in *Arabidopsis*, including homologs of LIN9 known as ALWAYS EARLY (ALY1, ALY2 and ALY3), the LIN54/TESMIN/TSO1-LIKE CXC homologs (TCX5 and TCX6), homologs of LIN52 (LIN52A and LIN52B), and homologs of ABNORMAL CELL LINEAGE PROTEIN 37 (LIN37A and LIN37B) (Kobayashi *et al.*, 2015; Ning *et al.*, 2020; Lang *et al.*, 2021). Functional studies have shown that the *Arabidopsis* DREAM complex transcriptionally regulates genes involved in cell cycle regulation and maintenance of DNA methylation (Kobayashi *et al.*, 2015; Ning *et al.*, 2020) and governs growth after DNA damage (Lang *et al.*, 2021).

To explore a possible role of the DREAM complex in reproductive development, we started by analyzing fertility-related metrics of single mutants of core MuvB components, i.e., *aly1, aly2, aly3, tcx5, tcx6, lin37a, lin37b, lin52a,* and *lin52b*, none of which differed notably from wild-type plants (WT). We then generated double mutants of presumed redundant components. While *lin37a/b, lin52a/b, aly1/3*, and *aly2/3* double mutants were indistinguishable from WT, *aly1/2* and *tcx5/6* mutants exhibited severe sterility, with reduced seed sets (WT, 60 ± 0.4; *aly1/2*, 35±1.8 ; *tcx5/6*, 11±1.6) and substantially reduced pollen viability (WT, 99.5% ± 0.2%; *aly1/2*, 91% ± 1.0%; *tcx5/6*, 86% ± 2.2%; $p<0.0001$ for all comparisons against WT; Figure 1.1A–D).

Furthermore, both *aly1/2* and *tcx5/6* mutants displayed pollen size variation (Figure 1.1C), hinting at gametophytic and/or meiotic defects. However, transmission efficiency of *tcx6* was unaffected when *tcx5* homozygous/*tcx6* heterozygous plants

were crossed with WT (male: 102%, female: 106%; Supplementary Table 1.1), indicating a sporophytic origin. Therefore, we analyzed male meiosis by acid spreads. Both mutants showed pairing defects at pachytene with unpaired regions (Figure 1.1E, g and m, arrowheads), whereas WT chromosomes were fully paired. Pairing defects are followed by incomplete synapsis at late pachytene (Supplementary Figure 1.1A). At diakinesis and metaphase I, univalents were observed in the mutants (Figure 1.1E, h, n, i, o), instead of the five bivalents seen in WT (Figure 1.1E, b and c). The average number of bivalence was 5.0 in WT, 3.8 in *aly1/2* and 3.3 in *tcx5/6* (n= 81, 48, and 46, respectively; aberrant metaphase I cells were excluded from this calculation). At interkinesis, lagging chromosomes and unbalanced chromosome pools after anaphase I (Figure 1.1E, j and p, white arrowheads) and the formation of triads and polyads after meiosis II could be observed (Figure 1.1E, l and s, Supplementary Figure 1.1B), instead of balanced tetrads as in WT (Figure 1.1E,f).

These meiotic abnormalities indicated severe defects in recombination in DREAM mutants. Next, we quantified chiasmata, the physical manifestations of crossovers (COs), during metaphase I (Figure 1.1F), finding significantly reduced numbers in *aly1/2* (6.5 ± 0.5) and *tcx5/6* (5.3 ± 0.5) compared to WT (9.5 ± 1.7; p<0.0001 for all comparisons against WT). Notably, 11% of *aly1/2* and 15% of *tcx5/6* meiocytes lacked chiasmata entirely, demonstrating that the DREAM complex is essential for crossover formation and faithful chromosome segregation in *Arabidopsis*.

To determine which recombination step was impaired in DREAM complex mutants, we assessed meiotic double-strand break (DSB) formation. SPO11-mediated DNA DSBs (Keeney, Giroux and Kleckner, 1997) generate 3' single-stranded DNA (ssDNA) overhangs coated by RAD51 and DMC1 to promote strand invasion and joint molecule (JMs) formation (Cloud *et al.*, 2012; Ines *et al.*, 2013). Quantification of RAD51 foci at zygotene showed no significant differences between *aly1/2*, *tcx5/6*, and WT (Supplementary Figure 1.1C,D), indicating normal DSB formation.

A subset of DSBs is processed into COs by two pathways: class I and class II (Bishop and Zickler, 2004; Baudat and de Massy, 2007; Zickler and Kleckner, 2015).

Class I COs, which account for ~85% of total COs in *Arabidopsis*, rely on ZMM proteins such as MER3, PTD, SHOC1, ZIP4, MSH4/5, and HEI10 (Bishop and Zickler, 2004; Chen *et al.*, 2005; Baudat and de Massy, 2007; Chelysheva *et al.*, 2007, 2012; Higgins *et al.*, 2008; Lu *et al.*, 2014; Zickler and Kleckner, 2015; Ren *et al.*, 2019). We assessed class I COs by quantifying HEI10 foci at late pachytene and could observe a significant reduction in *aly1/2* (6.2 ± 0.5) and *tcx5/6* (5.8 ± 0.6) compared to WT (10.0 ± 0.2; $p<0.0001$ for all comparisons against WT; Figure 1.1G,H), indicating DREAM function is required for class I CO formation.

Consistent with their function in meiosis, ALY1 and TCX5 localized on chromosomes from leptotene to the tetrad stage as revealed by using genomic reporter lines that nearly completely restored fertility in the respective double mutants (Figure 1.1I, Supplementary Figure 1.2, and Supplementary Figure 1.3). Consistently, DREAM complex homologs in *C. elegans* and mice localize on chromatin in germline cells, suggesting a conserved role for the DREAM complex in meiotic chromosome regulation (Jiang *et al.*, 2007; Tabuchi *et al.*, 2011; Zhang *et al.*, 2021; Goetsch and Strome, 2022; Oura *et al.*, 2022).

To elucidate the molecular basis of the meiotic defects, we compared the transcriptomes of male meiocytes from *aly1/2*, *tcx5/6*, and WT. Whole-transcriptome sequencing yielded over 72 million reads per sample (three replicates per genotype), with >91% of the reads achieving 99.99% base-calling accuracy (Supplementary Table 1.2). A total of 17,775 genes were identified in WT, 17,840 in *aly1/2*, and 18,110 in *tcx5/6*. Among them, 17,176 genes were coexpressed across all genotypes, while 262 genes in WT, 122 in *aly1/2*, and 415 in *tcx5/6* were uniquely expressed (Figure 1.2A). Differential expression analysis revealed 655 upregulated and 256 downregulated genes in *aly1/2*, and 1,358 upregulated and 685 downregulated genes in *tcx5/6* (Figure 1.2B, C). The greater number and magnitude of gene expression changes in *tcx5/6* correlate with its more severe recombination defect relative to *aly1/2* (Figure 1.1F). Possibly, ALY3 may partially compensate for the loss of *ALY1/2*, as corroborated by the embryonic lethality of *aly1/2/3* triple mutants indicating functional redundancy (Ning *et al.*, 2020).

To identify the biological pathways represented among differentially expressed genes (DEGs), we performed a gene ontology (GO) enrichment analysis on upregulated genes in *aly1/2* and *tcx5/6* compared to WT. Both showed significant enrichment for the cell cycle GO term (Figure 1.2D, E), with 53 genes in *aly1/2* (FDR = 1.50×10^{-15}) and 123 in *tcx5/6* (5.60×10^{-37}), consistent with a conserved role of the DREAM complex in cell cycle regulation (Sadasivam and DeCaprio, 2013; Fischer *et al.*, 2016; Fischer and Müller, 2017). Additionally, GO terms “DNA repair” and “DNA metabolic process” are significantly enriched in *tcx5/6* (62 genes, FDR = 3.30×10^{-17} and 104 genes, FDR = 5.10×10^{-27}, respectively; Figure 1.2D, E).

To uncover the molecular basis of reduced COs in DREAM mutants, we focused on the expression of genes involved in meiotic recombination. Two patterns emerged that may account for the CO defects: (i) upregulation of CO-suppressing factors, such as FANCM, RECQ4A, and RMI1, and (ii) downregulation of the CO-promoting factor MER3 (Table 1.1).

CO-suppressing factor FANCM promotes DSB repair via synthesis-dependent strand annealing (SDSA) (Girard *et al.*, 2014), while RECQ4A/B, forming the RTR complex together with TOP3α and RMI1, resolves double Holliday Junctions (dHJs) into non-crossovers (NCO)s (Higgins *et al.*, 2011; Séguéla-Arnaud *et al.*, 2015b). Mutants in *FANCM*, *RECQ4*, and *RMI1* exhibit elevated CO numbers due to increased class II COs (Crismani *et al.*, 2012; Séguéla-Arnaud *et al.*, 2015b; Serra *et al.*, 2017). Although upregulation of these suppressors has not previously been associated with reduced CO levels, it is tempting to speculate that their increased expression contributes to the CO defects observed in DREAM mutants.

MER3, a conserved eukaryotic helicase, promotes CO formation by catalyzing D-loop migration and dHJ formation. Like other ZMM proteins, *mer3* exhibits decreased levels of COs leading to univalent formation recapitulating the defects seen in *aly1/2* and *tcx5/6* (Mercier *et al.*, 2005).

To address whether the observed transcriptional de-regulation could be a result of the direct regulation by the DREAM complex, we performed CUT&Tag using anthers of GFP-TCX5 transgenic plants, identifying 3470 TCX5-enriched genes.

Among these, 271 were upregulated and 98 downregulated in *tcx5/6*, indicating a significant overlap between TCX5-enriched targets and differentially expressed genes in the mutant (Figure 1.2F).

TCX5 CUT&Tag reads were predominantly enriched around transcription start sites (TSS) within promoter regions (Figure 1.2G, H and Supplementary Figure 1.4A). HOMER motif enrichment analysis of these regions identified several overrepresented motifs, with the most enriched being the “GC rich motif” (*p*=1e-858), followed by an “E-box-like” motif (*p*=1e-246, Figure 1.2I). We also detected motifs recognized by tesmin/TSO1-like CxC domain-containing (TCX) proteins (*p*=1e-36) and canonical DREAM-associated transcription factors, including MYB3Rs (*p*=1e-25) and E2Fs (*p*=1e-21).

GO analysis of genes both TCX5-enriched and upregulated in *tcx5/6* revealed significant enrichment for categories related to DNA repair and cell cycle (Figure 1.2J). Reflecting shared meiotic defects of *aly1/2* and *tcx5/6*, 141 of the 655 genes upregulated in *aly1/2* were direct TCX5 targets, with 119 also upregulated in *tcx5/6* (Supplementary Figure 1.4B, C). GO enrichment of these 119 genes similarly highlighted DNA repair and cell cycle categories, supporting a shared regulatory role for ALY1/2 and TCX5/6 during meiosis (Supplementary Figure 1.4D).

Notably, we found no evidence of TCX5 binding at the promoters of *RECQ4A* or *FANCM*, indicating their upregulation is unlikely to be directly mediated by TCX5. In contrast, TCX5 was detected at the promoter of *RMI1* (Supplementary Table 1.3). Although *RMI1* transcript levels were elevated in *tcx5/6* meiocytes, it remained unchanged in *aly1/2* (Table 1.1), and no upregulation was observed for *TOP3α*, the third component of the RTR complex (Hartung *et al.*, 2008; Séguéla-Arnaud *et al.*, 2015b). These findings suggest that increased RMI1 expression alone is unlikely to account for the reduced COs observed in plants with impaired DREAM complex activity.

To test whether *MER3* downregulation contributes to reduced recombination in DREAM complex mutants, we first confirmed strong TCX5 enrichment at the *MER3* promoter, suggesting direct transcriptional regulation (Figure 1.3A). To bypass

DREAM-mediated repression, we generated a construct expressing genomic MER3 fused to mEGFP under the meiosis-specific *DMC1* promoter. This construct fully restored fertility in homozygous *mer3* mutants (Figure 1.3B, D, and Supplementary Figure 1.5A), validating its functionality. MER3-GFP localization was confined to male meiocytes, with no detectable expression in surrounding anther tissues (Figure 1.3C). We next introduced this construct into *tcx5*$^{-/-}$ *tcx6*$^{+/-}$ and *aly1*$^{-/-}$ *aly2*$^{+/-}$ mutants to assess whether MER3 overexpression could restore CO formation defects.

Interestingly, in *aly1/2* and *tcx5/6* anthers, MER3-GFP was not only detected in meiocytes but was also found in the surrounding tapetal cells (Figure 1.3C, Supplementary Figure 1.5B). This suggests that the DREAM complex may also restrict the appropriate spatial activity of the *DMC1* promoter and possibly also other meiotic gene expression to meiocytes (Figure 1.3C, marked by yellow arrowheads).

Strikingly, *MER3-GFP* expression in *aly1/2* increased the proportion of meiocytes with five bivalents from 40% to 55%, while cells with two, one or no bivalents were longer observed (Figure 1.3D). In *tcx5/6*, *MER3* expression reduced the fraction of cells with no bivalents from 14% to 1%, and those with one bivalent from 9% to 4% (Figure 1.3D). Importantly, *MER3* overexpression significantly increased the average bivalent numbers from 3.8 to 4.8 in *aly1/2* ($p< 0.0001$) and from 3.3 to 4.1 in *tcx5/6* ($p<0.008$, Figure 1.3B;e,g, D). However, it also elevated the incidence of chromosome entanglements, potentially contributing to the chromosome fragmentation seen in anaphase I (Figure 1.3B l, n). These findings identify *MER3* as a major target of the DREAM complex. However, the limited CO restoration by *MER3* overexpression, particularly in *tcx5/6*, suggests that additional misregulated meiotic genes contribute to this phenotype.

Interestingly, the DREAM complex functions as both a transcriptional repressor and activator depending on the specific developmental context. To further explore this dual role, we compared TCX5 binding profiles from seedlings (reanalyzed TCX5-FLAG ChIP-Seq data from Ning *et al.*, 2020) and anthers (CUT&Tag), identifying 1,011 shared target genes, with 2,459 and 1,732 genes uniquely bound in anthers and seedlings, respectively (Supplementary Figure 1.6A). Among genes repressed in

tcx5/6 meiocytes, 126 were common TCX5 targets in both tissues and cell cycle-related GO terms were enriched, suggesting a shared repressive role of the DREAM complex (Supplementary Figure 1.6B,C). In contrast, TCX5-activated targets showed no overlap between tissues, indicating that its activator role is specific to anthers within this comparison (Supplementary Figure 1.6D).

Next, we examined 132 genes with established meiotic functions to assess their transcriptional regulation and TCX5 binding in seedlings and meiocytes. Consistent with previous findings (Ning *et al.*, 2020), 85 of these genes were both bound by TCX5 and transcriptionally repressed by the DREAM complex (Figure 1.4A). These include genes involved in class I and II CO formation, DSB formation and repair, and synaptonemal complex assembly (Supplementary Table 1.3), reflecting the repressive function of dREAM in *C.elegans* somatic cells (Bujarrabal-Dueso *et al.*, 2023).

Our analysis in reproductive tissues revealed four distinct regulatory patterns among the 132 meiotic genes (Fig. 4B): (I) 63 genes not bound by TCX5 at their promoters, including most ZMM genes, suggesting a transcriptional release from DREAM-mediated repression in anthers; (II) 32 genes bound by TCX5 in anthers but not differentially expressed in meiocytes of DREAM complex mutants, such as those involved in axis and synaptonemal complex formation, indicating a potential regulation in anthers but not in meiocytes; (III) 35 genes repressed in meiocytes by TCX5 binding, primarily genes associated with DNA repair; and (IV) 2 genes both bound and transcriptionally activated by TCX5, *MER3* and *SDS*.

In anthers, TCX5 binds the promoters of several key meiotic DSB repair genes, where its association correlates with their transcriptional repression (Supplementary Table 1.3), mirroring its role in seedlings and supporting a conserved repressive function of DREAM complex across reproductive and somatic tissues. These genes fall into the third category described above and include *DMC1, RAD51, RMI1, XRCC3, FAS1, MEI1,* and *RPA* (Grelon *et al.*, 2003; Bleuyard and White, 2004; Kirik *et al.*, 2006; Hinch *et al.*, 2020). Their misregulation may contribute to the chromosome entanglement and fragmentation observed in *aly1/2* and *tcx5/6* meiocytes, although

the direct consequences of their overexpression on meiotic progression remains unclear.

While the DREAM complex represses DNA repair genes in both tissues, its activator role appears to be specific to meiocytes. Supporting this, we observed no significant overlap between TCX5-bound genes and downregulated genes in seedlings (Supplementary Figure 1.6E), whereas such an overlap was evident in *tcx5/6* male meiocytes and TCX5-bound genes in anthers (Figure 1.2F).

In addition to *MER3*, the DREAM complex likely also activates the meiotic cyclin *SOLO DANCERS* (*SDS*) (Azumi *et al.*, 2002), a plant-specific cyclin which is essential for chromosome pairing, synapsis, and recombination (Supplementary Figure 1.7). Although initially described as a repressor, the DRM in *C. elegans,* the dREAM and testis-specific DREAM-like tMAC complex in *D. melanogaster* have been shown to act as an activator in germ cells (Jiang and White-Cooper, 2003; Beall *et al.*, 2007; Georlette *et al.*, 2007; Tabuchi *et al.*, 2011, 2013; Goetsch and Strome, 2022). Thus, dual repressor-activator roles may represent a conserved feature of DREAM paralogs.

DREAM complex homologs play conserved roles in reproductive development across species. In *Drosophila*, the testis-specific tMAC complex activates G2/meiosis transition genes, while the canonical dREAM complex represses inappropriate gene expression in spermatocytes (Laktionov *et al.*, 2018). The LIN54 homolog Mip120, orthologous to *Arabidopsis TCX5/6*, is essential for meiosis in both sexes, and its loss results in meiotic arrest, although it remains unclear whether recombination defects are involved (Cheng *et al.*, 2017). In *C. elegans*, germline LIN-54 activates a distinct set of reproduction- and growth-associated genes and mutants are sterile (Tabuchi *et al.*, 2011, 2013). In mice, the testis-specific LIN54 paralog TESMIN is required for spermatogenesis, with Tesmin-deficient males arresting at pachytene but retaining homologous recombination (Oji *et al.*, 2020; Zhang *et al.*, 2021). Thus, the role of DREAM in germline regulation is broadly conserved, though its specific functions may vary by lineage.

Together, these cross-species findings reinforce the idea that DREAM complex homologs are critical regulators of meiosis and reproductive development. Our study

establishes a direct function for the *Arabidopsis* DREAM complex in transcriptional control of meiotic recombination, providing a blueprint for related studies in other organisms.

Methods

Plant materials

The *Arabidopsis thaliana* accession Columbia (Col-0) was used as a wild-type reference throughout this study. All mutants and transgenic lines used in this study were in Col-0 background. The T-DNA insertion lines *tcx5-1* (SALK_047165), *tcx6-1* (GK-453H07), *aly1-1* (SALK_073108), *aly2-2* (SALK_118765C), *aly3-4* (SALK_125138C), *lin37a-2* (SALK_057175), *lin37b-3* (SALK_103139C), *lin52b-1* (GK_854A11), and *mer3-2* (SALK_091560) were isolated from GABI-KAT, SAIL, and SALK T-DNA collections and described previously (Chen *et al.*, 2005; Lang *et al.*, 2021). The *lin52a-c1* mutant is generated via CRISPR/Cas9 and described in our previous study (Lang *et al.*, 2021). Transgenic lines harboring PRO_{RPS5A}*:TagRFP:TUA5* (Komaki and Schnittger, 2017) and PRO_{ASY3}*:ASY3:RFP* (Yang *et al.*, 2019) reporter constructs were crossed with mEGFP-TCX5, mEGFP-TCX6, mEGFP-ALY1 transgenic reporter lines generated in this study. All plants were grown in growth chambers with a 16 h light/21°C and 8 h/18°C dark cycle at 60% humidity.

Plasmid construction and plant transformation

To generate PRO_{TCX5}*:mEGFP:TCX5* and PRO_{TCX6}*:mEGFP:TCX6* reporter constructs, genomic sequences of *TCX5* (5557 bp) and *TCX6* (5158 bp) were amplified by PCR and subsequently integrated into *pDONR221* vector by Gateway BP reaction. A *Sma*I site was then inserted right after the start codon by PCR. Resulting constructs were linearized by *Sma*I restriction and ligated with *mEGFP* fragments. To generate the PRO_{ALY1}*:ALY1-mEGFP* construct, the genomic sequence of *ALY1* (9,252 bp) and the mEGFP coding sequence were amplified by PCR and inserted into the *pENTR* vector via SLiCE reaction. The *mEGFP* sequence was positioned immediately upstream of the *ALY1* stop codon to produce a C-terminal fusion.

To generate PRO_{DMC1}*:MER3:mEGFP:*TER_{REC8} genomic sequences of MER3 (6259 bp) and mEGFP were amplified by PCR and incorporated into *SmaI* restriction linearized *pENTR* vector harboring PRO_{DMC1}*:SmaI:*TER_{REC8} by SLICE reaction. These

constructs were then transferred into the binary expression vector pGWB501 (Nakagawa *et al.*, 2007) by Gateway LR reaction. *Arabidopsis thaliana* transgenic lines were generated by *Agrobacterium*-mediated transformation (Zhang *et al.*, 2006).

Pollen and seed viability assessment

Pollen viability was assessed as previously described (Peterson *et al.*, 2010). 3 open flowers per plant were dipped into 12 μL of Peterson staining solution (10% ethanol, 0.001% malachite green, 25% glycerol, 0.005% acid fuchsin, 0.0005% orange G, 4% acetic acid). Slides were covered with a cover slip and incubated on a pre-heated hotplate at 80°C for 5 min and screened using a light microscope (Axioskop, Carl Zeiss GmbH, Oberkochen, Germany) and 20× objective. 600 pollen grains of 5 different plants were counted per line. To assess seed viability, seeds were evaluated from 5 siliques of at least 5 different plants per line.

Cell spreads

Cell spreads of transgenic lines were prepared as previously described (Ross *et al.*, 1996). Briefly, fresh flower buds were fixed in ethanol/acetic acid (3:1) for 48 h at 4 °C and washed with 75% ethanol three times and stored in 70% ethanol at 4 °C. For spreading, flower buds between 0.3 and 0.5 mm in size were digested in an enzyme solution (10 mM citrate buffer containing 1.5% cellulose, 1.5% pectolyase, and 1.5% cytohelicase) for 3 h at 37 °C. Three digested flower buds were transferred onto a glass slide and mashed with a bent needle. Cell suspension was spread on an adhesive slide on a 46 °C hot plate after adding 10 μL of 45% acetic acid. The slide was then rinsed with ice-cold ethanol/acetic acid (3:1) solution and mounted in 15 μL of VECTASHIELD medium with DAPI (Vector Laboratories). Slides were observed using an Axiophot microscope (Zeiss) with 63× oil-immersion objective.

Immunostaining

Immunostaining was performed as previously described (Sims *et al.,* 2021). Briefly, flower buds were dissected using needles, and anthers were transferred to a droplet of artificial pond water (0.5 mM NaCl, 0.4 mM $CaCl_2$, 0.2 mM $NaHCO_3$, 0.05 mM KCl, in deionized water) on a polylysine-coated slide. Anthers were gently squeezed to

release meiocytes, which remained grouped in syncytia. The isolated meiocytes were collected into a 1.5 mL tube on ice and subsequently digested in 15 μL of digestion solution (1% cytohelicase, 1.5% sucrose, and 1% polyvinylpyrrolidone) in the dark for 30 min. Following digestion, meiocytes were transferred to a clean,charged microscope slide. Next, 20 μL of 1% Lipsol was added, and the sample was spread by tilting the slide. After a 4-min incubation at room temperature, 24 μL of 4% formaldehyde was added, and the slide was left to air dry. The slides were washed twice with 2× SCC (0.3 M NaCl and 30 mM $Na_3C_6H_5O_7$) for 5 min each. Primary antibody mix was then added, and the slide was covered by a piece of parafilm. Slides were incubated overnight at 4 °C in a humid chamber Slides were washed twice with 2× SCC for 5 min, followed by addition of the secondary antibody mix. Slides were again covered with parafilm, and incubated for 1 h at 37 °C in a humid chamber. Finally, slides were washed twice with 2× SCC for 5 min in the dark. 15 μL of VECTASHIELD medium with DAPI was added to the slide and covered with a glass cover slip and sealed using nail polish. Following dilutions were used for the primary and secondary antibodies: anti-ASY1 1:10,000 (Sims *et al.,* 2021), anti-RAD51 1:300 (Kurzbauer *et al.*, 2012), anti-ZYP1 1:500 (Higgins, Vignard, *et al.*, 2008), anti-HEI10 1:300, anti-guinea pig Alexa 488 1:400 (Abcam #ab150185), anti-rabbit Alexa 568 1:400 (Abcam #ab175471), anti-rat Alexa 647 (Abcam #ab150159)

Microscopy

To detect protein localization, in reporter lines, young anthers o were dissected from floral buds in a drop of artificial pond water (APW) and imaged directly using an upright Zeiss LSM900 confocal microscope equipped with 60× water-immersion objective. Meiotic stages were determined based on chromosome morphology, cell shape, or microtubule shape in the presence of *PRO$_{RPS5A}$:TagRFP:TUA5* marker. GFP was excited at 488 nm and detected at 495–560 nm and TagRFP was excited at 561 nm and detected at 570–650 nm.

For imaging immunohistochemical stained samples, high-resolution imaging was performed using a Zeiss LSM 880 confocal microscope equipped with an Airyscan detector (Zeiss, Oberkochen, Germany), using a 63×/1.4 NA oil-immersion objective.

Airyscan mode was used to improve resolution and signal-to-noise ratio. Z-stacks were acquired at optimal intervals for 3D reconstruction and processed using the Zeiss Zen Black software (ZEN 2.3 SP1).

Male meiocyte isolation and RNA extraction

Anthers at developmental stage 6–11 anthers, covering all meiotic stages, were dissected and collected in artificial pond water supplemented with 1 U/μl RNasin Ribonuclease Inhibitor (Promega, N2511). Anthers were gently squashed to release meiotic columns, and ~300 columns per sample were transferred into ZR BashingBead Lysis Tubes (Zymo Research, S6003-50) containing lysis buffer from the RNAqueous™-Micro Total RNA Isolation Kit (Thermo Fisher, AM1931), then immediately flash-frozen in liquid nitrogen. Dissections and collections were performed at 4 °C from 16 plants per genotype, across three biological replicates. Samples were homogenized using a mechanical shaker, and total RNA ´was extracted according to the manufacturer's protocol. RNA quality was assessed using an Agilent 2100 Bioanalyzer with the NanoChip Kit, and all samples showed high integrity (RIN > 8.0).

Transcriptome sequencing and data analysis

RNA sequencing libraries were prepared by Novogene and sequenced on an Illumina HiSeq X Ten platform using 150 bp paired-end reads (PE150). Raw read quality was assessed using *FastQC*. The reference genome index was built with *HISAT2* (v2.0.5), and paired-end reads were aligned to the genome using the same version. Gene-level read counts were obtained using *featureCounts* (v1.5.0-p3). Transcript assembly and quantification were performed with *StringTie* (v1.3.3b), and gene expression levels were reported as fragments per kilobase of exon per million fragments mapped (FPKM). Next, we used DESeq2 to identify differentially expressed genes (DEGs) with the thresholds: adjusted *p*-value < 0.05 and |log2FoldChange| > 0.5. Gene Ontology (GO) enrichment analysis of DEGs was performed using agriGO v2.0 (https://systemsbiology.cau.edu.cn/agriGOv2/). GO terms with an adjusted $p<0.05$ were considered significantly enriched.

CUT&Tag sample preparation from Arabidopsis anthers

Anthers at stage 6–11 from the *PRO$_{TCX5}$:mEGFP:TCX5 tcx5* transgenic line were dissected to capture all stages of meiosis and collected in Nuclei Extraction Buffer (0.25 M sucrose, 10 mM Tris-HCl pH 8.0, 10 mM $MgCl_2$, 1% Triton X-100) supplemented with protease inhibitor cocktail (cOmplete™ ULTRA Tablets, Roche, 05892791001). Anthers were homogenized using a glass Dounce tissue grinder and incubated on a rotating wheel at 4 °C for 10 min. The homogenate was filtered through 50 μm filters and nuclei were pelleted by centrifugation at 1,000 × g for 10 min at 4 °C. Nuclei were washed three times with the same extraction buffer. The final pellet was resuspended in sucrose buffer (0.25 M sucrose, 10 mM Tris-HCl pH 8.0, 10 mM $MgCl_2$) containing protease inhibitor cocktail (cOmplete™ ULTRA Tablets) and 10% DMSO. Extracted nuclei were cryopreserved at –80 °C in a controlled-rate freezing container. CUT&Tag was performed using the CUT&Tag-IT® Assay Kit, Anti-Rabbit (Active Motif, 53160), with an anti-GFP antibody (ThermoFisher, A-11122) used to target GFP-tagged TCX5. Library preparation was carried out according to the manufacturer's protocol.

CUT&TAG data analysis

Paired-end reads of CUT&TAG raw data were trimmed by using Fastp (v0.23.2). Using Bowtie2 (v2.5.4), the cleaned reads were aligned on the Arabidopsis reference genome assembly TAIR10. Duplicated reads were removed and reads were filtered to keep only high quality alignments (MAPQ score > 30) using SAMtools (v1.9) Afterwards, peaks were called using MACS3 (https://github.com/macs3-project/MACS) with the threshold *q*-value <0.05. ChIPseeker from the R package was used to investigate genomic distribution of CUT&TAG peaks. To visualize the signals of CUT&TAG, RPGC normalized bigWig files were generated using the bamCoverage option from Deeptools (v3.5.6). Motif enrichment analysis of TCX5 binding sites was conducted using findMotifsGenome.pl from HOMER, identifying motifs enriched with p-value < 0.05 , which was determined by binomial test.

Image processing and HEI10 and RAD51 foci quantification

For image analysis of RAD51 and HEI10 immunostainings, maximum intensity projections were generated using the Z Project function in Fiji/ImageJ (Version 2.14.0/1.54f). RAD51and HEI10 foci were manually counted on merged channels. Only RAD51 and HEI10 foci colocalizing with the chromatin (DAPI) were included in the analysis. To ensure consistency across samples, all images were adjusted with identical brightness and contrast settings

Statistical analysis

All statistical analyses (as indicated in the figure legends) were performed using GraphPad Prism software (GraphPad Software Version 10.4.1). Error bars indicate standard deviations.

Data availability

The RNA-seq and CUT&TAG data have been deposited in GEO under GSE302287 and GSE302286 respectively.

Figures & table

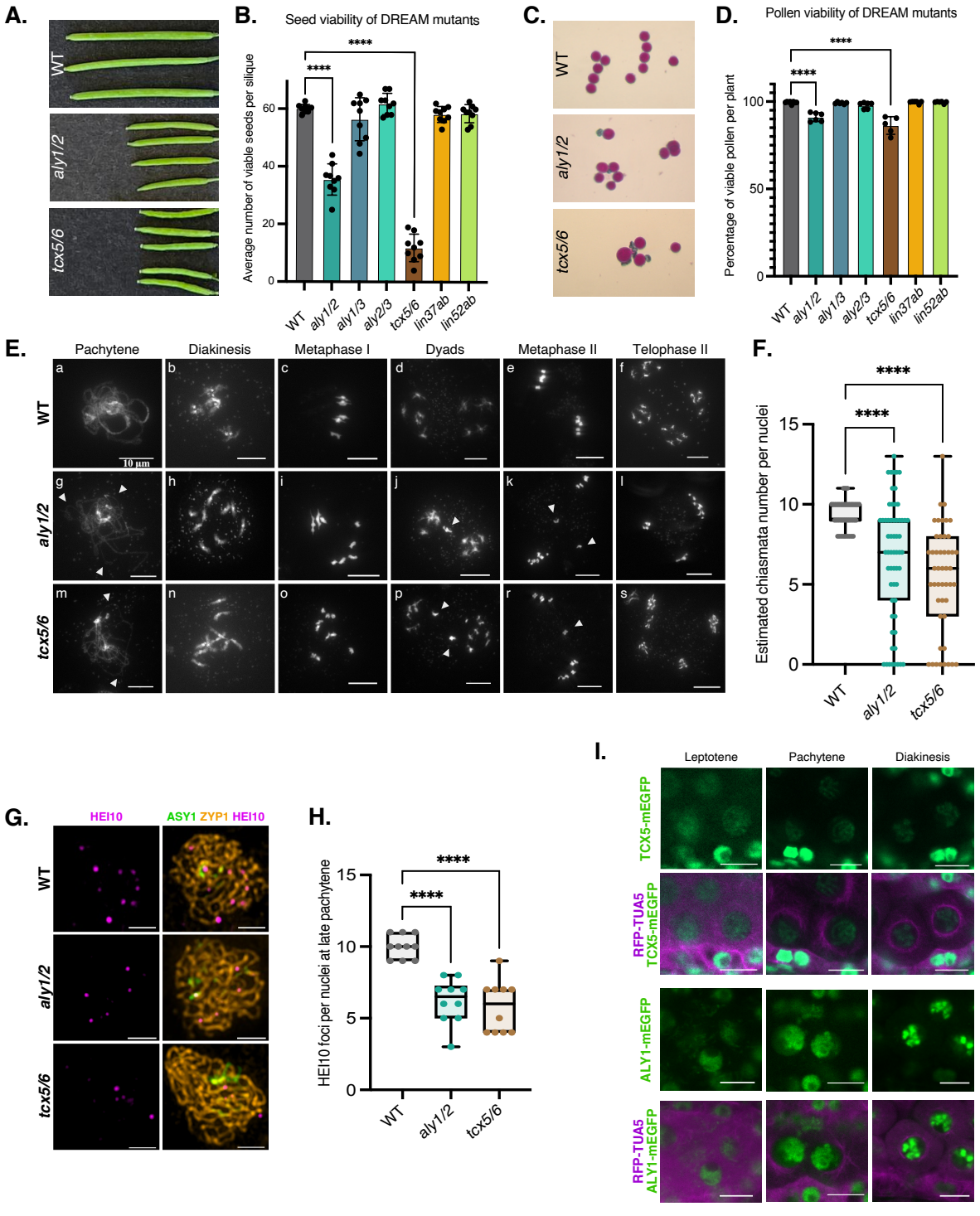


Figure 1.1. DREAM complex plays an important role in meiosis.

(A) The DREAM mutants *aly1/2* and *tcx5/6* show reduced length of siliques. **(B)** Seed viability assessment of mutants of the core DREAM components (n = 10 for all, p <0.0001). **(C)** Pollen size variation and death observed in *aly1/2* and *tcx5/6*. **(D)** Pollen viability assessment of core mutants of the core DREAM components (n = 10 for all, p <0.0001). **(E)** Meiosis progression in WT (a-f), *aly1/2* (g-

l) and *tcx5/6* (m-s) double mutants was observed via acid spreads. DREAM mutants have defects in synapsis, crossover formation, chromosome segregation. Representative pictures of pachytene (a,g,m), diakinesis (b,h,n), metaphase I (c,i,o), dyads (d,j,p), metaphase II (e,k,r), and telophase II (f,l,s) shown for each genotype. White arrowheads indicate pairing defects at pachytene (g,m) and lagging chromosomes at dyad stage (j,p) and metaphase II (k,r). Scale bars, 10 μm. **(F)** Estimated chiasmata numbers were calculated based on at metaphase I cells (n = 40, 47 and 59 for WT, *aly1/2* and *tcx5/6* respectively; p <0.0001) **(G)** HEI10 foci at late pachytene in WT, *aly1/2* and *tcx5/6* mutants was observed via immunohistochemical staining of HEI10 (magenta), ASY1 (green) and ZYP1 (orange). Scale bars, 2 μm. **(H)** The DREAM mutants exhibit a reduced number of HEI10 foci at late pachytene compared to WT (n = 10 for all; p <0.0001). ONE-WAY ANOVA, Dunnett's multiple comparison test used for B, D, F, and H. **(I)** ALY1 and TCX5 (both green) expressed in meiocytes and localized to chromosomes, clearly visible in pachytene and diakinesis. RFP-TUA5 (magenta) serves as a meiotic stage marker. Scale bars, 10 μm.

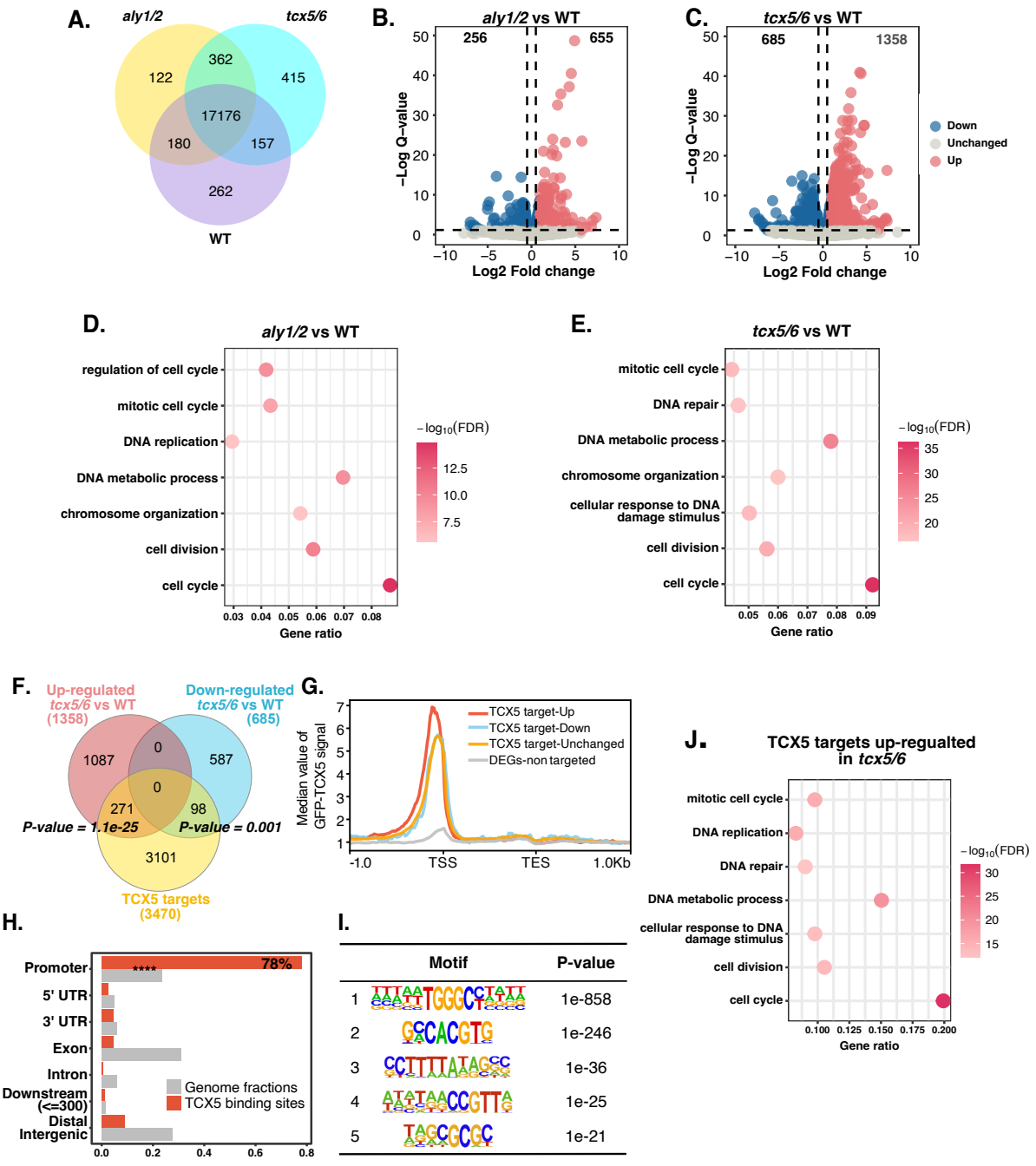


Figure 1.2. Transcriptome analysis of DREAM mutants and CUT&Tag with GFP-TCX5 reveals roles in cell cycle regulation and DNA repair.

(A) Venn diagram showing the number of genes uniquely or co-expressed in WT, *aly1/2*, and *tcx5/6* male meiocytes. **(B, C)** Volcano plots depicting differentially expressed genes in *aly1/2* **(B)** and *tcx5/6* **(C)** male meiocytes compared to WT. **(D, E)** GO enrichment analysis of upregulated genes in *aly1/2* **(D)** and *tcx5/6* **(E)**, highlighting enrichment in biological pathways related to cell cycle and DNA repair. **(F)** Venn diagram showing the overlap between upregulated genes (pink), downregulated genes (blue) in *tcx5/6* male meiocytes, and TCX5 targets (yellow) identified by CUT&Tag using GFP-TCX5 in anthers (Hypergeometric test: p=1.1e−25 and p=0.0001). **(G)** Meta-plot showing median GFP-TCX5 CUT&Tag

signal across gene bodies. The pink line represents genes upregulated in *tcx5/6*, blue for downregulated genes, yellow for non-differentially expressed genes, and grey for non-targeted DEGs. TSS: Transcription Start Site; TES: Transcription End Site. **(H)** Bar graph indicating that 78% of TCX5 targets are bound at their promoter regions (Hypergeometric test, **** $p<0.0001$). **(I)** HOMER known motif enrichment analysis of TCX5 binding sites showing significant binding motifs and their *p*-values. **(J)** GO enrichment analysis of TCX5 targets that are upregulated in *tcx5/6* male meiocytes.

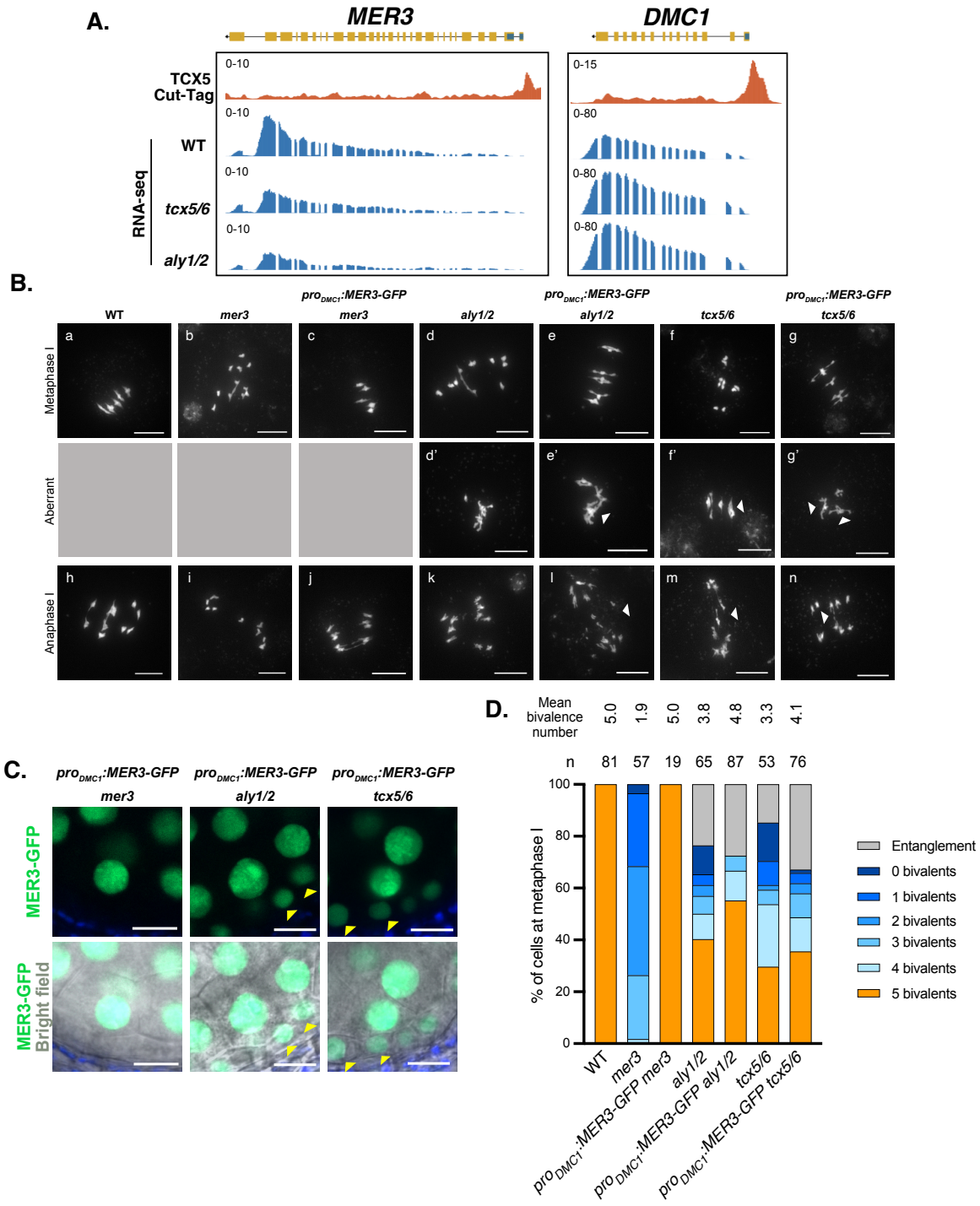


Figure 1.3. The DREAM complex activates *MER3* transcription. Overexpression of *MER3* in *aly1/2* and *tcx5/6* partially recovers CO loss.

(A) Genome browser snapshot of *MER3* and *DMC1* transcript levels derived from RNA-seq in WT, *tcx5/6*, and *aly1/2* male meiocytes (blue tracks), aligned with CUT&Tag signal for GFP-TCX5 in anthers (dark orange track). **(B)** Metaphase I and anaphase I chromosomes displayed for each genotype; WT (a,h), *mer3* (b,i), *PRO$_{DMC1}$:MER3:GFP mer3* (c,c'j), *aly1/2* (d,d'k), *PRO$_{DMC1}$:MER3:GFP aly1/2* (e,e',l), *tcx5/6* (f,f',m), *PRO$_{DMC1}$:MER3:GFP tcx5/6* (g,n). White arrowheads mark chromosome entanglement

at aberrant metaphase I (d´,e´,f´,g´) and chromosome fragmentation at anaphase I (l,m,n). Scale bars, 10 μm. **(C)** MER3-GFP localization at anthers of *PRO$_{DMC1}$:MER3:GFP mer3*, *PRO$_{DMC1}$:MER3:GFP aly1/2*, and *PRO$_{DMC1}$:MER3:GFP tcx5/6*. First row shows the MER3-GFP signal in green and autofluorescence in dark blue. Second row shows a merged image with a bright field to determine cell shape. Yellow arrowheads indicate MER3-GFP signal at tapetal cells. Scale bars, 10 μm. **(D)** Frequency of observed bivalence numbers and chromosome entanglement at metaphase I. Above the chart, "n" represents the number of metaphase I cells observed and average bivalence number for each transgenic line.

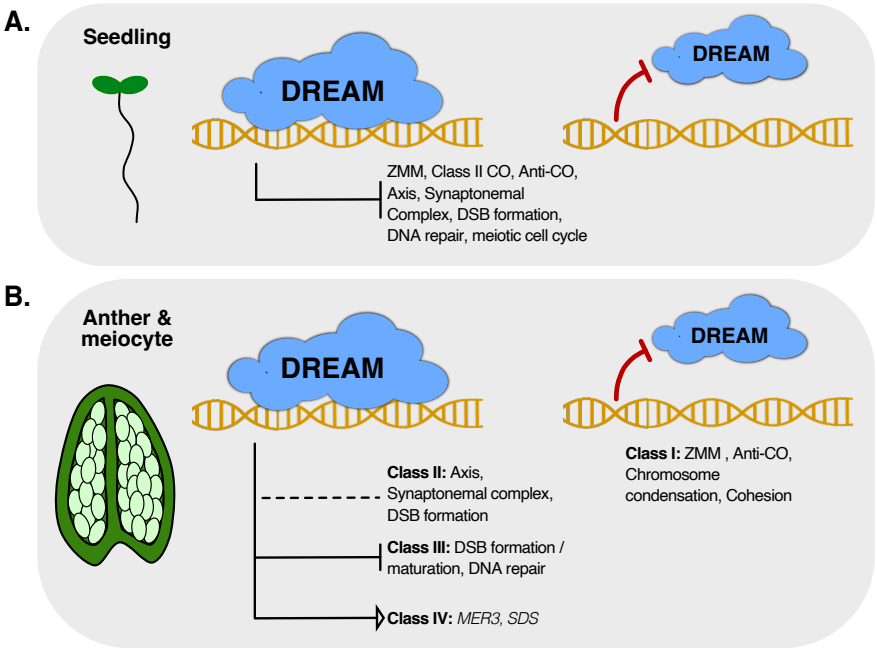


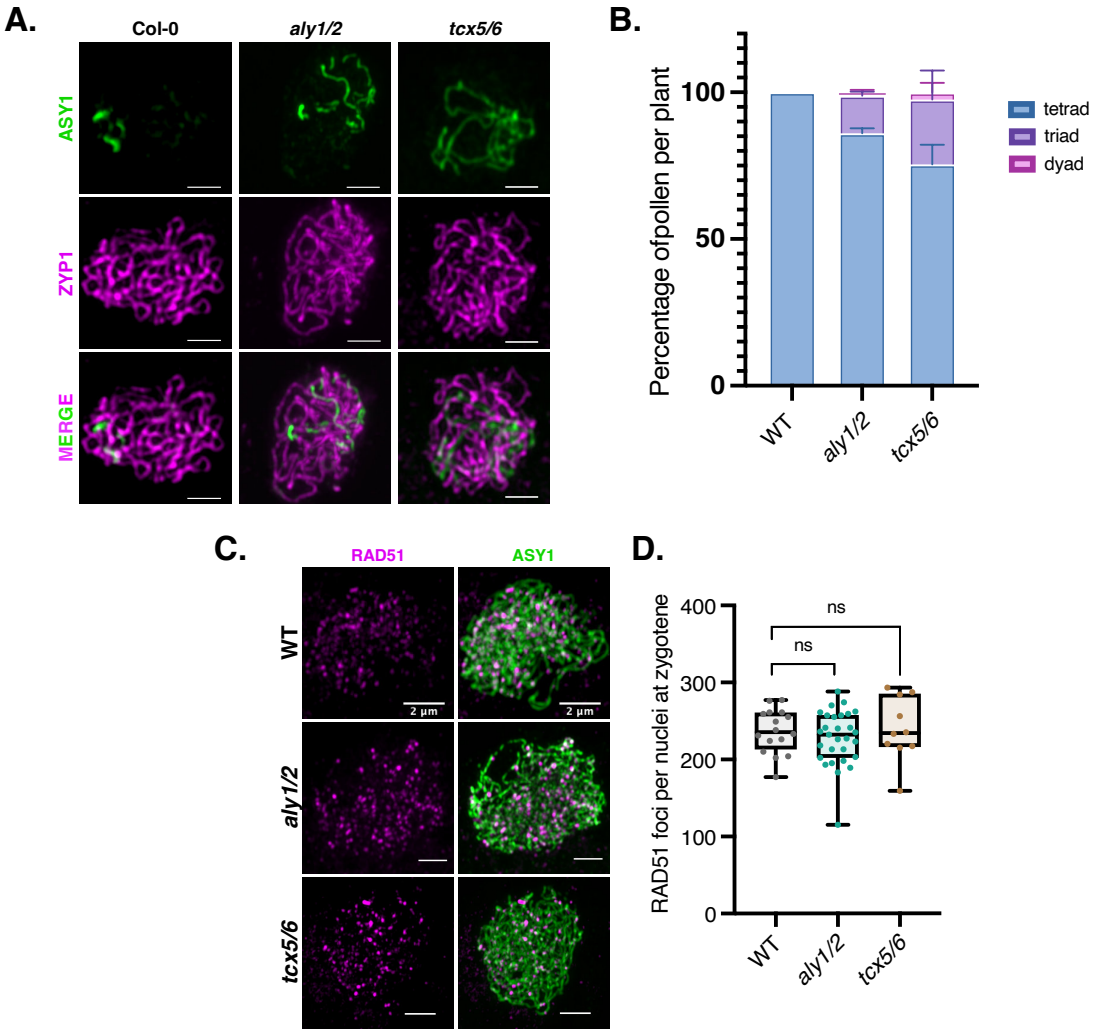
Figure 1.4. A brief summary of DREAM complex regulating meiotic genes (A) in seedlings and (B) in anthers/meiocytes.

Table 1.1. Differential expression of genes in *aly1/2* and *tcx5/6* meiocytes, involved in recombination pathways.

For each gene log_2(Fold-change) values and adjusted *p*-values (padj) are listed, along with annotated gene functions.

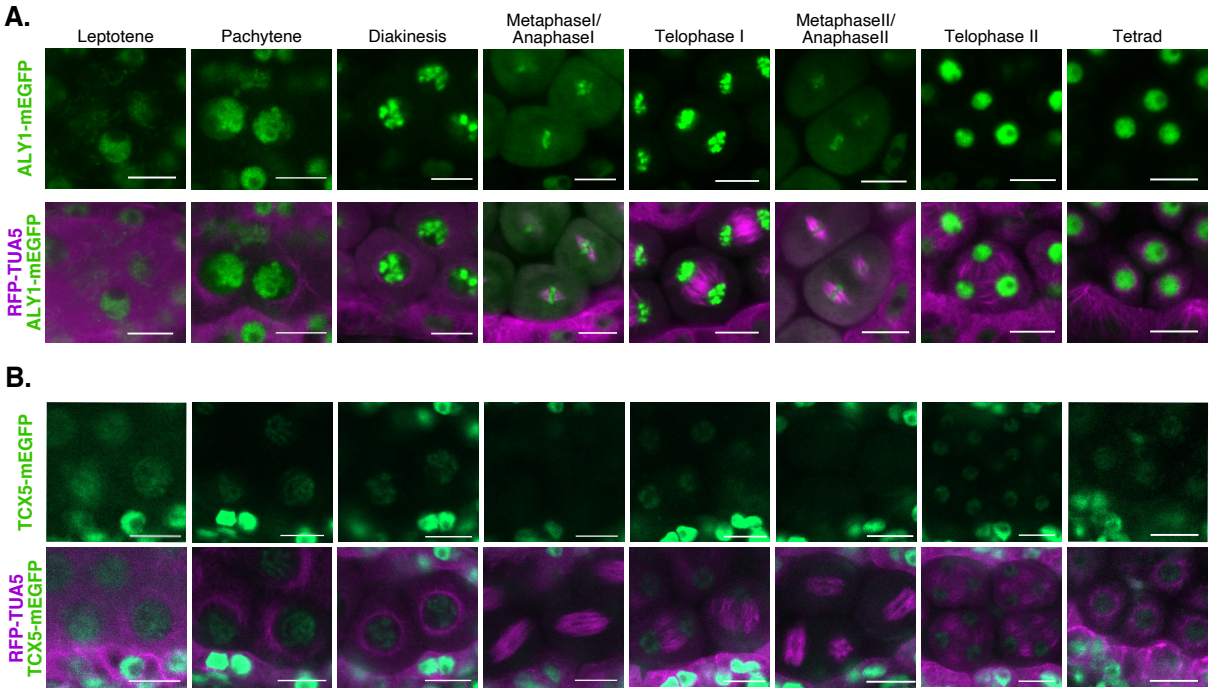
	***aly1/2* vs WT**		***tcx5/6* vs WT**		
	log_2(Fold-change)	**padj**	**log_2(Fold-change)**	**padj**	**Function**
MER3	-0.8870	0.0454	-0.9107	0.0029	ZMM protein
FANCM	0.6340	0.0788	1.2987	9.2730E-08	Anti-CO factor
RECQ4A	0.6771	0.0091	0.9473	3.3297E-06	Anti-CO factor
RMI1	unchanged		0.8594	0.0041	Anti-CO factor
DMC1	0.8584	0.0012	0.6823	0.0152	DSB processing

Suplemental data



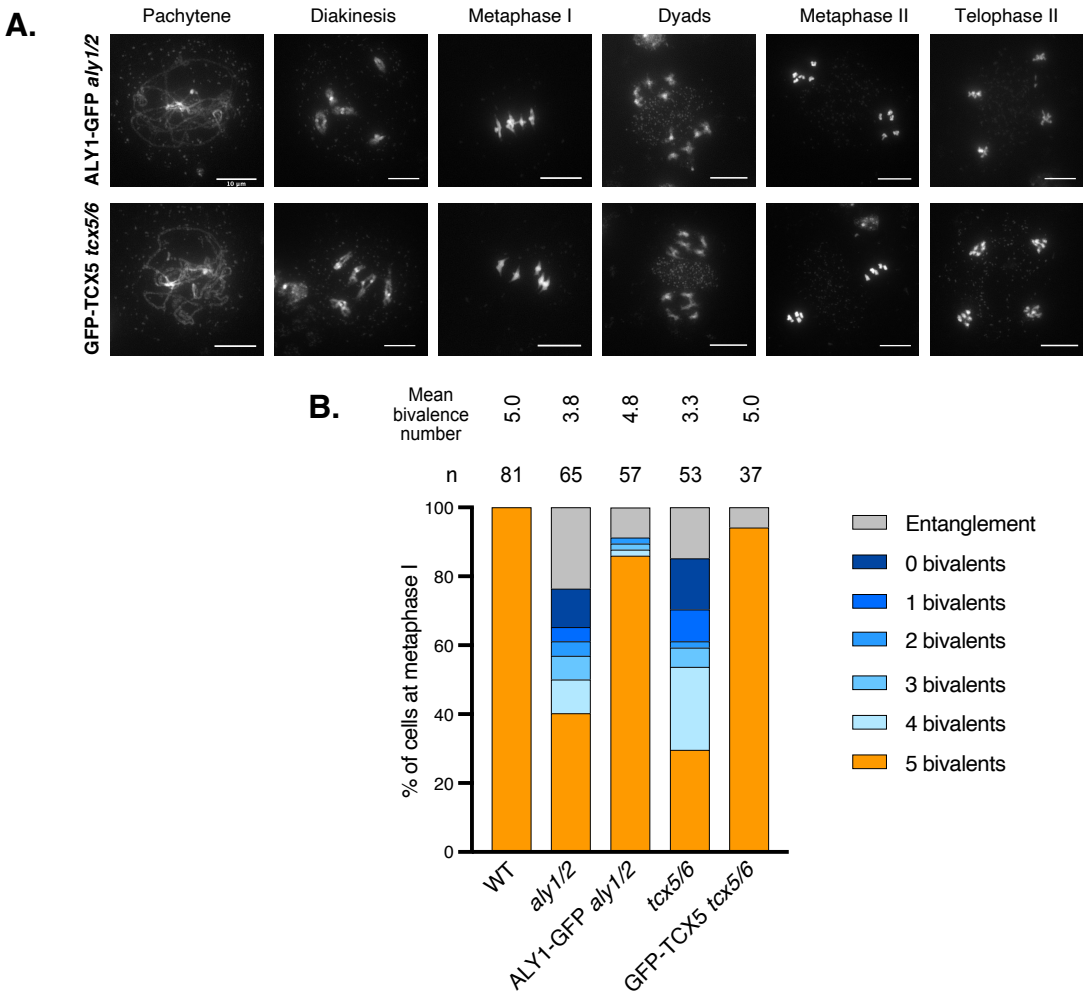
Supplementary Figure 1.1. DREAM mutants exhibit incomplete synapsis and form dyads and triads; however DSB formation occurs at WT level.

(A) Synapsis is incomplete in *aly1/2* and *tcx5/6* mutants. Immunostaining of ASY1 (green) and ZYP1 (magenta) at late pachytene in wild type (WT), *aly1/2*, and *tcx5/6* reveals that ASY1 is largely removed from chromosomes, except at rDNA regions, and ZYP1 fully decorates the chromosome axes in WT. In contrast, both ASY1 removal and ZYP1 loading are incomplete in *aly1/2* and *tcx5/6*. **(B)** At the end of meiosis, DREAM mutants more frequently produce triads and dyads instead of normal tetrads, compared to WT. **(C, D)** DSB formation is not impaired in *aly1/2* and *tcx5/6*. **(C)** Immunostaining of RAD51 (magenta, left panel) and ASY1 (green, merged with RAD51 at right panel) at zygotene in WT, *aly1/2*, and *tcx5/6*. **(D)** Quantification of RAD51 foci shows no significant difference between WT, *aly1/2*, and *tcx5/6*. Statistical analysis was performed using one-way ANOVA followed by Dunnett's multiple comparison test. Scale bars, 2 µm.



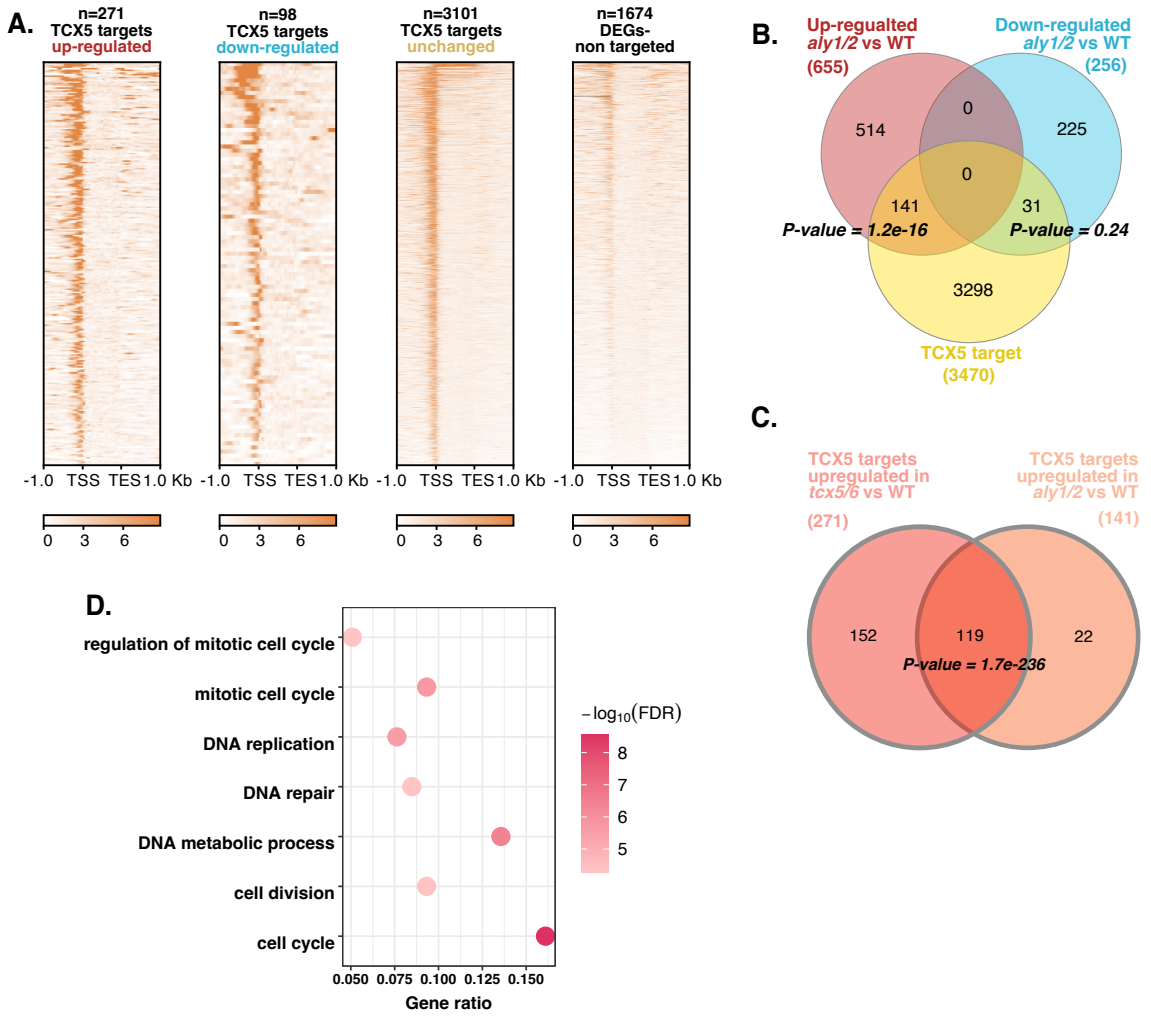
Supplementary Figure 1.2. ALY1 and TCX5 are present throughout meiosis and localized to chromosomes.

(A–B) Confocal images showing the localization patterns of GFP-tagged ALY1 (green) **(A)**, TCX5 (green) **(B)**, alongside RFP-tagged TUA5 (magenta), which serves as a meiotic stage marker. Scale bars, 10 μm.



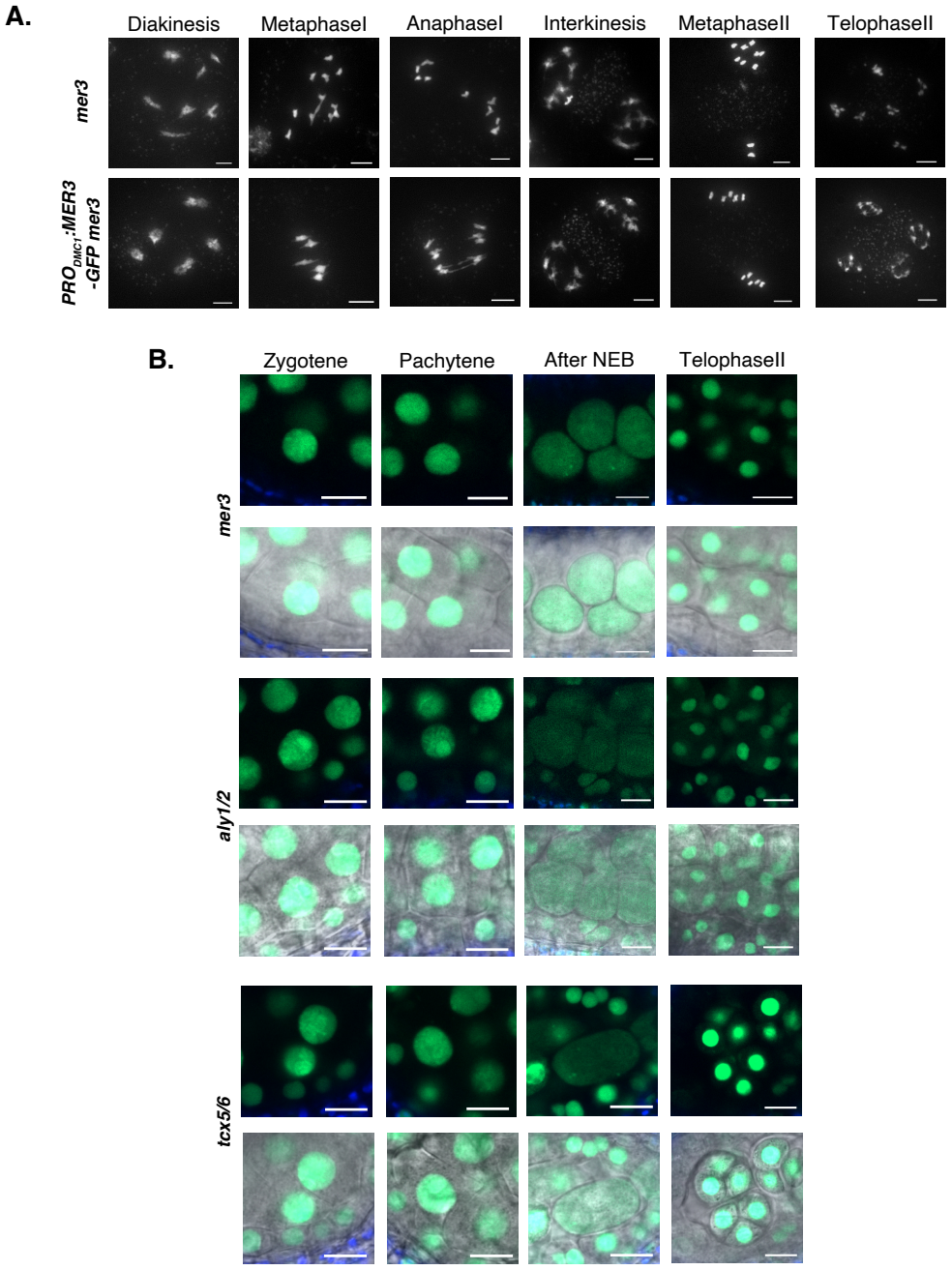
Supplementary Figure 1.3. ALY1-GFP and GFP-TCX5 reporter lines rescue fertility defects in the respective double mutants.

(A) Representative images from acid spreads showing meiotic progression in ALY1-GFP *aly1/2* and GFP-TCX5 *tcx5/6*. Scale bars, 10 *μ*m. **(B)** Quantification of bivalents at metaphase I in WT, *aly1/2*, ALY1-GFP *aly1/2, tcx5/6*, and GFP-TCX5 *tcx5/6* indicates that complementation with ALY1 and TCX5 restores proper bivalent formation. Frequency of observed bivalence numbers and chromosome entanglement at metaphase I. Above the chart, "n" shows the number of metaphase I cells observed and average bivalence number for each transgenic line.



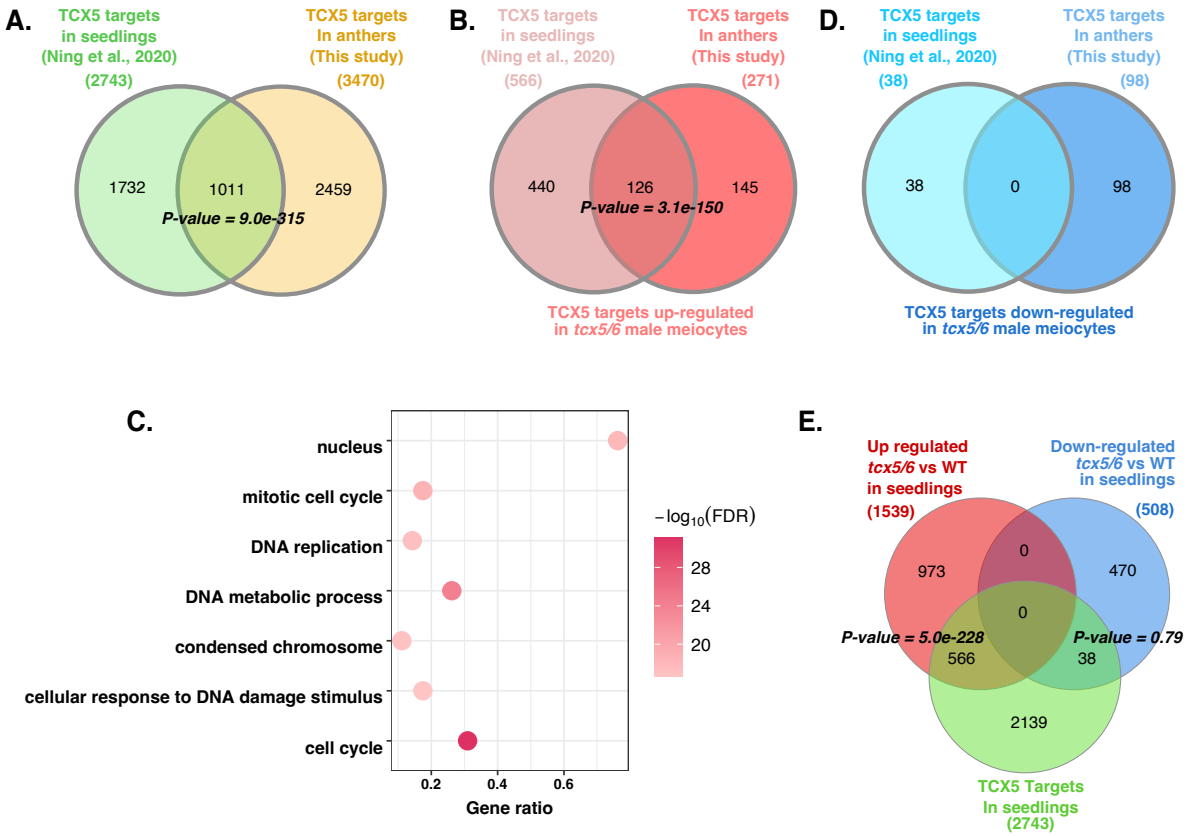
Supplementary Figure 1.4. Integration of transcriptomic and CUT&Tag data reveals direct TCX5 targets among misregulated genes in *aly1/2* and *tcx5/6*.

(A) Heatmap representation of high-confidence GFP-TCX5 CUT&Tag peaks across gene bodies and flanking regions of upregulated (pink, *n* = 271), downregulated (blue, *n* = 98), and non-differentially expressed (orange, *n* = 3101) genes in *tcx5/6* male meiocytes. Also shown are genes that are differentially expressed in *tcx5/6* but not targeted by TCX5. Enrichment signals cluster near transcription start sites (TSS) across all categories. **(B)** Venn diagram illustrating the intersection between genes upregulated (pink) or downregulated (blue) in *aly1/2* male meiocytes and TCX5-bound loci identified by CUT&Tag using GFP-TCX5 in anthers. Statistical significance was assessed using a hypergeometric test (*p* = 1.2e−16 and *p* = -0.24). **(C)** Venn diagram depicting the overlap of TCX5 targets that are transcriptionally upregulated in both *tcx5/6* (dark pink) and *aly1/2* (light pink). Statistical significance of the overlap was assessed using a hypergeometric test (*p* = 1.7e-236). **(D)** GO enrichment analysis of TCX5-bound genes that are consistently upregulated in *tcx5/6* and *aly1/2* male meiocytes.



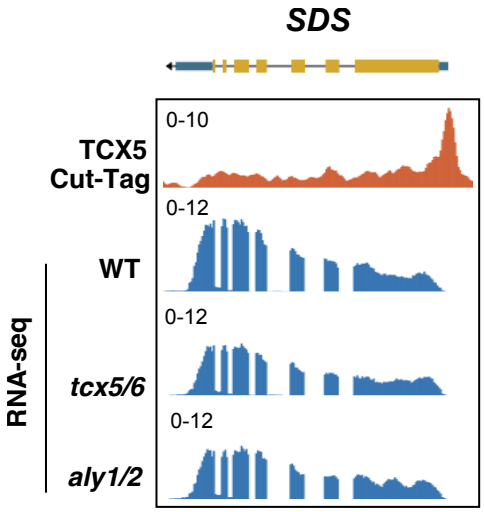
Supplementary Figure 1.5. A *MER3-GFP* genomic reporter under the meiosis-specific *DMC1* promoter produces functional MER3 protein and rescues CO defects in *mer3*.

(A) Cytological analysis of meiotic progression in *mer3* and *proDMC1:MER3-GFP mer3* via acid spreads. **(B)** Confocal images of MER3-GFP at zygotene, pachytene, after nuclear envelope breakdown (NEB), and telophase II in *mer3*, *aly1/2*, and *tcx5/6*. MER3-GFP is specifically expressed in meiotic cells within anthers in *mer3*, while ectopic expression is observed in tapetal cells in *aly1/2* and *tcx5/6*. The localization pattern of MER3-GFP in meiotic cells is comparable across genotypes. Scale bars, 10 μm.



Supplementary Figure 1.6. Comparative analysis of TCX5 targets across tissues reveals shared regulatory roles in seedlings and anthers.

(A) Venn diagram comparing TCX5 target genes identified in seedlings (light green) and anthers (light yellow), highlighting shared and tissue-specific binding (p = 9.0e-315). **(B)** Venn diagram showing the number of genes up regulated in *tcx5/6* male meiocytes that overlap with TCX5 targets identified in seedlings and anthers (p = 3.1e-150). **(C)** GO enrichment analysis of *tcx5/6* upregulated genes in male meiocytes that are bound by TCX5 in both seedlings and anthers. **(D)** Venn diagram showing the number of genes downregulated in *tcx5/6* male meiocytes that overlap with TCX5 targets identified in seedlings and anthers. **(E)** Venn diagram illustrating the intersection between upregulated (pink) and downregulated (blue) genes in *tcx5/6* seedlings and TCX5-bound loci identified via ChIP-seq using TCX5-FLAG (p = 5.0e–228 and p = 0.79, respectively). Statistical significance was assessed using a hypergeometric test in A, B, and E.



Supplementary Figure 1.7. The DREAM complex activates *SDS* transcription.

Browser view of *SDS* transcript levels obtained from RNA-seq in male meiocytes of WT, *tcx5/6*, and *aly1/2* shown in blue, while GFP-TCX5 peaks obtained from CUT&TAG with anther samples shown in dark orange.

Supplementary Table 1.1. Transmission analysis of the *tcx6* allele in a *tcx5* mutant background indicates no gametophytic defect.

Reciprocal crosses were performed between WT and plants homozygous for *tcx5* and heterozygous for *tcx6*. F_1 progeny was genotyped to assess the inheritance of the *TCX6* mutant and WT alleles. Results suggest that the *tcx5 tcx6* mutation combination does not impair gamete transmission.

female x male	Wildtype	*tcx6-1*	# of F1 plants checked
WT x *tcx5* $^{-/-}$ *tcx6* $^{+/-}$	93.70%	106.30%	96
tcx5 $^{-/-}$ *tcx6* $^{+/-}$ x WT	97.80%	102%	96

Supplementary Table 1.2. Sequencing quality metrics for RNA-seq of *aly1/2*, *tcx5/6*, and WT male meiocytes.

Summary of whole transcriptome sequencing statistics, including the number of raw reads, total base counts, clean reads, error rate, GC content, and the proportion of bases falling within Q20 and Q30 quality thresholds, corresponding to base call accuracies of 99% and 99.9%, respectively.

Sample	Raw reads	Raw bases	Clean reads	Clean bases	Error rate	Q20	Q30	GC_pct
*aly1/2*_rep1	72916398	10.94G	72091052	10.81G	0.03	97.35	92.69	44.66
*aly1/2*_rep2	76614758	11.49G	75805972	11.37G	0.03	96.97	91.79	44.41
*aly1/2*_rep3	71233128	10.68G	70734904	10.61G	0.03	97.43	92.86	44.16
*tcx5/6*_rep1	83175446	12.48G	82240380	12.34G	0.03	96.91	91.64	44.48
*tcx5/6*_rep2	77062404	11.56G	76369590	11.46G	0.03	96.73	91.29	44.52
*tcx5/6*_rep3	75309418	11.3G	74620488	11.19G	0.03	97.47	92.94	44.08
WT_rep1	78701654	11.81G	78137760	11.72G	0.03	97.51	93.07	44
WT_rep2	71316336	10.7G	70603748	10.59G	0.03	97.31	92.62	45.11
WT_rep3	71454840	10.72G	70588366	10.59G	0.03	97.59	93.2	44.06

Supplementary Table 1.3. List of meiotic genes and their differential transcriptional levels in *aly1/2* and *tcx5/6* male meiocytes compared to WT.

The table indicates whether these genes are identified as TCX5 targets based on CUT&Tag data from anthers, as well as their differential expression in *tcx5/6* seedlings (data from Ning *et al.*, 2020) and TCX5 target status based on ChIP data from seedlings (Ning *et al.*, 2020). (–: not targeted, +: TCX5 target) If a gene shows no differential expression, it is marked as "unchanged"; *ns* indicates not statistically significant.

			Seedling (Ning *et al.* 2020)		Meiocyte (this study)		Anther (this study)
BP	**Gene ID**	**Name**	***tcx5/6***	**TCX5 ChIP**	***aly1/2***	***tcx5/6***	**TCX5 C&T**
Class I CO (ZMM)	AT1G53490	HEI10	3.9568	+	unchanged	unchanged	-
	AT4G17380	MSH4	2.5436	+	unchanged	unchanged	-
	AT3G20475	MSH5	2.9702	+	unchanged	unchanged	-
	AT5G48390	ZIP4	4.6256	+	unchanged	0.8472	-
	AT5G52290	SHOC1	3.9759	+	unchanged	unchanged	+
	AT1G12790	PDT	0.8473	-	unchanged	unchanged	+
	AT3G27730	MER3	1.9167	+	-0.8870	-0.9107	+
	AT4G09140	MLH1	unchanged	+	unchanged	unchanged	-
	AT4G35520	MLH3	1.8438	+	unchanged	0.8016	-
Class II CO	AT4G30870	MUS81	1.3074	-	0.8330	1.2725	-
	AT4G14970	FANCD2	1.9273	+	unchanged	unchanged	-
	AT2G21800	EME1A	1.9164	+	unchanged	1.0549	-
	AT2G22140	EME1B	not expressed	+	unchanged	unchanged	-

			Seedling (Ning *et al.* 2020)		Meiocyte (this study)		Anther (this study)
BP	**Gene ID**	**Name**	***tcx5/6***	**TCX5 ChIP**	***aly1/2***	***tcx5/6***	**TCX5 C&T**
DSB formation/ maturation	AT3G13170	SPO11-1	2.8927	+	unchanged	unchanged	+
	AT1G63990	SPO11-2	0.4909	+	unchanged	unchanged	+
	AT4G14180	PRD1	0.6481	+	unchanged	unchanged	-
	AT5G57880	PRD2/MPS1	0.4071	-	unchanged	unchanged	-
	AT1G01690	MER2/PRD3	1.3144	+	unchanged	unchanged	+
	AT3G52115	COM1/SAE2	1.3149	+	unchanged	0.8934	-
	AT1G10710	PHS1/REC114	3.8127	+	unchanged	unchanged	+
	AT4G29170	MND1	1.1400	-	unchanged	unchanged	+
	AT3G22880	DMC1	2.6767	+	0.8584	0.6823	+
	AT5G20850	RAD51	1.6726	+	ns	1.2349	+
	AT4G24710	PCH2	1.6109	+	unchanged	unchanged	-
	AT5G54260	MRE11	0.6064	+	unchanged	unchanged	-
Axis/SC	AT1G67370	ASY1	3.7509	+	unchanged	unchanged	+
	AT2G46980	ASY3	1.9693	+	unchanged	unchanged	+
	AT2G33793	ASY4	1.2920	+	unchanged	unchanged	+
	AT5G05490	REC8	unchanged	+	unchanged	unchanged	+
	AT1G22260	ZYP1a	2.6228	+	unchanged	unchanged	+
	AT1G22275	ZYP1b	unchanged	+	unchanged	unchanged	+

			Seedling (Ning *et al.* 2020)		Meiocyte (this study)		Anther (this study)
BP	**Gene ID**	**Name**	***tcx5/6***	**TCX5 ChIP**	***aly1/2***	***tcx5/6***	**TCX5 C&T**
Anti CO / DNA repair	AT1G10930	RECQ4A	1.0525	+	0.6771	0.9473	-
	AT1G60930	RECQ4B	1.5873	+	unchanged	unchanged	-
	AT1G35530	FANCM	2.5329	-	ns	1.2987	-
	AT5G50930	MHF1	2.7016	-	unchanged	unchanged	-
	AT1G78790	MHF2	0.6342	-	unchanged	unchanged	+
	AT5G63540	RMI1	2.2338	+	unchanged	0.8594	+
	AT5G63920	TOP3alpha	1.6885	+	unchanged	unchanged	+
	AT3G05740	RECQI1	1.0262	+	0.6381	0.8993	+
	AT5G57450	XRCC3	1.9864	+	ns	1.0829	+
	AT1G65470	FAS1	1.6342	+	unchanged	0.6898	+
	AT1G77320	MEI1	1.6907	+	unchanged	0.6424	+
	AT4G19130	RPA1E	2.6941	+	0.908326207	1.5063	+
	AT5G22750	RAD5A	1.1882	+	unchanged	0.5482	+
	AT1G20750	FANCJ	5.8328	+	2.1505	3.4613	+
	AT5G49110	FANCI	2.1053	+	unchanged	unchanged	-
	AT1G51130	NSE4A	1.4350	+	unchanged	0.5880	+
	AT1G79950	RTEL1	0.6277	+	unchanged	unchanged	+
	AT3G02920	RPA32B	0.9971	+	unchanged	0.6588	+
	AT1G08130	LIG1	0.8361	+	unchanged	0.5275	+

			Seedling (Ning *et al.* 2020)		Meiocyte (this study)		Anther (this study)
BP	**Gene ID**	**Name**	***tcx5/6***	**TCX5 ChIP**	***aly1/2***	***tcx5/6***	**TCX5 C&T**
Anti CO / DNA repair	AT3G25100	CDC45	0.6163	+	0.659563052	0.7157	+
	AT5G61460	SMC6B/RAD18	1.9297	+	unchanged	0.7599	+
	AT4G21070	BRCA1	1.2407	+	0.7510	1.2760	-
	AT4G00020	BRCA2A	0.5352	+	unchanged	unchanged	+
	AT5G01630	BRCA2B	1.8545	+	unchanged	unchanged	+
	AT2G06510	RPA1A	0.7882	+	unchanged	unchanged	-
	AT3G02920	RPA32B	not expressed	+	unchanged	0.6588	+
	AT2G24490	RPA32A	0.5324	+	unchanged	unchanged	+
	AT4G19130	RPA1E	2.6941	+	0.9083	1.5063	+
	AT3G07800	TK1A	1.4088	+	1.1717	1.3854	+
	AT2G45280	RAD51C	1.1252	-	0.4206	0.5592	-
	AT3G48900	SEND1 (GEN2)	1.9774	+	0.9158	1.2453	-
	AT5G08020	RPA1B	unchanged	+	unchanged	0.4537	+
	AT5G45400	RPA1C	0.5605	+	0.4939	0.9395	+
	AT5G61000	RPA1D	0.5105	+	0.4465	0.7480	+
	AT5G27680	RECQSIM	0.9172	-	unchanged	0.8142	+
	AT4G25120	SRS2	1.4814	-	unchanged	1.4249	-
	AT1G01880	GEN1	ns	+	unchanged	unchanged	-
	AT2G31970	RAD50	unchanged	-	unchanged	unchanged	-

			Seedling (Ning *et al.* 2020)		Meiocyte (this study)		Anther (this study)
BP	**Gene ID**	**Name**	***tcx5/6***	**TCX5 ChIP**	***aly1/2***	***tcx5/6***	**TCX5 C&T**
Anti CO / DNA repair	AT3G18524	MSH2	0.6315	+	unchanged	0.4609	-
	AT3G48190	ATM	unchanged	-	unchanged	unchanged	+
	AT4G02460	PMS1	0.9560	+	unchanged	ns	+
	AT3G52630	RPA3-1	unchanged	+	unchanged	unchanged	+
	AT4G18590	RPA3-2	unchanged	-	unchanged	unchanged	-
	AT4G35740	RECQ3	unchanged	-	unchanged	unchanged	-
	AT5G40820	ATR	1.8395	-	unchanged	unchanged	-
	AT5G43530	RAD5B	2.2158	+	unchanged	unchanged	-
	AT4G18470	SNI1	1.6151	+	1.0031	1.1111	-
	AT5G48720	XRI1	unchanged	-	unchanged	unchanged	-
Chromosome condensation and cohesion	AT2G27170	SMC3/TTN7	0.3391	-	unchanged	unchanged	-
	AT3G59550	SYN3	1.4806	+	0.7317	1.3743	-
	AT3G54670	SMC1/TTN8	0.3429	-	unchanged	unchanged	-
	AT5G15540	SCC2	0.2977	-	unchanged	unchanged	-
	AT5G15920	SMC5	0.5805	+	0.5539	0.7265	+
	AT5G40840	SYN2	unchanged	-	unchanged	unchanged	+
	AT5G62410	CAP-E1/TTN3	1.4224	+	0.6855	1.0742	-
	AT2G47980	SCC3	0.3488	-	unchanged	unchanged	-
	AT3G47460	CAP-E2	0.8441	-	unchanged	0.8658	-

			Seedling (Ning *et al.* 2020)		Meiocyte (this study)		Anther (this study)
BP	**Gene ID**	**Name**	***tcx5/6***	**TCX5 ChIP**	***aly1/2***	***tcx5/6***	**TCX5 C&T**
Chromosome condensation and cohesion	AT5G48600	SMC4/CAP-C	1.5845	+	0.7410	1.4184	-
	AT3G57060	CAP-D2	1.1460	+	unchanged	0.6041	+
	At4G31400	CTF7	0.6932	+	unchanged	unchanged	-
	At2G47980	ESP1	0.3488	+	unchanged	unchanged	-
	AT5G61460	SMC6B/RAD18	1.9297	+	unchanged	0.7599	+
	At5G07660	SMC6	2.6669	+	unchanged	1.0585	-
	AT5G23610	DYAD	unchanged	+	unchanged	unchanged	-
	AT4G15890	CAP-D3	2.0508	+	unchanged	0.7167	+
	AT2G32590	CAP-H	1.6077	+	0.7214	1.4365	+
	AT5G37630	CAP-G	1.2902	+	0.6233	1.1290	-
	AT1G64960	CAP-G2	0.4242	+	unchanged	unchanged	-
	AT4G18470	SNI1	1.6151	+	1.0031	1.1111	-
	AT3G15150	NSE2 /MMS21	1.3184	+	unchanged	0.7182	+

			Seedling (Ning *et al.* 2020)		Meiocyte (this study)		Anther (this study)
BP	**Gene ID**	**Name**	***tcx5/6***	**TCX5 ChIP**	***aly1/2***	***tcx5/6***	**TCX5 C&T**
Meiotic cell cycle	AT1G14750	SDS	1.6690	+	unchanged	-0.7345	+
	AT1G16330	CYCB3;1	1.0900	+	unchanged	unchanged	-
	AT1G77390	TAM	1.6463	-	unchanged	unchanged	+
	AT3G48750	CDKA;1	unchanged	-	-0.6013	-0.7485	-
	AT5G63370	CDKG;1	unchanged	-	unchanged	unchanged	+
	AT3G57860	OSD1	1.3563	+	ns	0.8982	+
	AT1G10710	PHS1	3.8127	+	unchanged	unchanged	+
	AT1G06660	JASON	0.8538	+	unchanged	0.6072	+
	AT1G29400	ML5/AML5	unchanged	-	unchanged	unchanged	-
	AT1G34355	PS1	0.8176	-	-0.7342	-0.9362	-
	AT1G63770	MPA1	-0.3416	-	unchanged	unchanged	-
	AT1G66170	MMD1/DUET	3.5362	-	unchanged	unchanged	+
	AT1G75950	ASK1	unchanged	-	unchanged	unchanged	-
	AT3G02680	NBS1	unchanged	-	unchanged	0.5575	+
	AT3G10440	SGO1	0.8261	+	unchanged	unchanged	+
	AT3G14190	PANS1	unchanged	+	unchanged	unchanged	+
	AT3G19590	BUB3.1	0.9945	+	0.5572	0.6294	+
	AT3G25980	MAD2	unchanged	-	unchanged	unchanged	-

			Seedling (Ning *et al.* 2020)		Meiocyte (this study)		Anther (this study)
BP	**Gene ID**	**Name**	***tcx5/6***	**TCX5 ChIP**	***aly1/2***	***tcx5/6***	**TCX5 C&T**
	AT3G43210	TETRASPORE (TES/STD)	1.1685	+	unchanged	unchanged	+
	AT4G20900	TDM1/MS5	not expressed	-	1.2303	1.3815	-
	AT4G21270	ATK1	1.1198	+	ns	0.8352	+
	AT4G22970	ESP /RSW4	1.7147	+	unchanged	0.6046	+
	AT4G29830	SKI8/VIP3	unchanged	-	unchanged	unchanged	+
	AT5G04320	SGO2	0.7046	-	unchanged	0.5657	+
	AT5G07290	AML4	unchanged	-	unchanged	unchanged	-
	AT5G19400	SMG7	unchanged	-	unchanged	unchanged	-
	AT5G21150	AGO9	unchanged	-	unchanged	unchanged	-
	AT5G42190	ASK2	unchanged	-	unchanged	unchanged	-
	AT5G61960	AML1	unchanged	-	unchanged	unchanged	-
	AT3G12280	RBR1	0.6523	+	unchanged	ns	+
	AT2G33560	BUBR1	0.4914	-	0.5578	ns	-

CHAPTER II. Dissecting the multifaceted roles of the DREAM complex in meiosis

1. INTRODUCTION TO CHAPER II

Meiosis is a specialized form of nuclear division that requires precise orchestration of several key molecular events, including programmed DSB repair, homologous chromosome pairing, CO formation, and balanced chromosome segregation. These events necessitates a distinct pattern of gene expression. Despite advances in our understanding of meiotic mechanisms, the regulatory networks that shape the meiotic transcriptome and coordinate these complex events remain poorly characterized.

One emerging regulatory complex in this context is the DREAM complex (composed of DP, RB-like, E2F, and MuvB-core proteins), a well-conserved transcriptional repressor complex initially characterized for its role in controlling the cell cycle in somatic cells (Fischer and Müller, 2017; Hoareau *et al.*, 2024). In Arabidopsis, all MuvB-core subunits are represented by several homologs, of which ALY1-3 (LIN9 homologs), TCX5/6 (LIN54 homologs), LIN37A/B, LIN52A/B and MSI1 have been precipitated in complex with RBR1and E2F/DP, reflecting plant DREAM versions in somatic cells, as well as in complex with several plant-specific components such as MYB3R transcriptional regulators and proteins of unknown function such as FLIC, FLAC, BTE1, and BTL1 (Ning *et al.*, 2020; Lang *et al.*, 2021, 2023; Y. Wang *et al.*, 2022).

In Chapter I, I showed that ALY1/2 and TCX5/6, representing two core DREAM components, are vital for unperturbed male meiosis, specifically involved in transcriptional regulation of male meiosis, specifically meiotic recombination, whereas others such as LIN37 and LIN52 homologs do not appear to play prominent roles during this stage.

Beyond a general function in mitotic cell cycle regulation, DREAM-like complexes have evolved specialized roles in reproductive development across species. In *Drosophila*, the testis-specific tMAC complex, composed of core dREAM components and spermatocyte-specific factors, activates genes essential for meiotic entry and spermatid differentiation, while the canonical dREAM represses represses somatically expressed genes in male germline cells (Beall *et al.*, 2007; Jiang *et al.*,

2007; Doggett *et al.*, 2011b; Laktionov *et al.*, 2014, 2018). In *C. elegans*, the DRM complex regulates germline-specific transcription, and loss of components like LIN-54 causes sterility (Tabuchi *et al.*, 2011, 2013; Bujarrabal-Dueso *et al.*, 2023). Similarly, in mice, the LIN54 paralog TESMIN forms a testis-specific complex critical for meiosis, with its loss leading to pachytene arrest and infertility (Oji *et al.*, 2020; Zhang *et al.*, 2021). These findings highlight a conserved yet diversified role for DREAM-like complexes in germline transcriptional regulation including meiosis, but their exact mechanisms and targets remain to be fully elucidated.

In this chapter, I focus on the meiotic roles of DREAM core components, particularly ALY1/2 and TCX5/6, and their potential coordination with other DREAM components. I explore the impact of DREAM mutants on key meiotic processes including DSB repair, CO formation, chromosome segregation, microtubule organization, and meiotic timing. Using live-cell imaging, a powerful approach that captures temporal dynamics otherwise obscured in fixed preparations (Prusicki *et al.*, 2019), I assessed the progression of meiosis in DREAM mutants, enabling high-resolution observation of meiotic timing, synchrony and MT rearrangements throughout meiosis.

Furthermore, because canonical protein-protein interaction assays such as co-immunoprecipitation and affinity prufication are difficult to perform in the low-abundance and transient context of meiotic cells, our understanding of the precise composition of a "meiotic DREAM complex" remains unexplored. Nonetheless, genetic analyses can provide critical insight into functional relationships. In this work, I investigated the genetic interplay between ALY1/2 and TCX5/6, examining the extent to which these proteins act cooperatively, redundantly, or in distinct pathways during meiosis. Additionally, I initiated a functional characterization of the MYB3R transcription factors, known components of DREAM complex in somatic contexts (Kobayashi *et al.*, 2015a; Kobayashi *et al.*, 2015b), to assess their potential involvement in reproductive development and meiotic regulation.

Together, this chapter aims to provide a comprehensive view of the roles of DREAM complex components in male meiosis. By integrating cytological analysis,

transcriptomics, and genetic approaches, I dissect the mechanisms by which DREAM-mediated transcriptional regulation ensures faithful meiotic progression. This work elucidates the diverse functions of DREAM complex members in male meiocytes and lays the groundwork for characterizing the composition of meiotic DREAM-like complexes.

2. RESULTS

2.1. DREAM mutants display defects in DSB repair

To investigate whether the reduced CO numbers observed in DREAM mutants (see Chapter I) can be compensated by disrupting anti-crossover pathways, I generated triple and quadruple mutant combinations of the DREAM mutants *aly1/2* and *tcx5/6* with the anti-CO mutants *fancm* and *recq4a recq4b* (hereafter referred to as *recq4ab*). Both FANCM and RECQ4A/B are known to limit Class II CO formation. In their absence, Class II COs are upregulated and can restore CO formation in Class I deficient *zmm* mutants (Crismani *et al.*, 2012; Séguéla-Arnaud *et al.*, 2015b). Given that DREAM mutants exhibit reduced COs at least in part due to MER3 downregulation (Figure 1.3), I aimed to test whether impairing anti-CO pathways could similarly compensate for the CO defect in DREAM mutants.

While *fancm* mutants show wild-type like behavior in chromosome spreads, it is to note that *recq4ab* mutants frequently display chromosome entanglements, with 53 % of cells exhibiting this phenotype (Figure 2.1A and B). These entanglements often persist and lead chromosome fragmentation at anaphase I, followed by the appearance of lagging chromosomes in anaphase I / telophase I (Supplementary Figure 2.1). However, in cells without entanglement, the average number of bivalents is 5 as in wild-type and *fancm* mutants. In the *aly1/2* mutant the average number of bivalents at metaphase I is reduced to 3.8; however, when combined with either *fancm* or *recq4ab*, bivalent numbers increase significantly to 5.0 and 4.9, respectively (Figure 2.1A and B), nearly restoring WT levels and indicating a substantial rescue of the CO defects (n=34 for *aly1/2*, n=97 for *aly1/2 fancm*, and n=65 for *aly1/2 recq4ab*; p<0.005). However, in the *aly1/2 fancm* triple mutant, the frequency of chromosome entanglements increases to 60%. In contrast, the *aly1/2 recq4ab* mutant also shows a restoration of bivalent formation with respect to the *aly1/2* single mutant, but with 29% the frequency of meiocytes showing entanglement is comparable to the 23% observed in *aly1/2* (Figure 2.1B) and even reduced with respect to *recq4a/b* double mutant (53%).

The same mutant combinations involving *tcx5/6* revealed additional phenotypes beyond those observed in *aly1/2*. In the *tcx5/6 fancm* triple mutant, the average number of bivalents per cell significantly increased to 4.3 compared to 3.3 in *tcx5/6* alone (n=44 and n=53, respectively; p<0.05), indicating a partial restoration of CO formation. As in the case of *aly1/2 fancm*, this rescue was accompanied by an increase in chromosome entanglement, rising from 14% in *tcx5/6* to 39% in *tcx5/6 fancm* (Figure 2.1 A and B). However, 10% of cells in *tcx5/6 fancm* also exhibited chromosome fragmentation at metaphase I, suggesting impaired DSB repair.

Strikingly, *tcx5/6 recq4ab* quadruple mutants displayed fully fragmented chromosomes at metaphase I (Figure 2.1 A, left panel). Chromosome spreads revealed no detectable meiotic stages beyond anaphase I in *tcx5/6 recq4ab*, likely due to meiotic arrest triggered by extensive chromosome fragmentation (Supplementary Figure 2.1). This severe defect results in complete sterility, as evidenced by the absence of pollen and seed production.

This outcome was unexpected, as *recq4ab* is known to restore CO formation in various *zmm* mutants (Séguéla-Arnaud *et al.*, 2015a). Since the *zmm* protein MER3 is downregulated in DREAM mutants, it was anticipated that combining *tcx5/6* with *fancm* or *recq4ab* would similarly rescue the CO defect, especially given that the *mer3 recq4ab* triple mutant shows complete restoration of CO formation (Supplementary Figure 2.2) without the presense of abberrant chromosome configurations at metaphase I.

Contrary to this expectation, neither *tcx5/6 fancm* nor *tcx5/6 recq4ab* restored CO formation to wild-type levels (Figure 2.1A and B). Instead, these combinations revealed that upon reduction of anti-CO repair pathways, DREAM mutants, particularly *tcx5/6*, exhibit pronounced defects in DSB repair, manifesting as chromosome fragmentation at metaphase I (Figure 2.1 A, left panel).

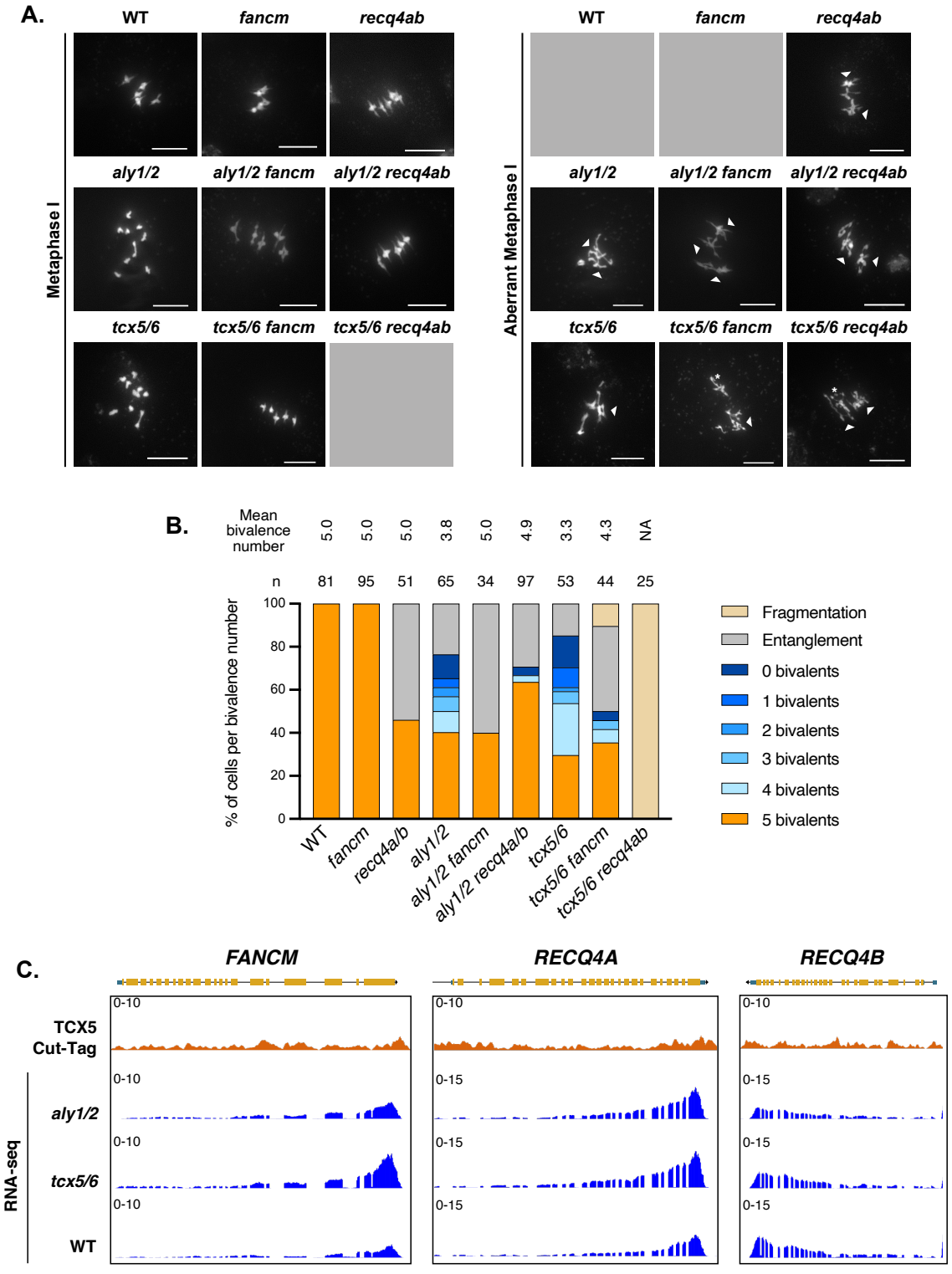


Figure 2.1. DREAM mutants display increased aberrant chromosome configurations at metaphase I in the absence of anti-CO factors.

(A) Representative images of metaphase I chromosome spreads for each genotype are shown on the left: WT, *fancm, recq4ab, aly1/2, aly1/2 fancm, aly1/2 recq4ab, tcx5/6, tcx5/6 fancm,* and *tcx5/6 recq4ab*. On the right, selected examples highlight aberrant metaphase I chromosome configurations,

including entanglement (indicated by white arrow heads) and chromosome fragmentation (indicated by stars). Notably, such abnormalities were observed in *recq4ab, aly1/2, aly1/2 fancm, aly1/2 recq4ab, tcx5/6, tcx5/6 fancm* and *tcx5/6 recq4ab*. Scale bars,10 *μ*m. (**B)** Quantification of bivalent numbers and the frequency of chromosome entanglement as well as fragmentation at metaphase I. Each bar represents the frequency distribution of bivalents per cell, entanglement and fragmentation. The total number of metaphase I cells analyzed is indicated above each column ("n"), along with the average bivalent number. (**C)** Genome browser view displaying the expression levels of *FANCM, RECQ4A* and *RECQ4B* derived from RNA-seq in WT, *tcx5/6*, and *aly1/2* male meiocytes (blue tracks), aligned with CUT&Tag signal for GFP-TCX5 in anthers (dark orange track).

Next, I aimed to determine to which extend the residual COs in DREAM mutants are mediated through the Class II pathway, which operates independently of ZMM proteins. To evaluate the functional contribution of the Class II CO pathway in DREAM mutants, I generated triple mutants combining mutant of MUS81, a key endonuclease in Class II CO formation, with *aly1/2* or *tcx5/6* and assessed their effects on CO formation. Previous studies (Higgins, Buckling, *et al.*, 2008) have shown that *mus81* single mutants does exhibit any meiotic mutant phenotype and are indistinguishable from WT, which is consistent with observations in this study (Figure 2.2A and B; and Supplementary Figure 2.3). In the *aly1/2 mus81* triple mutant, the average bivalence was not significantly different from *aly1/2* alone. However, the proportion of cells exhibiting complete loss of bivalents increased slightly from 13% in *aly1/2* to 17% in *aly1/2 mus81* (Figure 2.2B).

Notably, *tcx5/6 mus81* triple mutants displayed a markedly more severe phenotype. The average bivalent number was dropped significantly from 3.3 in *tcx5/6* to 2.2 in *tcx5/6 mus81* (n=31 and n=53 respectively, p value=0.005, Figure 2.2B). Furthermore, the frequency of cells lacking bivalents entirely increased from 15% in *tcx5/6* to 42% in the *tcx5/6 mus81* combination. Interestingly, the frequency of cells with five bivalents remained unchanged upon the loss of MUS81. Overall, these results indicate that in *tcx5/6* mutants, a substantial portion of the residual COs are dependent on the Class II pathway, particularly on MUS81 activity, highlighting a compensatory role in the absence of proper DREAM function.

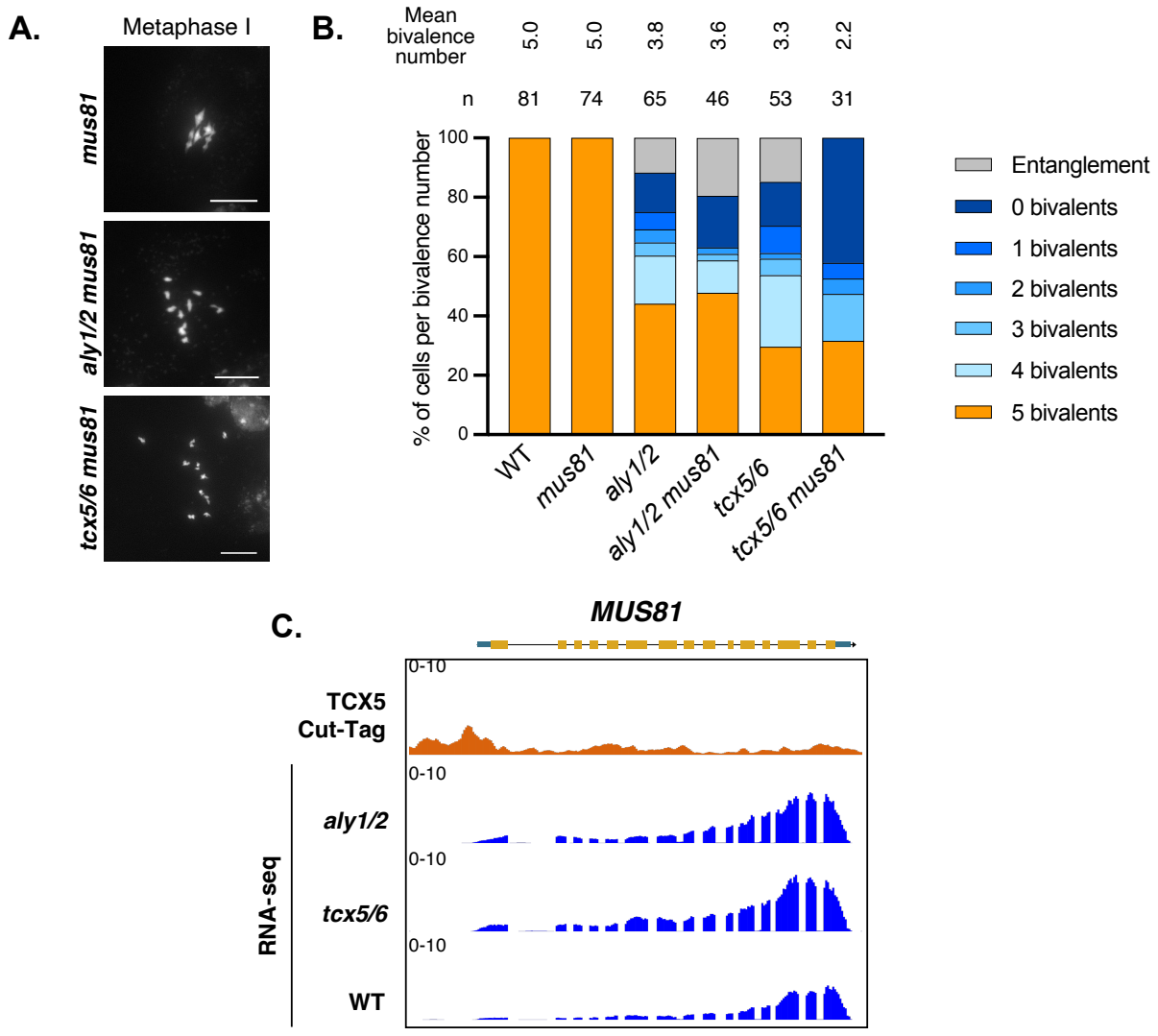


Figure 2.2. MUS81 expression and functional contribution to the meiotic recombination in DREAM mutants.

(A) Representative images of metaphase I chromosomes in *mus81, aly1/2 mus81* and *tcx5/6 mus81*. **(B)** Quantification of bivalent numbers, as well as the frequency of chromosome entanglement at metaphase I. Each bar displays the frequency distribution of bivalents per cell, along with the proportion of cells showing chromosome entanglement. The total number of metaphase I cells analysed for each genotype ("n") and the corresponding average number of bivalents are indicated above the columns. **(C)** Genome browser view showing *MUS81* transcript levels (blue tracks) from RNA-seq data in WT, *tcx5/6*, and *aly1/2* male meiocytes, aligned with CUT&Tag signal for GFP-TCX5 in anthers (dark orange track).

Transcriptomic analysis revealed an upregulation of *MUS81* (Supplementary Table 1.3 and Figure 2.2C). However, CUT&Tag experiments using GFP-TCX5 in anthers showed no TCX5 enrichment at the *MUS81* promoter (Figure 2.2C), suggesting that *MUS81* is not directly regulated by the DREAM complex.

Moreover, transcriptome analysis revealed that *FANCM* and *RECQ4A* are upregulated in *aly1/2* and *tcx5/6* male meiocytes, whereas *RECQ4B* expression remains unchanged (Table 1.1, Supplementary Table 1.3, and Figure 2.1C). Hever, CUT&Tag profiling using GFP-TCX5 in anthers did not detect any enrichment at the promoter regions of these genes, suggesting that their transcriptional regulation is not directly mediated by the DREAM complex. Nonetheless, the increased expression of *FANCM* and *RECQ4A* in DREAM mutants may reflect a compensatory mechanism, where anti-crossover pathways are upregulated to help maintain genome stability when the DREAM complex is not functioning properly during meiotic DSB repair.

Together, these findings highlight the essential role of the DREAM function in promoting proper CO formation and maintaining DSB repair fidelity during meiosis. In Chapter I, we show that in DREAM mutants, CO formation is defective due to down regulation of ZMM protein MER3. While combining *aly1/2* with anti-CO mutants *fancm* and r*ecq4ab* partially restores bivalent numbers via the Class II CO pathway, this rescue is accompanied by increased chromosome entanglement in *aly1/2 fancm*, indicative of error-prone repair. Particularly severe defects, including complete chromosome fragmentation and sterility, were observed in *tcx5/6 recq4ab* mutants, suggesting a critical reliance on anti-CO pathways for DSB repair when DREAM function is compromised. Overall, the DREAM complex emerges as a central player in safeguarding meiotic DSB repair and ensuring balanced CO formation through coordination of both Class I and Class II pathways.

2.2. Impaired DREAM complex activity hinders meiotic progression

Chromosome spreads allow a detailed characterization of meiotic phenotypes but only capture snapshots and do not reveal changes in the dynamics of meiosis. To overcome this limitation, I used an established live-cell imaging method for meiosis (Prusicki *et al.*, 2019) to quantify both the overall duration of meiosis and the stage-specific dynamics of spindle microtubule behavior in DREAM mutants compared to the wildtype.

For this purpose, I generated DREAM mutants harboring double reporter constructs PRO_{REC8}*:REC8:mEGFP* and PRO_{RPSA5}*:TagRFP:TUA5*, previously

validated for defining meiotic landmarks (Prusicki *et al.*, 2019). In this study, meiotic stages were assigned based on microtubule (MT) array morphology, which can be classified into fourteen discrete states, as described in (De Jaeger-Braet *et al.*, 2022). Briefly, MT organization in male meiocytes can be classified into 14 discrete array states (Prusicki *et al.*, 2019), which can be grouped into 7 easily distinguishable groups (De Jaeger-Braet *et al.*, 2022 and Supplementary Figure 2.4). During G_2- early leptotene, MTs form a uniform network with the nucleus centrally positioned (state 1). As cells progress through late leptotene to early pachytene, MTs polarize into a half-moon-like structure on one side of the nucleus (states 2-3-4). Throughout pachytene, diplotene, and diakinesis, this structure develops into a full moon-like assembly encircling the nucleus (states 5-6). Following nuclear envelope breakdown, the pre-spindle reorganizes into the meiosis I spindle (states 7-8-9). At telophase I and during interkinesis, MTs assemble around the two daughter nuclei and form a transient phragmoplast-like structure (states 10 -11). The second division begins with two pre-spindle arrays that mature into metaphase II and anaphase II spindles (states 12 -13). Finally, phragmoplast-like arrays reappear at telophase II (state 14), completing cytokinesis and yielding the four daughter cells of the tetrad.

Durations of meiotic stages are altered in DREAM mutants

As an initial analysis, I quantified the duration of each meiotic stage in *aly1/2, tcx5/6*, and WT controls. To assess whether more subtle alterations in meiotic dynamics occur in DREAM complex mutants that retain fertility, I also included *lin37ab*, a core DREAM component mutant that exhibits no obvious meiotic or fertility defects. By comparing stage lengths across these four genotypes, I aimed to uncover both pronounced and mild perturbations in meiotic timing associated with loss of specific DREAM subunits.

To quantify meiotic timing, I tracked individual meiocytes through live-cell imaging and recorded the interval between the onset and completion of each phase, as defined by transitions in MT array state. During live-cell imaging, frames were taken every 10 min of 15 min for *aly1/2, lin37ab* and WT, *tcx5/6*, respectively. For each genotype (WT, *aly1/2, tcx5/6* and *lin37ab*), I identified the frame in which a given MT state first appeared and the frame in which it transitioned to the next state, and

converted frame counts to elapsed time. This allowed me to calculate the duration of late leptotene - early pachytene (states 2-3-4), pachytene-diakinesis (states 5-6), metaphase I - anaphase I (states 7-9), telophase I-interkinesis (states 10-11), metaphase II - anaphase II (states 12–13) and telophase II (state 14).

From late leptotene to early pachytene, the median duration for MT states 2-3-4 in WT was 795 minutes (95% Confidence Interval (CI): 750-795 min, Figure 2.3A).This was followed by states 5-6 with a median of 450 min (CI: 420-525 min, Figure 2.3B) covering the pachytene and diakinesis stages. The median duration for metaphase I and anaphase I was 45 minutes (CI: 45-60 min, Figure 2.3C) and 75 minutes for telophase I and interkinesis (CI: 60-75 min, Figure 2.3D). The second meiotic division proceeded with a median of 60 minutes for metaphase II and anaphase II (CI: 60-60 min, Figure 2.3E), finishing the meiotic division with 225 min for telophase II (CI: 225-370 min, Figure 2.3E).

The duration of late leptotene to early pachytene was significantly prolonged in both *lin37ab* and *tcx5/6* mutants, with median durations of 1010 min and 930 min, respectively (CI: 1010-1010 min, and CI 855-960 min, respectively; $p<0.0001$). In contrast, *aly1/2* did not exhibit a significant difference from WT, showing a median duration of 810 minutes (CI: 740-840 min, Figure 2.3A). In *tcx5/6*, an extension of duration was observed for the pachytene and diakinesis stage (median duration: 525 min, CI: 495-555 min; $p<0.005$). Conversely, this stage was significantly shorter in *aly1/2* and *lin37ab*, with mean durations of 360 and 415 min, respectively (CI: 330–430 min and 410–420 min; $p<0.0001$ and $p<0.02$, respectively). Additionally, *lin37ab* showed a significantly reduced median duration of metaphase I and anaphase I (median 40 min, CI: 40–50 min; $p<0.0001$) compared to WT, (Figure 2.3C), whereas *aly1/2* and *tcx5/6* did not differ from WT during this stage.

The duration of telophase I and interkinesis was not significantly different in *aly1/2* and *lin37ab* relative to WT, but was significantly prolonged in *tcx5/6*, with a median duration of 105 min (CI: 90–120 min; $p<0.0008$; Figure 2.3D).

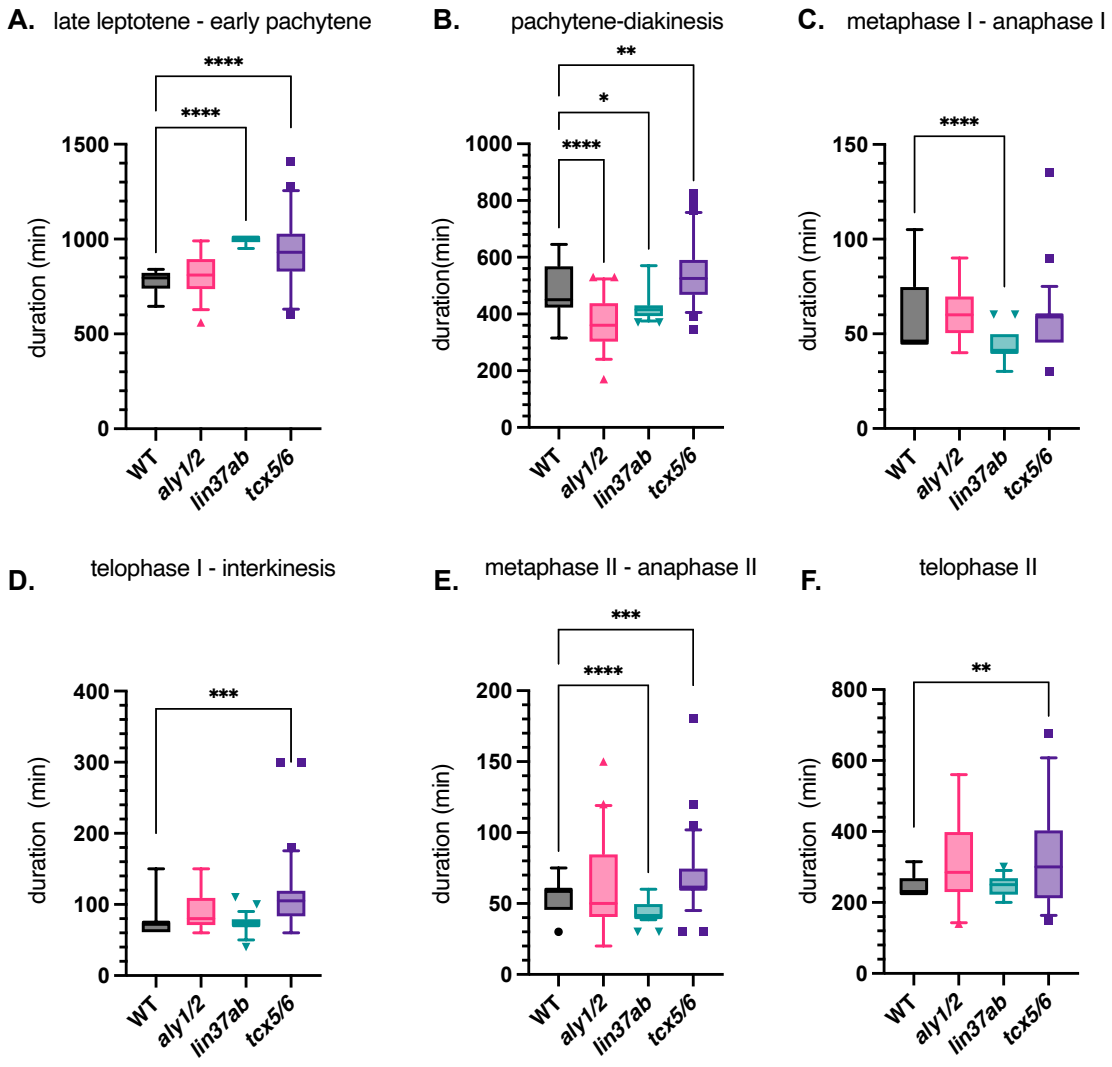


Figure 2.3. Duration of meiotic stages (in minutes) across WT, *aly1/2*, *lin37ab*, and *tcx5/6* genotypes.

Data are presented with box-and-whisker plots showing the median time with 95% confidence intervals, interquartile range, and minimum-to-maximum values. Outliers were defined as values outside 1.5 times the interquartile range and are indicated as individual points beyond the whiskers. **(A)** Late leptotene and pachytene, **(B)** pachytene and diakinesis, **(C)** metaphase I and anaphase I, **(D)** telophase I and interkinesis, **(E)** metaphase II and anaphase II, and **(F)** telophase II. One-way ANOVA was used followed by Dunnett's T3 multiple comparisons test. Statistical significance is indicated as follows: * $p \leq 0.05$, ** $p \leq 0.01$, *** $p \leq 0.001$ ****, $p \leq 0.0001$; n ≥ 40 for all stages.

Metaphase II and anaphase II were also significantly prolonged in *tcx5/6* (median time 60 min, CI: 60–75 min; $p<0.0004$), whereas they were shorter in *lin37ab* (median time 40 min, CI: 40–50 min; $p<0.00001$;Figure 2.3E). Telophase II duration was significantly

increased in *tcx5/6* (median time 300 min, CI: 285–390 min; $p<0.001$), while *aly1/2* and *lin37ab* did not differ significantly from WT (Figure 2.3F).

In summary, nearly all meiotic phases, except metaphase II and anaphase II, were prolonged in *tcx5/6*, whereas *lin37ab* generally exhibited accelerated progression, except during late leptotene and early pachytene. Although *lin37ab* did not display overt meiotic defects like *aly1/2* and *tcx5/6*, it still showed altered meiotic timing. Unlike *tcx5/6*, *aly1/2* exhibited meiotic timing comparable to WT for most stages, with the exception of a shortened pachytene and diakinesis.

Meiosis progression is asynchronous in *tcx5/6*

In *Arabidopsis*, meiocytes within the same pollen sac typically progress through meiosis almost synchronously (Prusicki *et al.*, 2019). Using live-cell imaging this synchrony can be observed as a gradual wave of progression, with metaphase I being first visible at one pole of the anther and then consecutively appearing in neighboring cells reaching the opposite pole approximately 15 minutes later. As shown in Figure 2.4A, in WT anthers, all meiocytes reach diakinesis simultaneously, characterized by the “full moon” microtubule structure, and proceed to metaphase I in in the above described wave-like manner.

In contrast, *tcx5/6* mutants display pronounced asynchrony in meiotic progression. In the top anther lobe (Figure 2.4B), meiocyte 1 is at metaphase I, while meiocyte 2 remains in diakinesis, meiocyte 3 is entering nuclear envelope breakdown, and meiocyte 4 has already reached metaphase II. In the lower anther lobe meiocyte 5 is at metaphase II; meiocyte 6 is in a late stage of telophase I, displaying two circular microtubule arrays encasing the segregated chromosomes; meiocyte 7 show a anaphase I MT array, while meiocyte 8 is also at telophase I, albeit not as far developed as meiocyte 6. Finally, meiocyte 9 has already progressed to telophase II.

Figure 2.5 illustrates the phase-by-phase meiotic progression of 10 cells within the same anther lobe, highlighting asynchrony in *tcx5/6* compared to WT. In WT, meiotic stages proceed in a mild wave-like manner, with cells typically differing by only one or two imaging frames as progression advances across the anther lobe. In

contrast, *tcx5/6* mutants exhibit pronounced temporal variability, with individual cells transitioning between stages at markedly different time points. This asynchrony is particularly evident in Figure 2.5B: examplified by cell 1 transitions earlier than the others, reaching late telophase II, while cell 10 remains significantly delayed at the pachytene/diakinesis stage. Meanwhile, cells 2 through 5 are observed at telophase I or interkinesis, further illustrating the disruption in coordinated progression. Notably, neighboring cells 3 and 4 proceed through most stages with only a one- to two-frame difference, except that cell 4 transitions from early leptotene (MT array 1) to late leptotene (MT arrays 2–4) earlier than cell 3. Cells 7, 8, and 9 exhibit an extended telophase I–interkinesis phase, and their transition to metaphase II–anaphase II is not observed, despite neighboring cells 1–6 progressing into these stages.

In contrast to *tcx5/6*, other core DREAM component mutants *aly1/2* and *lin37ab* displayed a more synchronous progression through meiosis similar to the WT (Supplementary Figure 2.5). These observations illustrate a striking loss of coordinated meiotic timing in *tcx5/6*, highlighting a unique role of TCX5/6 in maintaining synchrony across meiocytes within an anther lobe.

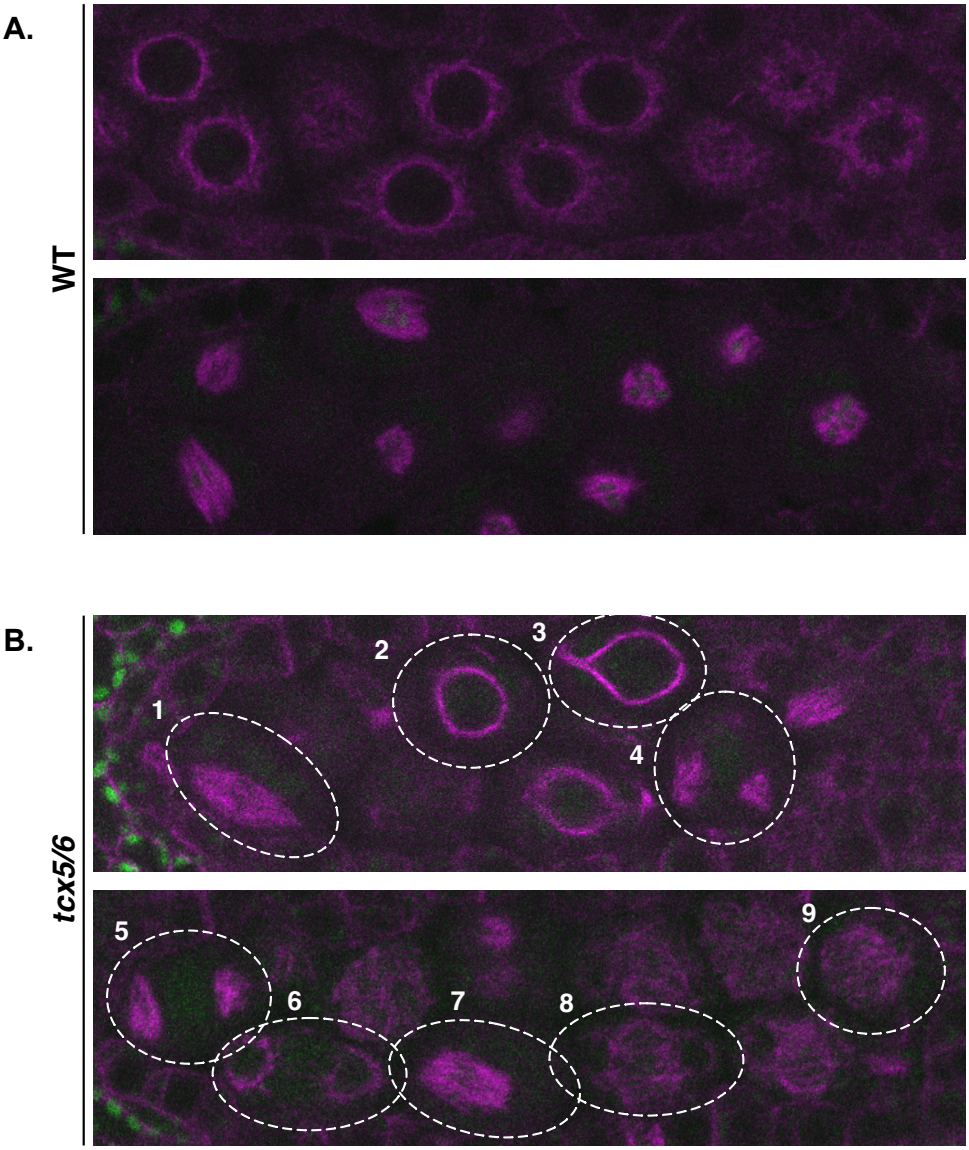


Figure 2.4. Meiosis progression is asynchronous in *tcx5/6.*

Confocal images of **(A)** WT and *tcx5/6* **(B)** anther lobes. Magenta indicates RFP-TUA5, green shows REC8-mEGFP. In **(B)**, circles and corresponding numbers denote individual meiocytes within the anther lobe, highlighting highly asynchronous progression in *tcx5/6.*

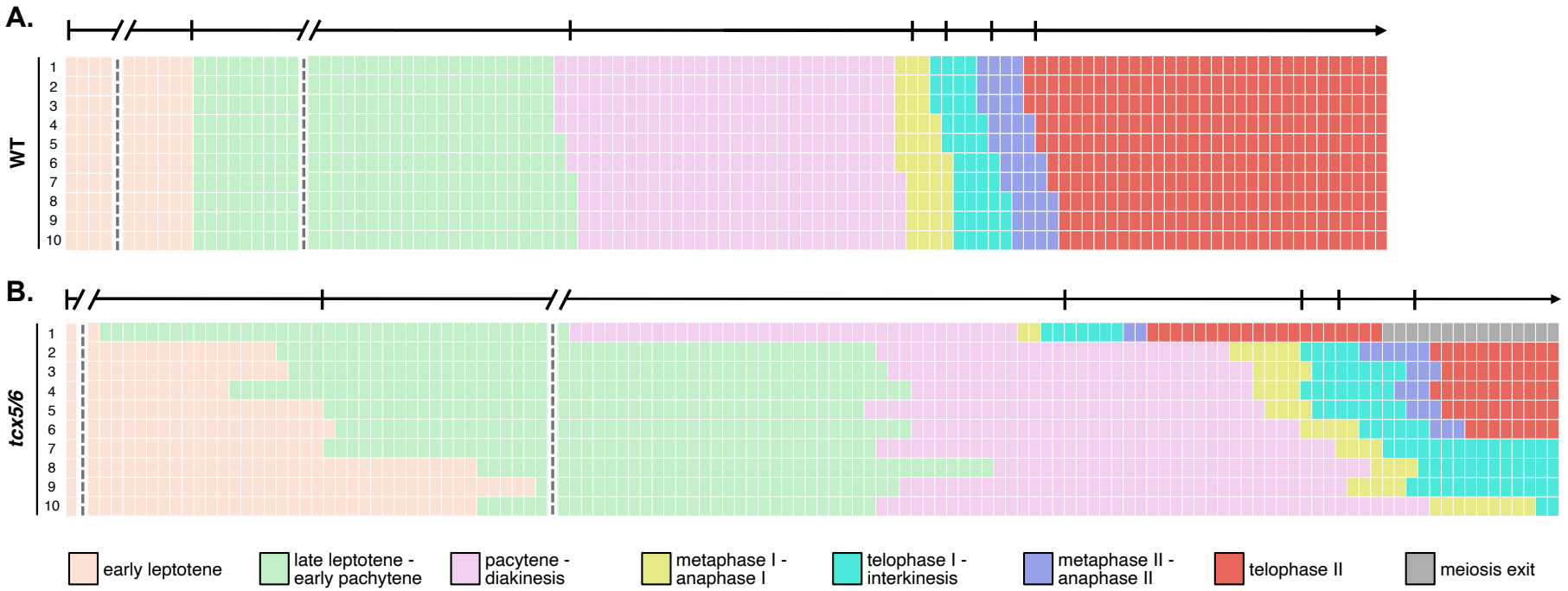


Figure 2.5. Quantification of meiotic synchrony in WT and *tcx5/6* male meiocytes

(A-B) Representation of phase-by-phase meiotic progression in **(A)** WT and **(B)** *tcx5/6* cells (n=10) within the same anther lobe. Each row is one cell, and each 15-min frame is one rectangle colored by the assigned meiotic phase: early leptotene (light orange), late leptotene and early pachytene (light green), pachytene and diakinesis (pink), telophase I and interkinesis (turquoise), metaphase II and anaphase II (purple), telophase II (orange) and meiotic exit defined by the occurance of tetrads (gray). Panels A illustrate the tight synchrony of WT meiocytes, while the variability in *tcx5/6* is shown in Panel B. Due to space constraints, 35 frames from early leptotene and 24 frames from late leptotene to early pachytene were omitted for both genotypes; these omissions are indicated by dashed lines and "//" on the timeline.

Differential expression of meiotic cyclins, CDKs, and their regulators in DREAM Mutants

Meiotic cyclins, cyclin-dependent kinases (CDKs), and their regulatory partners are central to coordinating the meiotic cell cycle, facilitating timely transitions through key stages such as prophase I, metaphase I/II, and cytokinesis. Several cyclins, including SDS and TAM, along with CDKs such as CDKA;1 and CDKG1, are known to play meiosis-specific roles (Zheng *et al.*, 2014; Yang *et al.*, 2019; Nibau *et al.*, 2020; Sofroni *et al.*, 2020).

To investigate whether the DREAM complex regulates meiotic cell cycle progression, I analyzed how the expression of cyclin-dependent kinases (CDKs), meiotic cyclins, and their regulatory partners change in *Arabidopsis* male meiocytes from *aly1/2* and *tcx5/6* mutants compared to WT, integrating this with CUT&Tag data to identify direct TCX5 targets (Table 2.2).

Among the CDKs, *CDKA;1*, a master regulator of meiosis, is significantly downregulated in both *aly1/2* (log_2FC = –0.60, adjusted *p-value* (*padj*) = 0.00686) and more strongly in *tcx5/6* (log_2FC = –0.75, *padj* = 0.00005), though it was not a direct TCX5 target. In contrast, *CDKD;1* is significantly upregulated in *aly1/2* (log_2FC = 0.72, *padj* = 0.00575) and identified as a direct TCX5 target, suggesting it may be under direct DREAM complex repression.

Among cyclins, multiple members of the CYCA2 family are upregulated. *CYCA2;4***,** which is not bound by TCX5, shows consistent upregulation in both *aly1/2* (log_2FC = 0.53, *padj*=0.01506) and *tcx5/6* (log_2FC = 1.28, *padj* < 0.00001). *CYCA2;1* is strongly induced only in *tcx5/6* (log_2FC = 3.24, *padj* < 0.00001), and also lack direct TCX5 association. *CYCA2;3*, in contrast, is slightly upregulated in *tcx5/6* (log_2FC = 0.47213, *padj* = 0.04709) and but identified as a direct TCX5 target, suggesting direct transcriptional de-repression in the *tcx5/6* mutant.

The meiosis-specific cyclin *SDS* is non-significantly downregulated in *tcx5/6* (log_2FC = -0.73448, *padj* = 0.05273), but marked as a direct TCX5 target pointing to a DREAM-mediated control of recombination-associated cyclins. *TAM (CYCA1;2)*,

another cyclin important for meiosis I, also directly bound by TCX5 but its expression is not de-regulated in DREAM mutants. *CYCB3;1*, on the other hand, important for suppressing ectopic cell wall formation, is slightly but significantly upregulated in *tcx5/6* ($log_2FC = 0.69419$, *padj* = 0.02796), though it is not a direct TCX5 target.

Among cyclin regulators, *OSD1*, which prevents premature meiotic exit, is significantly upregulated in *tcx5/6* ($log_2FC = 0.89821$, *padj* = 0.00394) and identified as a direct TCX5 target, indicating a direct regulatory link. Similarly, *THREE-DIVISION MUTANT/ MALE STERILE 5 (TDM1/MS5)*, which promotes meiotic exit, is significantly induced ($log_2FC > 1.2$, *padj* < 0.00001) in both backgrounds, though it is not directly bound by TCX5.

Overall, these data indicate that the DREAM complex directly and indirectly modulates the expression of several key regulators of the meiotic cell cycle. The integration of transcriptional profiling and CUT&Tag indicates a complex regulatory network, consistent with a major role of DREAM-like complexes in orchestrating meiotic progression.

Table 2.1. Differential expression of meiotic cyclins, CDKs, and their regulators in *tcx5/6* and *aly1/2* male meiocytes.

Log_2 fold change (log_2FC) and adjusted *p*-values (*padj*) are presented for selected genes involved in the meiotic cell cycle,comparing expression in *aly1/2* and *tcx5/6* meiocytes relative to wild-type. The final column indicates direct TCX5 binding in anthers, as determined by CUT&Tag analysis ('+' denotes TCX5 occupancy in the promoter region) Genes displaying statistically significant changes and/or mentioned in the text, are highlighted in bold.

			aly1/2		***tcx5/6***		**TCX5**
	Gene ID	Gene Name	log2FC	*padj*	log2FC	*padj*	**CUT&Tag**
Meiotic CDKs	**AT3G48750**	**CDKA;1**	**-0.60132**	**0.00686**	**-0.74845**	**0.00005**	-
	AT5G63370	CDKG;1	-0.17373	0.65721	-0.03733	0.93812	-
	AT1G73690	**CDKD;1**	**0.72087**	**0.00575**	0.16510	0.16510	**+**
	AT1G66750	CDKD;2	0.31192	0.33751	0.30073	0.30073	-
	AT1G18040	CDKD;3	0.22336	0.51984	0.11373	0.11373	-
Meiotic Cyclins	**AT1G14750**	**SDS**	-0.18744	0.84539	-0.73448	0.05273	**+**
	AT1G77390	**TAM (CYCA1;2)**	0.20004	0.73160	0.41436	0.40064	**+**
	AT5G25380	**CYCA2;1**	0.65308	0.75185	**3.23797**	**0.00000**	-
	AT5G11300	CYCA2;2	-0.29754	0.53951	-0.22717	0.55817	-
	AT1G15570	**CYCA2;3**	0.19770	0.62792	**0.47213**	**0.04709**	**+**
	AT1G80370	**CYCA2;4**	**0.52700**	**0.01506**	**1.28403**	**0.00000**	-
	AT1G47210	CYCA3;2	0.00748	0.99419	-0.07719	0.88985	-
	AT1G47220	CYCA3;3	4.22926	1.00000	4.93512	1.00000	-
	AT1G47230	CYCA3;4	0.08937	0.86503	0.30544	0.19593	-
	AT1G16330	**CYCB3;1**	0.45503	0.22794	**0.69419**	**0.02796**	-
Regulators	**AT3G57860**	**OSD1 (GIG)**	0.47156	0.13847	**0.89821**	**0.00394**	**+**
	AT5G19400	SMG7	0.12087	0.72877	0.25253	0.25852	-
	AT4G20900	**TDM1/MS5**	**1.23031**	**0.00000**	**1.38151**	**0.00000**	-

Aberrant meiotic microtubule organization observed in *tcx5/6*

Proper MT organization is essential for accurate chromosome segregation and cytokinesis during meiosis. To assess whether the DREAM complex influences MT dynamics, we examined MT architecture of meiocytes from wild WT, *aly1/2*, *lin37ab*, and *tcx5/6* mutants by live-cell imaging. At late leptotene and early pachytene, MTs formed characteristic half-moon–like structures across all genotypes (Figure 2.6a-d). By diakinesis, these progressed into full-moon arrangements. However, in *tcx5/6* mutants, an additional cap-like layer of MTs appeared outside of the full-moon structure (Figure 2.6h´,h´´, indicated by white arrows), while this feature is absent in *aly1/2* and *lin37ab*.

During nuclear envelope breakdown (NEB), *tcx5/6* meiocytes exhibited atypical MT arrangements (Figure 2.6l´, l´´, indicated by white arrows), including prominent tail-like extensions and ring-like structures surrounding the nascent spindles. At metaphase I, spindles in *tcx5/6* were notably enlarged (Figure 2.6p´, p´´), often spanning nearly the full length of the cell, as outlined by dashed circles. These early spindle defects were compounded at metaphase II, where *tcx5/6* meiocytes frequently displayed more than two spindles (Figure 2.6t´, t´´, indicated by numbers), in contrast to the two perpendicular spindles observed in WT and other mutants (Figure 2.6q-s) .

By telophase II, WT, *aly1/2*, and *lin37ab* meiocytes consistently formed balanced tetrads with symmetrical MT polarization (Figure 2.6u-w). In *tcx5/6* mutants, however, MT polarization was uneven and disorganized (Figure 2.6t´, t´´). These observations indicate a *tcx5/6*-specific function relevant for proper MT organization during meiosis, albeit a dosage effect cannot be excluded, as due to ALY3, *aly1/2* does not represent a complete loss of ALY.

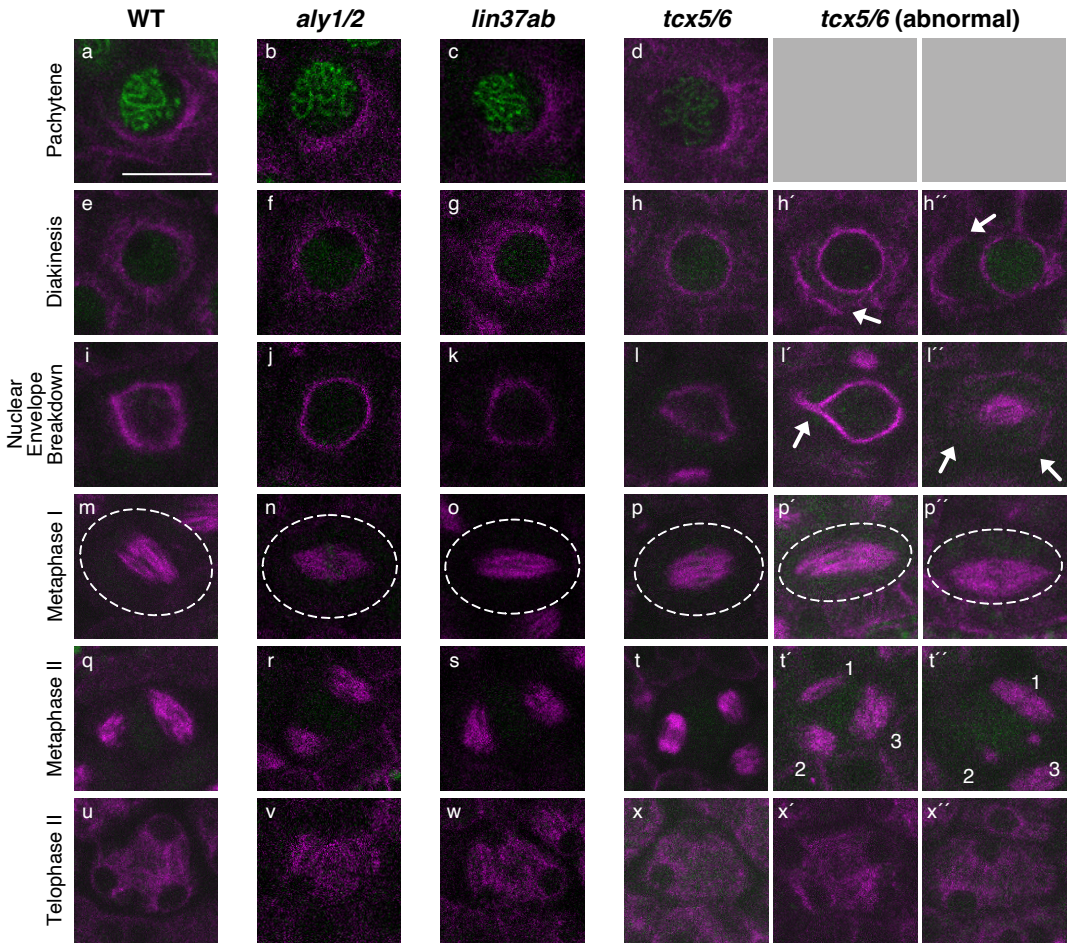


Figure 2.6. Abnormal microtubule dynamics during meiosis in *tcx5/6* mutants revealed by live imaging.

Live imaging of male meiocytes co-expressing RFP-TUA5 (magenta; microtubules) and REC8-mEGFP (green; chromosome cohesion) shows meiotic MT dynamics in WT, *aly1/2*, *lin37ab*, and *tcx5/6* genotypes. Representative frames are shown for key meiotic stages: pachytene (a-d); diakinesis (e-h), including abnormal MT structures in *tcx5/6* (h′, h′′); nuclear envelope breakdown (i-l, with abnormalities in *tcx5/6* shown in l′, l′′); metaphase I (m-p, with *tcx5/6* abnormalities in p′, p′′); metaphase II (q-t, with *tcx5/6* abnormalities in t′, t′′); and telophase II (u-x, with *tcx5/6* abnormalities in x′, x′′). Abnormal MT structures in *tcx5/6* include cap-like layers at diakinesis, tail- and ring-like formations during NEB (indicated by white arrows), enlarged spindles at metaphase I (cell boundaries marked by white dashed circles), multiple spindles at metaphase II (indicated by numbered structures), and unbalanced MT polarization at telophase II. Scale bars, 10 μm.

2.3. Towards understanding the meiotic DREAM complex

Previous studies have characterized the complete composition of Arabidopsis DREAM complex in somatic tissues using affinity purification and protein–protein interaction assays (Ning *et al.*, 2020; Lang *et al.*, 2021). However, it remains unclear whether the complex maintains the same composition during meiosis and which components are responsible for transcriptional regulation of meiotic genes. To address this, I not only concentrated on the MUV-B core components as described in the previous paragraphs but also investigated the potential role of MYB3R transcription factors in meiotic regulation. Additionally, I examined possible interactions between the ALY1/2 and TCX5/6 modules to understand their functional interplay. Finally, I assessed whether other DREAM components are misregulated in *aly1/2* and *tcx5/6* double mutants, aiming to uncover potential feedback mechanisms within the complex.

The interplay between ALY1/2 and TCX5/6

Previous studies in mice showed that a homolog of TCX5 (MTL5) requires ALY (LIN9) for its translocation into nucleus, where both together promote meiotic progression. Our understanding of the interdependencies among components of the Arabidopsis DREAM complex is limited. Notably, both ALY1/2/3 and TCX5/6 possess predicted DNA-binding domains (Bhatt *et al.*, 2004; Andersen *et al.*, 2007), yet it is unclear, if both can bind DNA independently, or if there is a dependency of one on the other for DNA association.

To clarify the reciprocal localization dependencies between TCX5/6 and ALY1/2, I introduced functional genomic reporter constructs, namely ALY1-GFP into *tcx5/6* double homozygous and heterozygous mutants, as well as functional GFP-TCX5 and GFP-TCX6 into *aly1/2* double homozygous and heterozygous mutants. In subsequent generations, I assessed GFP localization patterns in double homozygous mutant lines. Notably, the absence of TCX5 and TCX6 did not alter ALY1-GFP localization; it consistently decorated meiotic chromosomes clearly and robustly, particularly evident during pachytene (Figure 2.7A; left panel). Conversely, the localization of GFP-TCX5 and GFP-TCX6 was significantly affected in *aly1/2* double mutants (Figure 2.7A; middle and right panel, respectively). Instead of distinct

chromosomal localization, both proteins appeared diffusely distributed within the nucleoplasm, lacking clear enrichment or concentrated GFP signals on the chromosome. These observations indicate that ALY1/2 are essential for wild type-like chromosomal recruitment and localization of TCX5 and TCX6 during meiosis, whereas the localization of ALY1 remains independent of TCX5/6.

Next, I investigated whether the transcript levels ALY1, ALY2, TCX5 and TCX6 are interdependent with respect to transcriptional regulation. As shown in Figure 2.7B (quantification shown at Table 2.2), *ALY1* transcript abundance was significantly elevated in *tcx5/6* double mutant relative to WT (log_2FC = 1.7271, *padj* = 5.29E-17). CUT&Tag analysis further confirmed direct binding of TCX5 to the *ALY1* promoter in anther tissue. Similarly, *ALY2* transcript levels were upregulated in *tcx5/6* (Supplementary Figure 2.6 and Table 2.2) and both *TCX5* and *TCX6* expression levels are increased in *aly1/2* background. Also, *ALY2, TCX5* and *TCX6* are bound by TCX5 in anther tissue. Together these data reveal direct transcriptional feedback loops between ALY1/2 and TCX5/6.

To test the functional relationship between ALY1/2 and TCX5/6, I generated quadruple homozygous mutants (*aly1/2 tcx5/6)* and observed meiotic progression via chromosome spreads of male meiocytes. At pachytene, the quadruple mutant displayed unpaired regions (arrowheads in Figure 2.7C; a) at a 25% frequency (*n*=53), closely matching the rates in *aly1/2* (23%, *n*=82) and *tcx5/6* (26%, *n*=92) double mutants, indicating no enhancement of this defect. During diakinesis and metaphase I, univalent formation instead of five bivalents was observed (Figure 2.7C; b and c). In the quadruple mutant, 60% of cells lacked all bivalents (*n* = 65), compared to 13% in *aly1/2* (*n*=54) and 15% in *tcx5/6* (*n*=33), with mean bivalent counts of 1.7 versus 3.8 and 3.3, respectively (*p*=0.005, Figure 2.7D).

Anaphase I and telophase I exhibited chromosome lagging and missegregation (Figure 2.7C; e and f). By metaphase II, 91% of cells (*n*=21) showed unbalanced chromosome pools, and 67% displayed premature sister-chromatid separation. Telophase II produced only triads or polyads with micronuclei in all observed cells (*n*=19; Figure 2.7C; h). These phenotypes are less severe and/or not observed in the

aly1/2 and *tcx5/6* double mutants. No viable pollen was recovered from the quadruple mutant. This complete male sterility is a drastic enhancement compared to 90% and 86% pollen abortion seen in *aly1/2* and *tcx5/6*, respectively (Figure 1.1).

Together, these findings demonstrate that the *aly1/2 tcx5/6* quadruple mutant exhibits an enhanced loss of crossover formation compared to each double mutant, indicating a synergistic interaction that exacerbates defects in meiotic recombination and bivalent formation, as well as chromosome segregation.

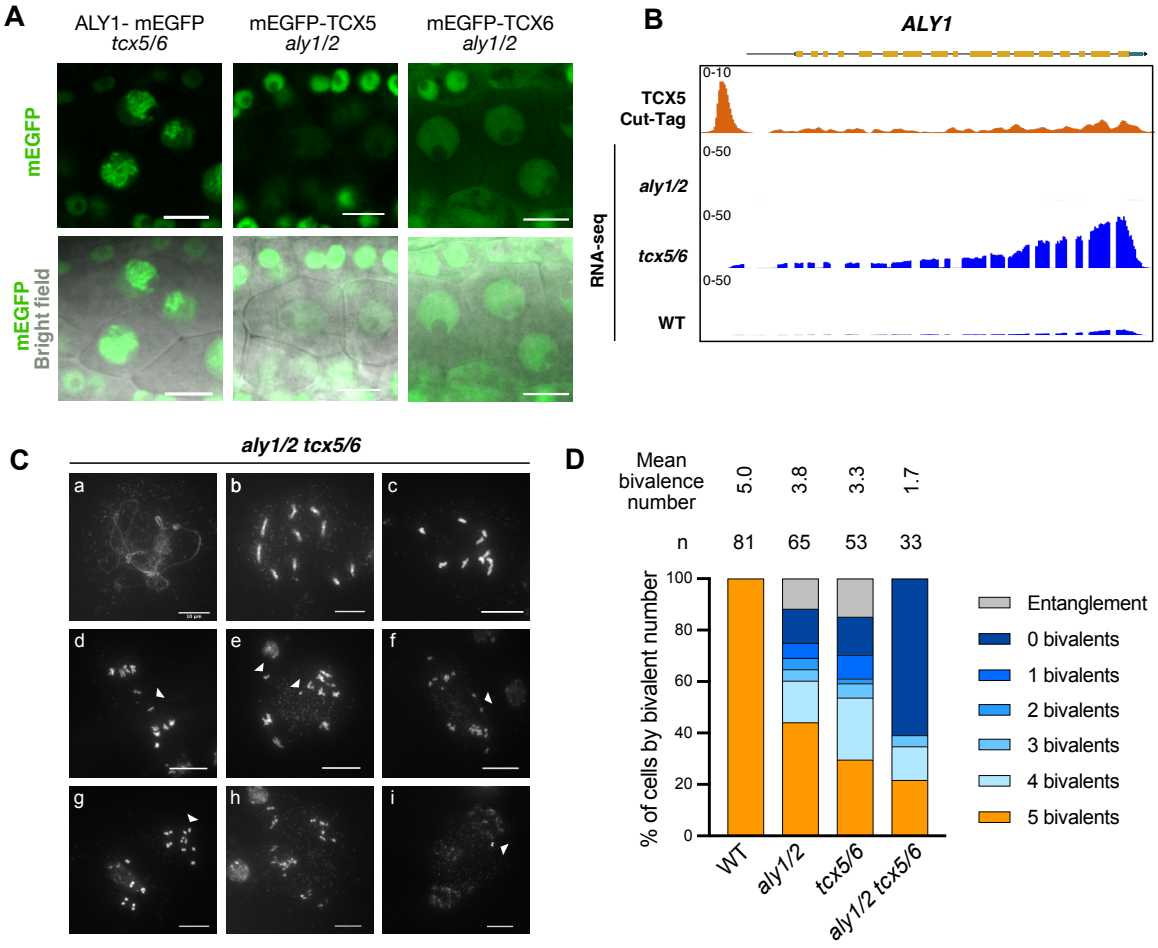


Figure 2.7. Localization dependency and functional interplay between ALY1/2 and TCX5/6 during meiosis.

(A) Confocal microscopy images illustrating the localization of ALY1-mEGFP (green, first column) in the *tcx5/6* mutant background, and mEGFP-TCX5 (green, second column) in the *aly1/2* mutant background at the pachytene stage. Bright-field merged images are shown in the second row for context. Scale bars, 10 *μ*m. **(B)** Genome browser visualization depicting *ALY1* transcript abundance (blue tracks) from RNA-seq analyses performed on WT, *aly1/2*, and *tcx5/6* meiocytes, overlaid with CUT&Tag data indicating GFP-TCX5 binding profiles in anther tissue (dark orange track). **(C)** Representative images of *aly1/2 tcx5/6* mutant chromosomes captured at distinct meiotic stages: pachytene (a), diakinesis (b), metaphase I (c), anaphase I (d), telophase I (e), metaphase II (f), anaphase II (g), telophase II (h), and tetrad stage (i). Scale bars, 10 *μ*m. **(D)** Quantification of bivalent numbers per cell at metaphase I, along with the frequency of chromosome entanglement, across WT, *aly1/2*, *tcx5/6*, and *aly1/2 tcx5/6* genotypes. Bars indicate the distribution of bivalents per cell and the proportion of cells exhibiting chromosome entanglement. The total number of metaphase I cells analyzed (n) and their respective average bivalent numbers are provided above each column.

Transcriptional up-regulation of DREAM Components in *aly1/2* and *tcx5/6* mutants

In both *aly1/2* and *tcx5/6* double mutants, we observed a compensatory upregulation of the reciprocal DREAM component pair (*TCX5/6* in *aly1/2* and *ALY1/ALY2* in *tcx5/6*, Table 2.2 and Supplementary Figure 2.6), likely indicating a feedback loop of the DREAM complex on itself. To determine whether additional MuvB-core DREAM subunits or plant-specific DREAM-associated proteins—namely FLIC, FLAC, BTE1, and BTL1—exhibit a similar response, we quantified their expression in *aly1/2* and *tcx5/6* male meiocytes using our RNA-seq datasets. We also mapped TCX5 occupancy at these loci in anthers via CUT&Tag. Finally, to assess whether this regulatory feedback extends beyond reproductive tissues, we compared these results with RNA-seq and ChIP data from *tcx5/6* seedlings, thereby highlighting both shared and tissue-specific aspects of DREAM complex regulation.

Among the MuvB-core components, both *LIN37A* and *MSI1* exhibited significant upregulation in *aly1/2* and *tcx5/6* meiocytes and were confirmed as direct TCX5 targets (Table 2.2). Consistent with this, their transcript levels also increased in *tcx5/6* seedlings, and TCX5 occupancy was detected at their promoters in ChIP with TCX5-FLAG lines (Ning *et al.*, 2020). By contrast, *ALY3* and *LIN37B* only showed an insignificant increase in meiocytes, and no TCX5 binding could be detected at their promoters in anthers. *LIN37B* also remained unchanged in *tcx5/6* seedlings despite being bound by TCX5. Notably, genomic reporter lines revealed no detectable ALY3 (Hansen, 2022) and LIN37B expression in meiocytes (Supplementary Figure 2.7B), whereas LIN37A showed an expression and localization pattern resembling ALY1, decorating chromosomes throughout meiotic division (Supplementary Figure 2.7A). Plant-specific DREAM components *FLIC, FLAC, BTE1*, and *BTL1* all exhibited significantly elevated expression in the *tcx5/6* background, and *BTE1* and *BTL1* also in the *aly1/2* background. Moreover, *FLIC* and *FLAC* promoters were directly bound by TCX5 in both meiocytes and seedlings.

We were unable to obtain reliable expression values for *LIN52A* and *LIN52B*, likely due to inefficient unique read mapping caused by their high sequence similarity

(Fold change values for these genes stated as non-available in Table 2.2). Nevertheless, visualization of RNA-seq read alignments suggests reduced transcript abundance in *aly1/2* and *tcx5/6* meiocytes compared to WT, particularly for *LIN52A* (Supplementary Figure 2.8). However, this observation is not quantitative and does not allow us to determine whether the difference is statistically significant. However, CUT&Tag data reveals clear enrichment of TCX5-GFP at the promoter regions of both *LIN52A* and *LIN52B* in anthers, while no binding was detected in seedlings (Table 2.2 and Supplementary Figure 2.8).

Together, these findings indicate that ALY1/2 and TCX5/6 predominantly function as repressors of the MuvB core and associated plant-specific factors. This negative feedback regulation appears to be largely direct and is observed in both seedlings and anthers.

Table 2.2. DREAM complex components expression in *aly1/2* and *tcx5/6* mutants.

Differential expression (log_2FC, *padj*) of DREAM related genes in *tcx5/6* seedlings versus WT, TCX5 target status (+/–) from seedling ChIP (Ning *et al.*, 2020). Differential expression (log_2FC, *padj*) of DREAM related genes in *aly1/2* and *tcx5/6* male meiocytes versus WT, TCX5 target status (+/–) from anther CUT&Tag (this study). – : not targeted, + : TCX5 target, NA indicates data not available.

			Seedling data (Ning *et al.* 2020)			**Male meiocytes and anthers (This study)**				
			tcx5/6		**TCX5**	***aly1/2***		***tcx5/6***		**TCX5**
	Gene ID	Name	log_2FC	*padj*	**ChIP**	log_2FC	*padj*	log_2FC	*padj*	**CUT&Tag**
MuvB-core DREAM components	AT5G27610	ALY1	2.7065	4.6247E-75	+	-3.7063	0.15601667	1.7271	5.29E-17	+
	AT3G05380	ALY2	1.0110	1.8512E-18	+	-7.3484	8.987E-104	1.0370	2.37E-12	+
	AT3G21430	ALY3	0.5103	1.6825E-05	-	0.0349	0.95198935	0.3623	0.05930403	-
	AT4G29000	TCX5	-0.9808	8.3222E-06	+	0.7086	0.00214916	-0.4777	0.09329362	+
	AT2G20110	TCX6	2.2686	5.4041E-32	+	1.5058	1.5566E-16	0.4116	0.36288955	+
	AT1G04930	LIN37A	0.8185	0.01458289	+	0.6957	0.00032612	0.9707	5.04E-07	+
	AT2G32840	LIN37B	0.4243	0.12928802	+	0.4248	0.48478061	0.7570	0.05596831	-
	AT2G45250	LIN52A	NA	NA	-	NA	NA	NA	NA	+
	AT4G38280	LIN52B	NA	NA	-	NA	NA	NA	NA	+
	AT5G65120	MSI1	1.1672	2.1294E-07	+	0.3277	0.18179794	0.8374	0.00000172	+
Plant-specific components	AT5G10110	FLIC	1.0941	2.2786E-08	+	0.4785	0.07135366	0.8369	0.0000605	+
	AT5G65120	FLAC	1.1672	2.1294E-07	+	0.3277	0.18179794	0.8374	0.00000172	+
	AT2G40630	BTE1	0.3768	0.06084218	+	0.7671	0.01979566	0.9633	0.00155493	-
	AT5G05240	BTL1	1.4310	2.9247E-17	+	1.2264	5.914E-10	1.5625	9.32E-15	-

Initial functional characterization of MYB3Rs in meiosis

Previous studies revealed via affinity purification and interaction assays that MYB3R1 and MYBR3 are components of the plant DREAM complex (Kobayashi, *et al.*, 2015; Lang *et al.*, 2021). In mitotic tissues, they bind RBR1, E2F/DP and the MuvB core to regulate the G_2/M transition. Here, I asked whether MYB3Rs similarly assemble into a DREAM complex during meiosis. To test this, I assessed fertility and chromosome behavior in loss-of-function mutants of repressive MYB3Rs (triple homozygous mutant *myb3r1/3/5*) and activator MYB3Rs (double homozygous mutant *myb3r1/4*) (Haga *et al.*, 2011; Kobayashi *et al.*, 2015) and used genomic reporter lines to determine their expression and localization during meiosis.

To evaluate fertility, I first quantified the seed set per silique. WT plants averaged 56 viable seeds per silique (Figure 2.8A), whereas *myb3r1/3/5* and *myb3r1/4* mutants averaged 50 and 41, respectively (*myb3r1/3/5* vs. WT, $p<0.001$; *myb3r1/4* vs. WT, $p<0.00001$). Next, pollen viability assays revealed a reduction from 99% viable pollen in WT to 94% in *myb3r1/3/5* ($p<0.0001$, Figure 2.8B). Additionally, both *myb3r1/3/5* and *myb3r1/4* populations displayed increased variance in pollen size, a hallmark of unbalanced chromosome segregation during meiosis (Figure 2.8B). These data indicate that loss of MYB3R function compromises both seed production and pollen viability.

Subsequently, to assess crossover formation, I estimated chiasma counts based on chromosome configurations at metaphase I, where *myb3r1/3/5* averaged 9.5 chiasmata per cell, indistinguishable from the 9.3 seen in WT, whereas *myb3r1/4* showed a significant increase to 10.0 ($n=39$ for WT, 22 for *myb3r1/3/5*, 34 for *myb3r1/4*; $p<0.001$).

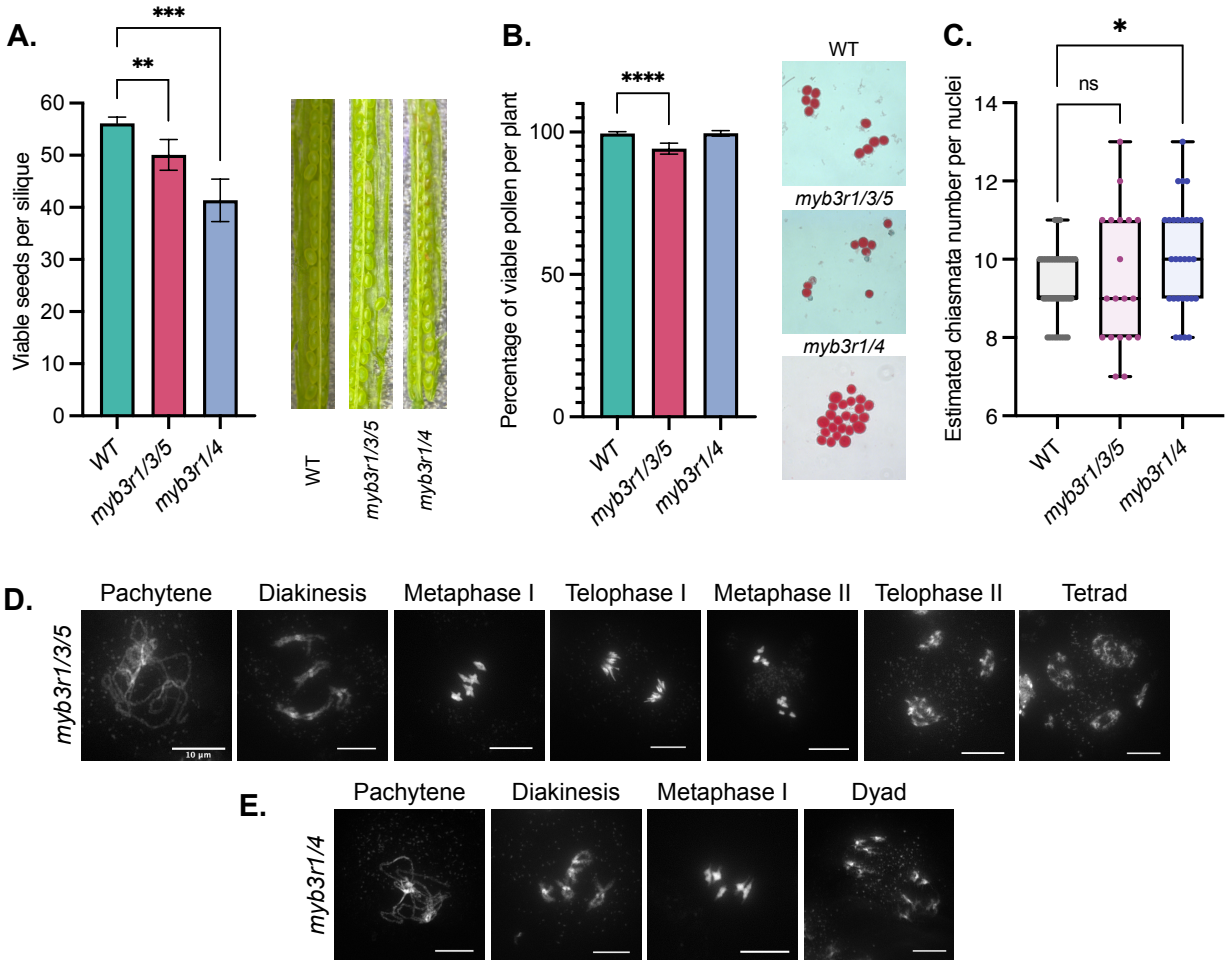


Figure 2.8. Reproductive and meiotic phenotypes of MYB3R mutants.

Seed **(A)** and pollen **(B)** viability assessment of WT, *myb3r1/3/5* and *myb3r1/4*. ** p<0.001, **** p<0.00001 **(C)** Estimated chiasma counts per cell at metaphase I (n=39 for WT; 22 for *myb3r1/3/5*; 34 for *myb3r1/4*). Bars indicate mean values; * p<0.01 (ONE-WAY ANOVA, Dunnett`s multiple comparisons test). **(D–E)** Representative meiotic stages in **(D)** *myb3r1/3/5* and **(E)** *myb3r1/4* mutants. Scale bars, 10 μm.

To determine whether MYB3R3 is present during meiosis, I examined a functional MYB3R3-mEGFP genomic reporter line (Kobayashi, *et al.*, 2015). As shown in Figure 2.9, the fusion protein is detectable as early as the S phase of pollen mother cells. During early prophase (zygotene) MYB3R3-mEGFP decorates the chromosomes, whereas in late prophase the signal disperses throughout the nucleoplasm. After nuclear-envelope breakdown the fluorescence is diffuse in the cytoplasm, with no distinct chromosomal enrichment. The mEGFP signal persist through the tetrad stage. This spatiotemporal pattern closely mirrors the chromosome-associated localization reported for the DREAM-core subunits TCX5/6 and ALY1.

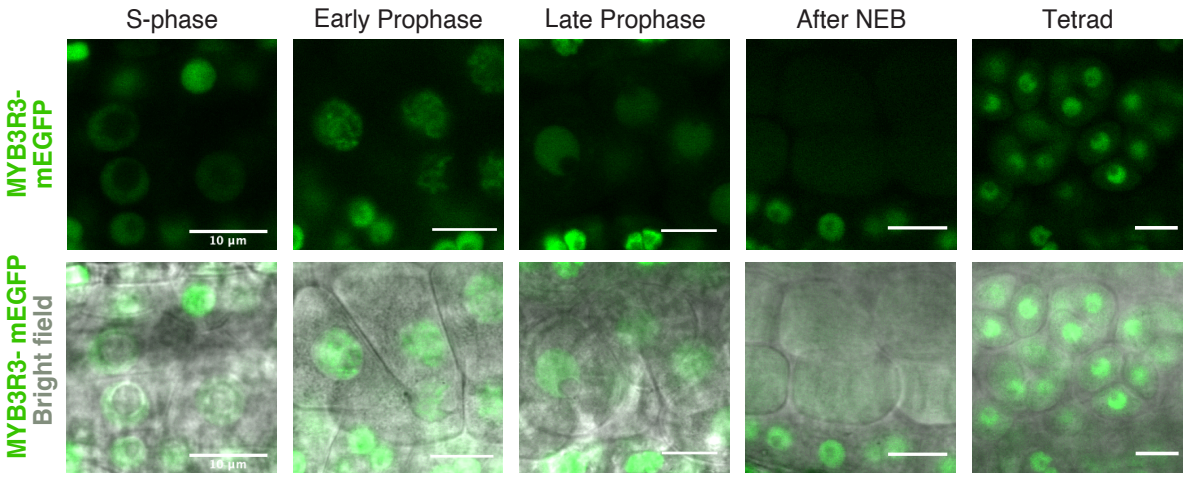


Figure 2.9. MYB3R3-mEGFP is expressed throughout meiosis and localizes to chromosomes.

Confocal images show MYB3R3–mEGFP fluorescence during S phase, early prophase, late prophase, post-NEB, and the tetrad stage. Bright field/fluorescence overlays are provided in the second row for context. Scale bars, 10 μm.

Together, these findings indicate that the MYB3R family possibly contributes to meiotic DREAM-like complexes that safeguard balanced chromosome segregation and gamete viability. Loss of the repressive MYB3Rs (*myb3r1/3/5*) compromises male fertility by causing unbalanced chromosome segregation and generating variance in pollen size, yet do not affect cross over formation unlike *aly1/2* and *tcx5/6* mutants. In contrast, loss of the activating MYB3Rs (*myb3r1/4*) elevates chiasmata numbers and might disrupt progression to meiosis II, resulting in an even stronger reduction in seed set.

The chromosome-associated MYB3R3-mEGFP signal in early prophase, mirroring ALY1 and TCX5/6, together with TCX5-dependent up-regulation of MYB3R1, MYB3R3, and MYB3R4 and TCX5 binding at their promoters in anther tissue (Supplementary Table 2.1), further supports the idea that MYB3Rs integrate with core DREAM components during male meiosis. These observations lay the groundwork for defining a bona fide meiotic DREAM complex.

3. DISCUSSION

The DREAM complex, a conserved transcriptional regulator of cell cycle processes, plays critical roles in meiosis as well. Although some of its somatic functions are well characterized, its composition and activity during meiosis remain largely unresolved. This uncertainty stems from the technical challenges of studying protein interactions in meiocytes, cells that are rare and difficult to isolate. Consequently, it is unclear whether the germline DREAM complex mirrors its somatic counterpart or adopts a meiosis-specific configuration. Despite these limitations, functional evidence suggests that DREAM components influence key meiotic processes.

In this chapter, I investigated the consequences of DREAM complex disruption in meiosis. My findings reveal a range of phenotypes, including defects in DSB repair, CO formation, meiotic synchrony, MT organization, and the duration of meiosis. These observations point to a multifaceted role for the DREAM complex in coordinating meiotic progression. The following sections discuss each of these aspects in detail, drawing connections between my results and broader mechanisms of germline regulation.

3.1. Regulation of DSB repair pathways by the DREAM complex

I discovered that anti-CO factors are upregulated in the absence of DREAM complex components via RNA-seq experiments using isolated meiocytes. Concurrently, the Class I CO pathway appears to be downregulated, likely due to the absence of an activating version of the DREAM complex (Table 1.1, Figure 1.3). Additionally, the Class II CO pathway gene *MUS81* was found to be upregulated. These observations prompted me to investigate the functional significance of these transcriptional changes by analyzing the phenotypic consequences of disrupting these pathways in DREAM mutant backgrounds.

Given the reduced number of COs observed in *tcx5/6* mutant combined with *mus81*, it is likely that the Class II CO pathway becomes upregulated in *tcx5/6* to compensate for the downregulation of *MER3*, i.e. the ZMM pathway. This

compensatory activation does not appear to be directly regulated by the DREAM complex, as no TCX5 enrichment was detected in the *MUS81* promoter region.

Aberrant recombination intermediates can result in entrapment of chromosomes that become physically obstructed during segregation. In such cases, removal of these intermediates via NCO formation is crucial to allow proper chromosome segregation. Unresolved chromosome entanglements, visible at metaphase I, leads to chromosome fragmentation in anaphase I. Interestingly, in *aly1/2 fancm* and *tcx5/6 fancm* double mutants, the CO defects are rescued, as reflected by an increased average number of bivalents per cell (Figure 2.1A,B). However, this restoration is accompanied by increased chromosome entanglements at metaphase I (Figure 2.1A, right panel). This suggests that in the absence of FANCM, abnormal recombination intermediates may accumulate, leading to defective chromosome segregation.

Additionally, in *aly1/2*, loss of RECQ4A/B restores CO levels with only a mild increase in entanglement, in contrast to the more pronounced effects seen in *aly1/2 fancm* (Figure 2.1B). This raises the question of whether FANCM and RECQ4A/B act on similar recombination intermediates, though they are known to function in parallel pathways. If so, these results suggest that, in the *aly1/2* background, FANCM-preferred substrates may preferentially accumulate.

However, the role of RECQ4A/B differs significantly between *aly1/2* and *tcx5/6* backgrounds. In the *tcx5/6 recq4ab* combination, severe chromosome fragmentation occurs at metaphase I, resulting in meiotic arrest and complete sterility (Figure 2.1A,B and Supplementary Figure 2.1), while *aly1/2 recq4ab* restores CO formation to near WT levels. Given that *recq4ab* mutants typically restore COs in ZMM-deficient backgrounds, meiotic arrest phenotype in *tcx5/6 recq4ab* was unexpected. It suggests that *tcx5/6* mutants may harbor additional defects in DSB repair beyond impaired Class I CO formation due to downregulation of *MER3*. These underlying defects become unmasked in the absence of RECQ4A/B, supporting the idea that DREAM mutants accumulate abnormal recombination intermediates that are normally resolved through anti-CO repair pathways. Notably, the absence of TCX5 enrichment in

FANCM and *RECQ4A/B* promoters indicates that *FANCM / RECQ4A/B* upregulation is likely independent of direct DREAM-mediated transcriptional control (Figure 2.1C).

According to literature, in *Arabidopsis*, *RECQ4A* and *RECQ4B* act to suppress excess COs but are not involved in resolving recombination intermediates (Higgins *et al.*, 2011). Instead, *RMI1* and *TOP3α* perform this role, functioning independently of their association in the RECQ4A/B–TOP3α–RMI1 (RTR) complex. Single mutants for RMI1 and TOP3α exhibit aberrant chromosome configurations at metaphase I (Hartung *et al.*, 2008; Séguéla-Arnaud *et al.*, 2017), resembling those seen in *aly1/2 fancm* and *aly1/2 recq4ab*.

In my observations, *recq4ab* mutants also exhibited entangled chromosomes at metaphase I, followed by chromosome fragmentation at anaphase I (Figure 2.1A,B and Supplementary Figure 2.1A). Notably, this phenotype was not reported in previous studies using the same insertion lines for *RECQ4A/B* (Hartung *et al.,* 2007; Séguéla-Arnaud *et al.*, 2015b; Jing *et al.*, 2025). Interestingly, although *recq4ab* mutants display fragmentation at anaphase I, *mer3 recq4ab* mutants recover CO formation without inducing fragmentation or entanglement (Supplementary Figure 2.2). This indicates that in ZMM-deficient backgrounds, Class II CO compensation does not inherently lead to aberrant chromosome interactions.

In *tcx5/6* combinations with *fancm* or *recq4ab*, however, fragmentation occurs in addition to entanglement, with *tcx5/6 recq4ab* showing the most extreme phenotype (Figure 2.1A, right panel and Supplementary Figure 2.1C). This suggests that the defects in *tcx5/6* are not solely due to unresolved entanglements, but also to impaired DSB processing. While fragmentation due to chromosome entanglements typically manifest at anaphase I, the fragmentation seen at metaphase I in *tcx5/6 recq4ab* indicates a failure in DSB repair or in the resolution of joint molecules and other recombination intermediates. Consistently, the fragmentation observed in *tcx5/6 recq4ab* mutants mirrors the phenotype of *com1* mutants (Uanschou *et al.*, 2007), in which DSBs remain unprocessed.

Notably, sites of entanglement are often associated with axis disassembly and diffuse chromatin (Holm and Rasmussen, 1980). Given the interdependence of

chromosome pairing and axis assembly, the unpaired configurations seen in DREAM mutants (Figure 1.1E; g,m) may reflect failures in axis stabilization due to entanglement.

Further investigation is needed to assess whether entanglements arise as interlocks during pachytene, and whether their nature and frequency differs between *aly1/2*, *tcx5/6* and WT. Combining these mutants with *spo11*, eliminating meiotic recombination via the absence of programmed DSBs, could help determine whether the observed defects are rooted in meiotic recombination machinery. Data in this chapter indicates that this is the case, as entanglement frequencies decrease in *aly1/2 tcx5/6* (Figure 2.7C,D) and *tcx5/6 mus81 (*Figure 2.2B,C*)* backgrounds where CO levels are reduced, and increase in *aly1/2 fancm* (Figure 2.1A,B) and *MER3* overexpression lines where COs are restored (Figure 1.3).

Taken together, these findings suggest that DREAM mutants exhibit multiple defects in meiotic DSB repair, which likely triggers a feedback mechanism that upregulates both Class II CO pathways as well as the anti-CO pathways, possibly due to guard a balance. When this balance is perturbed, as in *tcx5/6 mus81* and *tcx5/6 recq4ab* mutants, meiotic abnormalities become more severe. Among these, the meiotic arrest and fragmentation observed in *tcx5/6 recq4ab* represent the most striking phenotype, highlighting the DREAM complex's critical role in safeguarding meiotic recombination fidelity.

3.2. Progression and duration of meiosis in the absence of MuvB-core DREAM components

To investigate the dynamics of meiotic progression in MuvB-core DREAM complex mutants, I performed live-cell imaging using REC8-mEGFP and TagRFP:TUA5 reporter lines (Prusicki *et al.*, 2019). In addition to analyzing *aly1/2* and *tcx5/6*, which show strong fertility and meiotic defects, I also included the *lin37ab* double mutant in this analysis. Although *lin37ab* does not exhibit overt fertility defects (Figure 1.1A-D) or meiotic mutant phenotype that could be revealed by fixed specimen, I aimed to determine whether subtle alterations in meiotic timing or dynamics could still be detected under live conditions.

The live cell imaging-based timing revealed distinct stage-specific effects. In *tcx5/6,* meiosis was consistently prolonged across nearly all stages, with significant delays from late leptotene through diakinesis, while metaphase I through anaphase I progressed at WT-like speed (Figure 2.3). In contrast, *aly1/2* showed mostly WT-like progression, except for a notably shortened pachytene to diakinesis**.** Surprisingly, *lin37ab* exhibited altered timing in meiotic progression, with faster transitions through pachytene - diakinesis, metaphase I - anaphase I and metaphase II - anaphaseII, and delayed timing in late leptotene - early pachytene compared to wild-type, despite the lack of visible fertility or chromosomal defects.

These results indicate that different DREAM subunits have distinct roles in regulating meiotic timing. A prolonged prophase I in *tcx5/6* may reflect delays caused by aberrant or unresolved recombination intermediates. In yeast, disruption of the ZMM pathway results in recombination blocks and checkpoint-induced arrest in prophase I, especially under stress conditions such as elevated temperature (Börner, Kleckner and Hunter, 2004). Likewise, unresolved recombination intermediates have been shown to delay nuclear division and cause chromosomal fragmentation (Tang *et al.*, 2015; Kaur, GN and Lichten, 2019; De Jaeger-Braet *et al.*, 2022). This interpretation aligns with the exacerbated chromosomal fragmentation and entanglement observed in *tcx5/6 recq4a recq4b*, suggesting that TCX5/6 activity is especially important for proper processing or resolution of recombination structures (Figure 2.1A).

Although transcriptional misregulation of meiotic cyclins and CDKs could contribute to the observed delays, the expression of TAM (CYCA1;2),a key cyclin required for proper meiotic timing (Magnard *et al.*, 2001; d'Erfurth *et al.*, 2010), was not significantly altered in *tcx5/6*. However, several other regulators of the meiotic cell cycle were differentially expressed in this mutant. Notably, *CDKA;1* was downregulated, while *CDKD;1, CYCA2;1, CYCA2;3, CYCA2;4,* and *CYCB3;1* were upregulated. In addition, SDS, a meiosis-specific cyclin-like protein crucial for DSB formation and crossover establishment (Azumi *et al.*, 2002), was downregulated, and both *OSD1* and *TDM1* (Bulankova *et al.*, 2010; Cromer *et al.*, 2012; Cifuentes *et al.*, 2016), which function in the meiotic exit network, were upregulated (Table 2.1). While

these changes point to widespread dysregulation of cell cycle control in *tcx5/6*, the precise outcome of these opposing transcriptional shifts is impossible to predict. Most functional insights into these genes come from loss-of-function mutant phenotypes, leaving open questions about how their overexpression or partial downregulation misregulation affects meiotic timing and fidelity. Our observations suggests that a more complex regulatory network is perturbed in *tcx5/6*, and its impact likely extends beyond individual gene effects to broader miscoordination of meiotic transitions.

Live imaging in addition revealed that *tcx5/6* meiocytes often proceeded through meiosis asynchronously, with clear variation in meiotic stage progression between cells within the same anther lobe (Figure 2.4 and Figure 2.5). Such asynchrony was not detected in WT, *aly1/2*, or *lin37ab* meiocytes (Supplementary Figure 2.5), possibly indicating a specific requirement for TCX5/6 in coordinating temporal fidelity across meiocytes. However, as *aly1/2* does not abolish all *ALY* function due to the presence of *ALY3*, it is possible, that the asynchrony phenotype was not observed due to residual ALY activity.

Synchrony among meiocytes is a well-established feature in flowering plants (Armstrong and Jones, 2003; Nonomura *et al.*, 2011). In Arabidopsis, TAM/CYCA1;2 has also been implicated in maintaining meiotic synchrony, with tam mutants showing slowed and less coordinated meiotic progression (Magnard *et al.*, 2001; Wang *et al.*, 2004). However, as TAM transcript levels were unchanged in *tcx5/6* (Table 2.1), it is likely not causative for the synchrony defects in this mutant. Still, the observed asynchrony in *tcx5/6* may result from the deregulation of other cell cycle regulators, including the several cyclins and CDKs that were differentially expressed in *tcx5/6* male meiocytes compared to wild type.

A *tcx5/6* comparable asynchrony phenotype is also seen in the *FEHLSTART (fst-1)* mutant, where premature meiotic entry leads to temporal uncoupling between meiocytes and is accompanied by abnormal spindle structures and asymmetric cell divisions (Li *et al.*, 2015). While *FST* is also not deregulated in our DREAM mutants (REF), it is tempting to speculate that the misregulation of cell cycle regulators detected in *tcx5/6* could likewise cause an uneven meiotic entry into meiosis leading

to asynchrony. In addition, the spindle defects observed in *tcx5/6*, such as tripolar spindles and disrupted MT arrays (Figure 2.6), could further reinforce asynchrony by altering the meiotic progression of individual meiocytes.

Together, this supports the idea that TCX5/6 is required for synchronized male meiosis**,** likely by maintaining transcriptional control over genes that coordinate meiotic entry, progression, and spindle organization.

The reasons for spindle defects in *tcx5/6* are so far unknown. The transcriptome data reveal several genes related to microtubule organization as deregulated in *tcx5/6*, some of which are direct TCX5 targets in anthers. However, also CDKA;1, which has previously been shown to be critical for meiotic spindle organization and bipolar spindle formation (Sofroni *et al.*, 2020), is downregulated in *tcx5/6* (Table 2.1). Thus the observed phenotypes might also reflect a broader disruption in the regulatory network that ensure proper MT organization and behaviour and nuclear partitioning during meiosis.

Together, these findings highlight the multifaceted role of TCX5/6 in orchestrating male meiosis. Its absence results in prolonged meiotic stages, loss of synchrony among meiocytes, and severe defects in spindle organization. While other core DREAM components like ALY1/2 and LIN37A/B influence specific stages or timing subtly, TCX5/6 emerges as a central regulator ensuring coordinated progression and structural fidelity of meiosis.

3.3. The functional interplay between ALYs and TCXs

To better understand the functional interplay between ALY and TCX, I examined their localization dependencies and found that TCX5/6 requires ALY1/2 for efficient chromosomal localization (Figure 2.7A). In addition to their shared meiotic phenotypes, ALY and TCX appear to be mutually required for repression of each other's expression, likely acting together as a repressive DREAM complex also in meiosis (Figure 2.7B and Supplementary Figure 2.6). Nevertheless, the precise nature of the functional interaction between ALY and TCX remains to be elucidated.

In Arabidopsis, the somatic DREAM complex includes ALY and TCX proteins, which both possess putative DNA-binding domains: a MYB domain in ALY (Bhatt *et al.*, 2004) and two cysteine-rich CXC domains in TCX (Andersen *et al.*, 2007). CXC domains have been widely implicated in sequence-specific DNA binding, yet the precise roles of these domains in Arabidopsis remain unclear. In primary human cells, the TCX5/6 homolog LIN54 binds DNA through its CXC domains (Schmit, Cremer and Gaubatz, 2009; Asthana *et al.*, 2022; Koliopoulos *et al.*, 2022), and mutation of two conserved cysteine residues (C525 and C527) disrupts this interaction. Similarly, mutation of the equivalent residue in TSO1, a TCX family member involved in flower development, impairs floral morphogenesis and cell division in Arabidopsis (W. Wang *et al.*, 2018). These findings support the hypothesis that TCX5 and TCX6 can also bind DNA via their CXC domains. Nonetheless, the functional importance of these domains in Arabidopsis meiosis remains to be determined, as does the question of whether ALY and/or TCX is responsible for guiding the DREAM complex to its genomic targets in male meiocytes.

The MYB domain–containing ALY is unique to plants (Bhatt *et al.*, 2004). In mammals, LIN9 does not bind DNA directly but serves as a scaffold to recruit other DNA- and chromatin-binding subunits such as LIN54 (Esterlechner *et al.*, 2013; Asthana *et al.*, 2022; Koliopoulos *et al.*, 2022). In *C. elegans*, LIN9 is recruited to chromatin through LIN-54 (Harrison *et al.*, 2006), and in Drosophila, the tMAC component Aly lacks a recognizable DNA-binding domain (Jiang and White-Cooper, 2003; Jiang *et al.*, 2007). Instead, chromatin-associated subunits like Topi and

Achi/Vis require interaction with Aly and Comr for nuclear entry, but they mediate chromatin localization. Although Arabidopsis ALY contains a MYB domain, its functional relevance remains uncharacterized. To assess whether ALY can directly bind DNA, DAP-seq experiments could be informative.

A key question is whether ALY1/2 and TCX5/6 directly regulate the same targets. The phenotypic similarities between *aly1/2* and *tcx5/6* mutants, such as CO defects, impaired pairing and synapsis, and comparable meiotic transcriptome profiles, support the idea that they act in the same complex. Determining whether ALY1 and ALY2 bind DNA, and if so, where, is crucial for clarifying their direct regulatory roles. To this end, I performed a CUT&Tag assay using anthers from ALY1-mEGFP lines. However, we were unable to precipitate DNA, likely due to technical limitations such as inefficient tagging or inaccessibility of ALY1-mEGFP to the mEGFP antibody.

In seedlings, Ning et al. used ChIP-PCR to show that other DREAM components, including ALY3, MSI1, and LIN37B, are enriched at the transcription start sites of TCX5/6 target genes, suggesting that DREAM subunits act together to repress genes in seedlings. To understand whether ALY1/2 binds to TCX5 targets in anthers, ChIP-PCR can be used as an alternative to CUT&Tag in anthers.

To further investigate the ALY1/2 -TCX5/6 interplay, I analyzed their localization in reciprocal mutant backgrounds. TCX5/6 localization to chromosomes diminished in *aly1/2*, whereas ALY localization was unaffected in *tcx5/6* mutants (Figure 2.7A). This dependency of TCX5/6 on ALY1/2 is consistent with observations in other organisms: in mice, TESMIN (the TCX5/6 homolog) is cytoplasmic in early spermatocytes and requires LIN9 for nuclear localization (Zhang *et al.*, 2021); in *Drosophila*, Tomb (TCX5/6 homolog) depends on Aly and Comr for nuclear stability (Jiang and White-Cooper, 2003; Jiang *et al.*, 2007). However, this dependency appears somewhat contradictory to the phenotypic severity, which *tcx5/6* mutants exhibit more pronounced meiotic defects than *aly1/2* mutants. For instance, loss of COs in *tcx5/6* is larger than in *aly1/2* (Figure 1.1), and the level of transcriptional regulation showed greater fold change in *tcx5/6* vs WT than in *aly1/2* vs WT (Table 2.1, Table 2.2).

Additionally, *tcx5/6* showed meiotic defects that are not observed in *aly1/2*, such as extreme DSB repair defects in *tcx5/6 recq4ab* (Figure 2.1), abnormal MT organization (Figure 2.6), meiotic asynchrony (Figure 2.4), and extended meiotic duration (Figure 2.3). Several explanations may account for these observations: I) ALY3 might partially compensate the absence of ALY1/2. Although ALY3 is not normally expressed in WT meiocytes, its expression might be upregulated in the *aly1/2* background. This hypothesis could be tested by analyzing ALY3 expression in *aly1/2* meiocytes and generating a meiosis-specific ALY3 knockout in the *aly1/2* background. II) In *aly1/2* mutants, residual chromosome localized TCX5/6 might still be sufficient for its function as transcriptional regulator. Indeed TCX5/6 still localize to the nucleus in the absence of ALY1/2, albeit with weaker chromosomal association (Figure 2.7A).

Interestingly, *aly1/2/3* mutant is embryonic lethal (Ning *et al.*, 2020), whereas *tcx5/6* mutant is viable despite severe meiotic defects. One possible explanation for this observation is that TCX5 and TCX6 are not fully knocked out in the double mutant as expression analyses show that parts of their C-terminal regions remain expressed (Supplementary Figure 2.6), potentially producing partially functional proteins. An alternative explanation is the involvement of a third TCX protein in the meiotic DREAM complex. TCX7, the most closely related homolog to TCX5/6 (Andersen *et al.*, 2007), is upregulated in *aly1/2* and *tcx5/6* meiocytes and is a known TCX5 target in seedlings and anthers (Supplementary Table 2.1). Although TCX7 is not found to be associated with the DREAM complex in seedlings, it becomes upregulated in the absence of TCX5/6, which could explain the viability of *tcx5/6* mutants compared to the lethality of *aly1/2/3*. Therefore, *tcx5/6/7* triple mutants can be generated to examine whether TCX7 might have redundant roles with TCX5/6.

Finally, the *aly1/2 tcx5/6* quadruple mutant exhibits a more severe phenotype than either double mutant alone. This synergy could be explained by a slightly destabilized DREAM complex in either double mutant, while the disruption of both components might lead to a more severely compromised complex. Alternatively, the enhanced phenotype could reflect the deregulation of distinct targets within the same biological pathway, resulting in complete failure of the process only when both sets of targets are simultaneously affected.

Collectively, these findings indicate that ALY and TCX proteins form a functional unit that is essential for the proper activity of the meiotic DREAM complex in Arabidopsis. While both protein families exhibit putative DNA-binding domains, the precise mechanisms by which they influence chromatin targeting and transcriptional repression remain unresolved. Future technically challenging experiments, including DNA-binding assays, interaction mapping in meiocytes will be crucial to more precisely define the composition and targets of the meiotic DREAM complex(es).

3.4. The meiosis-specific DREAM complex

The composition of the Arabidopsis DREAM complex has been characterized in somatic tissues (Kobayashi *et al.*, 2015; Ning *et al.*, 2020; Lang *et al.*, 2021); however, its roles in reproduction, particularly during meiosis, remain largely unexplored. In this study, I identified roles for the core DREAM components ALY1/2 and TCX5/6 in the transcriptional regulation of male meiosis. Nevertheless, the exact composition of the "meiotic DREAM complex" may differ from that in seedlings. It is therefore plausible that a subset of the canonical complex, or a modified version of it, mediates regulatory functions unique to meiotic progression.

Whether the architecture of the somatic DREAM complex is conserved in the germline, or whether meiosis-specific subunits or post-translational modifications alter its structure and activity, remains unknown. A significant challenge in addressing this question is the technical difficulty of performing protein-protein interaction assays in isolated meiocytes. These cells are rare, transient, and embedded within complex tissues, complicating their isolation and biochemical characterization. Moreover, the dynamic nature of meiosis likely necessitates high temporal resolution to capture stage-specific or transient interactions.

To identify the core components of the meiotic DREAM complex, germline-specific proximity labeling using ALY1/2 or TCX5/6 could be informative. A recent study in mice used germline-specific proximity labeling to identify TESMIN-associated proteins, revealing that MYBL1, LIN9, and LIN37 interact with TESMIN in the germline (Oura *et al.*, 2022). Inspired by this, we attempted to generate meiosis-specific constructs expressing ALY1 and LIN37A fused to TURBO-ID and GFP under control

of the *DMC1* promoter. However, these constructs also showed expression in the surrounding tapetal cells, indicating insufficient meiotic specificity despite using a meiosis-associated promoter (Flores Sanchez, 2024).

Despite current limitations in identifying meiosis-specific DREAM interactions, reverse genetics and comparative expression analyses, possibly revealing feedback mechanisms, can provide insights into candidate components of the meiotic DREAM complex. For instance, assessment of pollen and seed viability showed no obvious reproductive defects in *lin37ab* and *lin52ab* mutants (Figure 1.1), suggesting that these components may not be essential for DREAM function during meiosis or may not participate in the meiotic DREAM complex.

In contrast, I demonstrated that MYB3R3 is expressed and localizes to chromosomes during meiosis (Figure 2.9), and that *myb3r1/3/5* triple mutants exhibit defects in meiosis II (Figure 2.8D), leading to unbalanced chromosome segregation. I also examined MYB3R4 expression using GFP-MYB3R4 reporter lines, but the signal was too weak to be detected in meiocytes or surrounding tapetal cells. (data not shown) Nevertheless, the presence of irregular pollen sizes in *myb3r1/4* mutants (Figure 2.8) and the difficulty in identifying meiosis II stages suggest that some meiocytes may skip the second division, potentially producing diploid pollen. This points to a possible role for MYB3R4 in regulating meiosis II as well.

Notably, TCX5 is enriched at the promoter regions of *MYB3R1*, *MYB3R3*, and *MYB3R4* in anthers (Supplementary Table 2.1), and all these genes are upregulated in *tcx5/6* male meiocytes. This suggests a possible negative feedback loop mediated by the DREAM, implying that these MYB3Rs could themselves be components of the meiotic DREAM complex.

Further evidence for a similar composition of somatic and meiotic DREAM complexes comes from previous work conducted under my supervision, which showed that FLIC and FLAC are expressed and localize to the nucleus after late pachytene (Flores Sanchez, 2024). Interestingly, *flic flac* double mutants exhibit chromosome segregation defects during meiosis II, often forming triads instead of tetrads, resembling the *myb3r1/3/5* phenotype. These defects may contribute to the reduced

seed viability observed in *flic flac* mutants (Lang *et al.*, 2023). Additionally, both *FLIC* and *FLAC* are differentially expressed in *tcx5/6* meiocytes and are directly bound by TCX5 in anthers (Supplementary Table 2.1), supporting their potential role as DREAM components in reproductive tissue.

Additionally, mEGFP-BTE1 is expressed and localizes to chromosomes throughout meiosis, while BTL1-mEGFP expression is restricted to the leptotene stage (Flores Sanchez, 2024). Expression of *BTE1* and *BTL1* is also upregulated in *aly1/2* and *tcx5/6* meiocytes, however they have not been identified as TCX5 targets in anthers. It will be informative to assess their role in meiosis by observing whether *bte1 btl1* double mutants exhibit meiotic defects similar to those of *aly1/2* and *tcx5/6*.

Together, the differences in phenotypes and expression patterns for different DREAM complex components suggest that the composition of the DREAM complex(es) in meiotic cells is variable depending on time and target, potentially involving meiosis-specific factors or modified associations of core components. While technical limitations currently hinder a comprehensive biochemical characterization, this thesis provides an extensive framework for understanding DREAM function in meiosis by integrating genetic, expression, and localization data. However, further refinement of techniques to characterize cell type specific transcriptional complexes and their DNA interaction sites, such as proximity labeling and CUT&Tag assays tailored for meiocytes will be essential to eventually unravel the full meiotic DREAM.

4. MATERIAL AND METHODS

4.1. Plant materials and growth conditions

Arabidopsis thaliana accession Columbia (Col-0) was used as the wild-type reference in all experiments. All mutant and transgenic lines employed in this study were in the Col-0 background. T-DNA insertion lines *tcx5-1* (SALK_047165), *tcx6-1* (GK-453H07), *aly1-1* (SALK_073108), *aly2-2* (SALK_118765C), *lin37a-2* (SALK_057175), *lin37b-3* (SALK_103139C), and *mus81-2* (SALK_107515) were obtained from the GABI-KAT, SAIL, and SALK T-DNA collections. Double and triple homozygous mutant lines *myb3r1/4* and *myb3r1/3/5* were kindly provided by Masaki Ito, as previously described by Kobayashi *et al.* (2015). The mutant lines *fancm-1*, *recq4a-4* (GABI_203C07), and *recq4b-2* (SALK_011357) lines were kindly provided by Raphaël Mercier and have been previously described (Crismani *et al.*, 2012; Séguéla-Arnaud *et al.*, 2015b).

A transgenic line expressing *PRO$_{REC8}$:REC8:mEGFP* and *PRO$_{RPSA5}$:TagRFP:TUA5*, developed for live-cell imaging (Prusicki *et al.*, 2019), was crossed with *tcx5/6*, *aly1/2*, and *lin37ab* double mutants to generate lines combining these reporters with the respective DREAM mutant backgrounds. A genomic MYB3R3-GFP reporter line, also kindly provided by Masaki Ito, was used as previously described (Kobayashi *et al.*, 2015). All plants were cultivated in controlled growth chambers under long-day conditions (16 h light at 21°C / 8 h dark at 18°C) with 60% relative humidity.

4.2. Plasmids and plant transformation

The construction of the plasmids *PRO$_{ALY1}$:ALY1:mEGFP*, *PRO$_{TCX5}$:mEGFP:TCX5* and *PRO$_{TCX6}$:mEGFP:TCX6* and as well as the plant transformation procedure, were previously described in Chapter I. The genomic reporter construct *PRO$_{ALY1}$:ALY1:mEGFP* was introduced into *tcx5* heterozygous *tcx6* homozygous plants. Homozygous *tcx5/6* double mutants were subsequently selected in the following generation to monitor ALY1-GFP expression and localization. Similarly, *PRO$_{TCX5}$:mEGFP:TCX5* and *PRO$_{TCX6}$:mEGFP:TCX6* constructs were introduced into *aly1* heterozygous *aly2* homozygous mutant plants. Double homozygous mutants carrying the respective reporter constructs were identified in the next generation and

used expression and localization analysis. For each construct, a total of 10 independent transgenic lines were analyzed.

4.3. Genotyping

Genomic DNA was extracted from the leaves of 1 week-old Arabidopsis thaliana plants. The leaves were put in 2 ml Eppendorf tubes with 2 metal beads in 400 µl magic buffer (50 mM Tris HCl (pH 7.5), 300 mM NaCl and 300 mM sucrose). Samples were homogenized using a Retsch mill at 25 rpm for 2 minutes. The tubes were then centrifuged at 14,000 rpm for 10 minutes, and the resulting supernatant, containing the extracted genomic DNA, was transferred to a fresh tube and stored at –20 °C.

Genotyping PCR was performed using either DreamTaq DNA polymerase (DreamTaq Green PCR Master Mix, 2X; Thermo Fisher Scientific, CAT# K1081) or Terra™ Direct PCR Polymerase Mix (2X; Takara Bio Inc., CAT# 639271). Each reaction contained the polymerase mix, 100 mM each of forward and reverse primers, and 1 µl of genomic DNA. Reactions were carried out in a thermocycler using protocol settings specific to each polymerase (Table 2.3).

PCR products were resolved by agarose gel electrophoresis on a 1% gel prepared with 1× TEA buffer (40 mM Tris-acetate, 2 mM EDTA) and stained with ethidium bromide (100 ng/ml). Electrophoresis was conducted at 120 V for 30–40 minutes. The sequences of genotyping primers are listed in Appendix Table 1.

Table 2.3. PCR program using DreamTaq or Terra polymerase. * Annealing temperature can change depending on primer pairs used.

Step	Time (DreamTaq/Terra)	Temperature (°C) (DreamTaq/ Terra)
1. Initial denaturation	5 min/2 min	95/98
2. Denatureation	30sec/10 sec	95/98
3. Primer annealing	30 sec/5 sec	55*
4. Elongation	1 min/kb	72/68
Repeat steps	30-35 cycles	
5. Final elongation	5 min	72/68
6. Hold	∞	

4.4. Pollen and seed viability assessment

Pollen and seed viability assays were conducted as described in Chapter I.

4.5. Cell spreads

Acid spreads were performed to monitor meiotic progression, following the protocol described in Chapter I. This technique allows for the visualization of meiotic chromosome behavior and staging. Detailed procedures for sample preparation, fixation, and staining are provided in the Methods section of Chapter I.

4.6. Confocal microscopy

To detect protein localization, young anthers from floral buds of the respective reporter lines were dissected in a drop of artificial pond water (APW) and imaged immediately. Imaging was performed using an upright Zeiss LSM900 confocal microscope equipped with a 60× water-immersion objective. Meiotic stages were identified based on chromosome morphology and cellular structure. GFP fluorescence was excited with a 488 nm laser and emission was detected within the 495–560 nm range.

4.7. Live cell imaging and quantitative analysisof the meiotic phases

Live-cell imaging was performed as previously described (Prusicki *et al.*, 2019). Time-lapse imaging was conducted at intervals of 10 minutes for REC8-GFP TagRFP-TUA5 in *aly1/2* and *lin37ab*, and 15 minutes for the same reporter in WT and *tcx5/6* backgrounds. At each time point, six Z-stacks were acquired with a spacing of 50 µm between planes. Due to sample movement during imaging, Z-planes were selected post-acquisition using the aMP imaging analysis and processing tool (Gosh, 2024), and XY drift was corrected using the StackReg plugin in Fiji (Version 2.14.0/1.54f).

The analysis of meiotic phase duration was based on the TagRFP-TUA5 reporter line. Meiocytes were manually classified into defined MT array states, corresponding to specific meiotic stages (Supplementary Figure 2.4). Phase duration was calculated from the number of time-lapse frames and the time interval between them. Only those meiotic stages for which both the onset and conclusion could be clearly observed were

included in the analysis. As a result, quantification was not possible for the early leptotene stage (MT array 1). Duration measurements were obtained from at least 40 meiocytes, representing a minimum of six anthers per genotype.

4.8. Transcriptome and CUT&Tag data anlaysis

Differentially expressed genes in *aly1/2* and *tcx5/6* male meiocytes relative to WT were analyzed in Chapter I as described in Methods. Specific subsets of these differentially expressed genes are listed in the present chapter. TCX5 target genes in anthers were identified using the CUT&Tag method. Sample and library preparation, as well as data analysis for the CUT&Tag experiment, were performed as described in the Chapter I Methods. JBrowse (Version 2.13.1) was used to visualize RNA-seq and CUT&Tag data at specific gene locus.

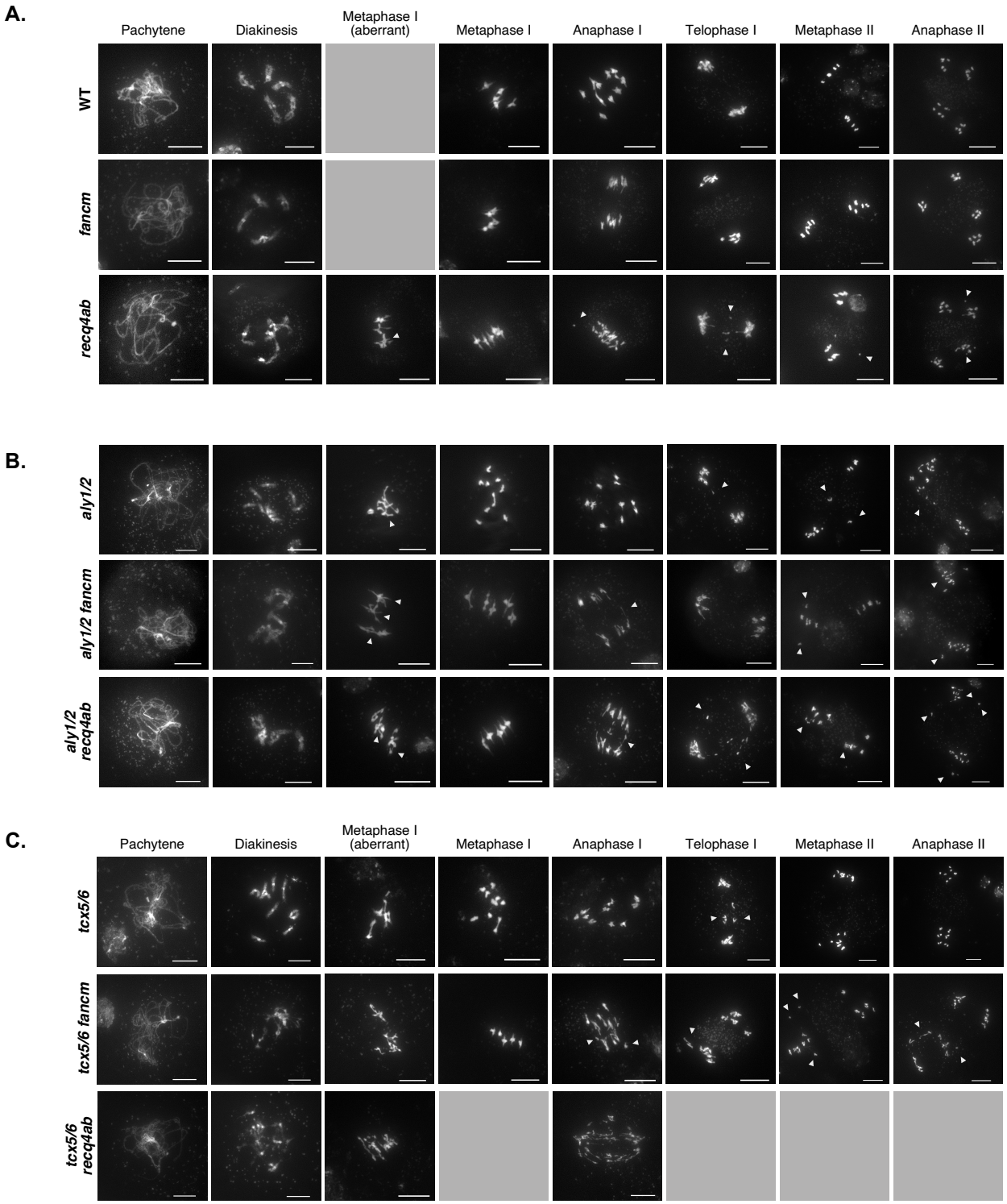
4.9. Statistical analysis

All statistical analyses and data visualizations were performed using GraphPad Prism 10 (version 10.4.2). To quantify the percentage of cells displaying a given number of bivalents, chromosome entanglement, or fragmentation within a genotype, the fraction of total analyzed cells was calculated.

For comparing bivalent numbers between genotypes, one-way ANOVA was used followed by Dunnett's T3 multiple comparisons test.

For each meiotic stage, genotype comparisons were performed using one-way ANOVA with Dunnett's post-hoc test, using WT as the control. Results were visualized as box-and-whisker plots showing the median, interquartile range, and minimum-to-maximum values. Outliers were defined as values outside 1.5 times the interquartile range and are indicated as individual points beyond the whiskers. All individual data points, each representing a single meiocyte, were plotted to ensure transparency. Statistical significance was defined as $p<0.05$.

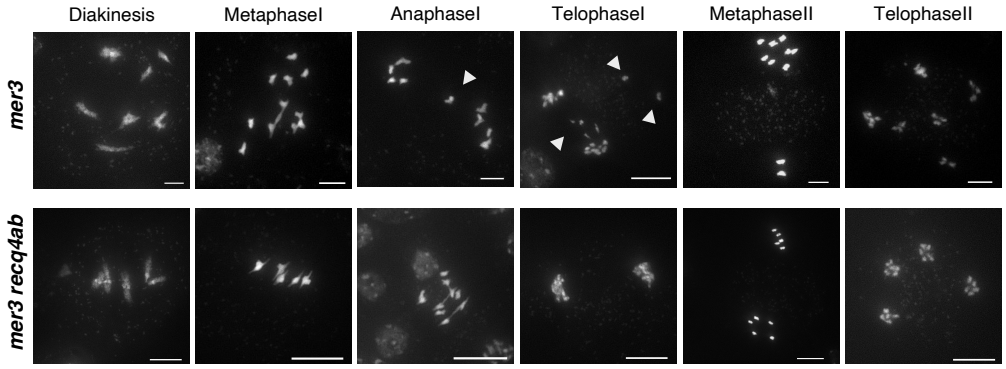
5. SUPPLEMENTAL DATA



Supplementary Figure 2.1. DREAM mutants display chromosome fragmentation and entanglement in their combination with *fancm* and *recq4ab*.

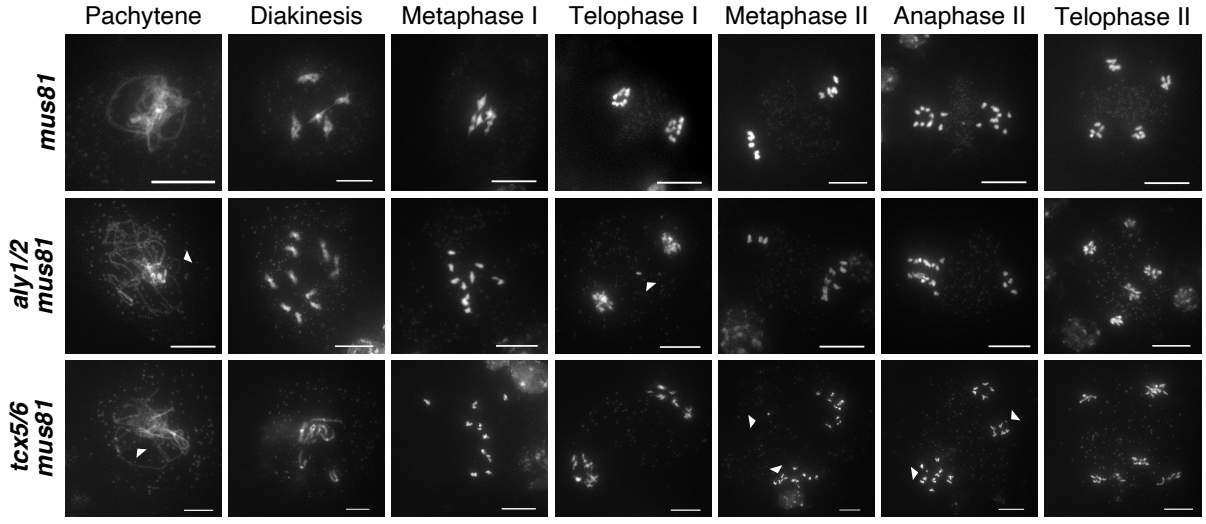
Representative pictures of pachytene, diakinesis, metaphase I (aberrant), metaphase I, anaphase I, telophase I, metaphase II and anaphase II in **(A)** WT (first row), *fancm* (middle row), *recq4ab* (bottom

row); **(B)** *aly1/2* (first row), *aly1/2 fancm* (middle row), *aly1/2 recq4ab* (bottom row); **(C)** *tcx5/6* (first row), *tcx5/6 fancm* (middle row), *tcx5/6 recq4ab* (bottom row). White arrow heads indicate chromosome entanglement at metaphase I (aberrant); chromosome fragmentation at anaphase I; lagging chromosomes and chromosome fragmentation at telophase I, metaphase II, and anaphase II. Sace bars, 10 μm



Supplementary Figure 2.2. Loss of RECQ4A/B recovers CO loss phenotype in *mer3.*

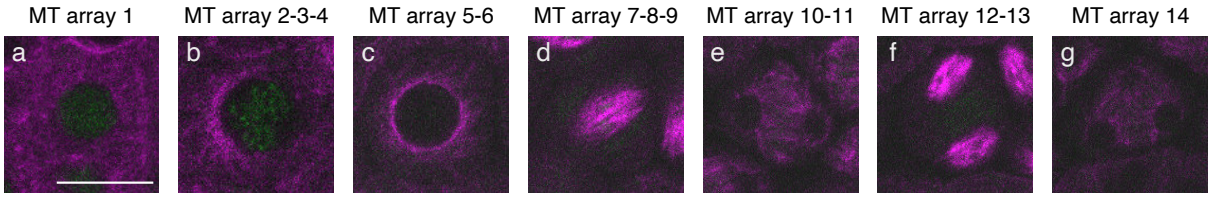
Representative pictures of diakinesis, metaphase I, anaphase I, telophase I, metaphaseII and telophase II in *mer3* (top row) and *mer3 recq4ab* (bottom row). Sace bars, 10 μm.



Supplementary Figure 2.3. Combination of *aly1/2* and *tcx5/6* with *mus81* elevates CO loss phenotype in DREAM mutants and chromosome segregation defects.

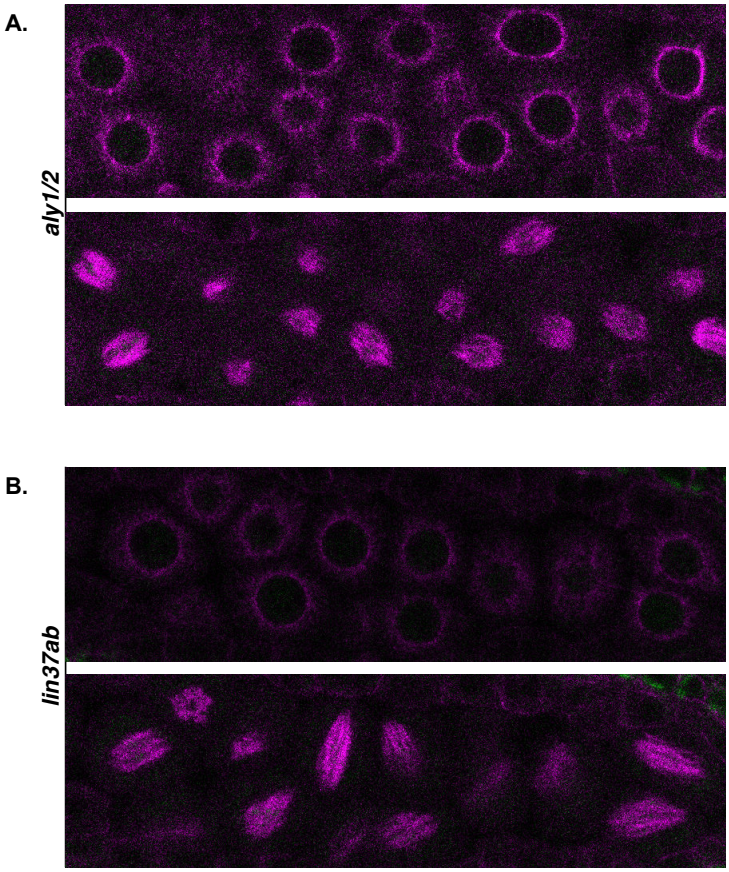
Representative pictures of pachytene, diakinesis, metaphase I, telophase I, metaphase II, anaphase II and telophase II in *mus81* (first row), *aly1/2 mus81* (middle row), and *tcx5/6 mus81* (bottom row). White

arrow heads mark unpaired regions in pachytene and chromosome fragmentation at metaphase II and anaphase II. Scalee bars, 10 μm.



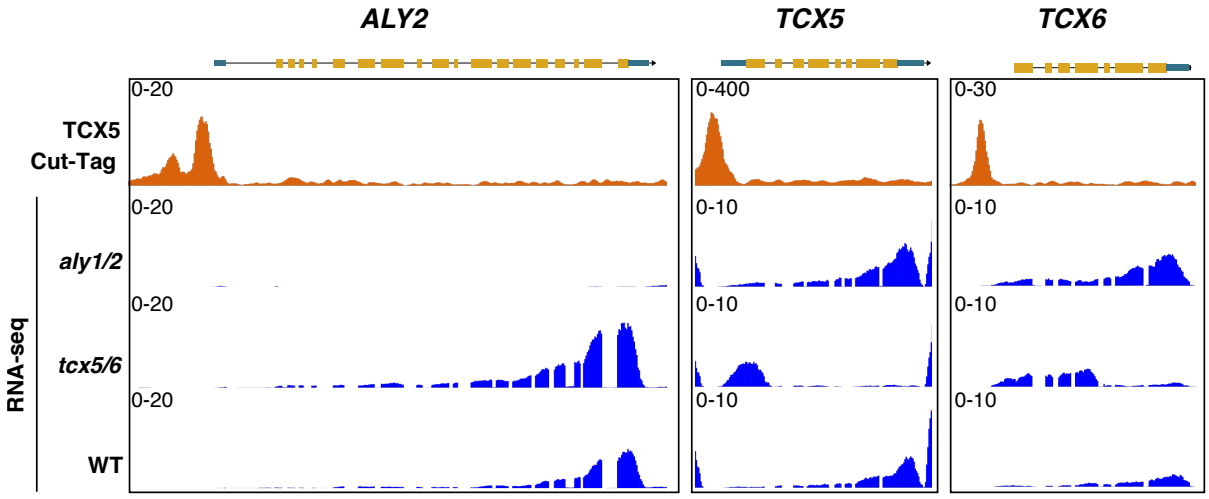
Supplementary Figure 2.4. MT array states of meiotic phases.

Representative confocal images of MT array states. (a) MT array state 1, from pre-meiosis to leptotene onward; (b) MT array state 2-3-4, late leptotene-early pachytene; (c) MT array state 5-6, pachytene-diakinesis; (d) MT array state 7-8-9, metaphase I-anaphase I; (e) MT array state 10-11, telophase I-interkinesis; (f) MT array state 12-13, metaphase II-anaphase II; (g) MT array state 14, telophase II. Scale bars,10 μm.



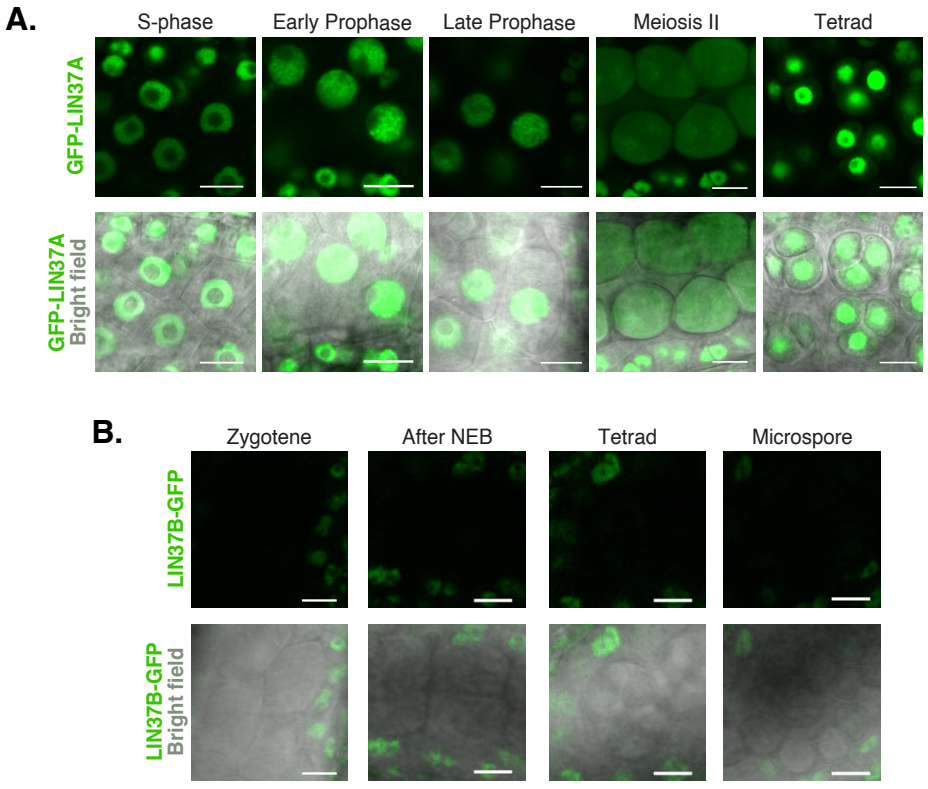
Supplementary Figure 2.5. Meiosis is synchronous in *aly1/2* and *lin37ab*.

Confocal images of (A) *aly1/2* and *lin37ab* (B) anther lobes captured just before NEB (top) and metaphase I (bottom). Magenta indicates RFP-TUA5, green shows REC8-mEGFP.



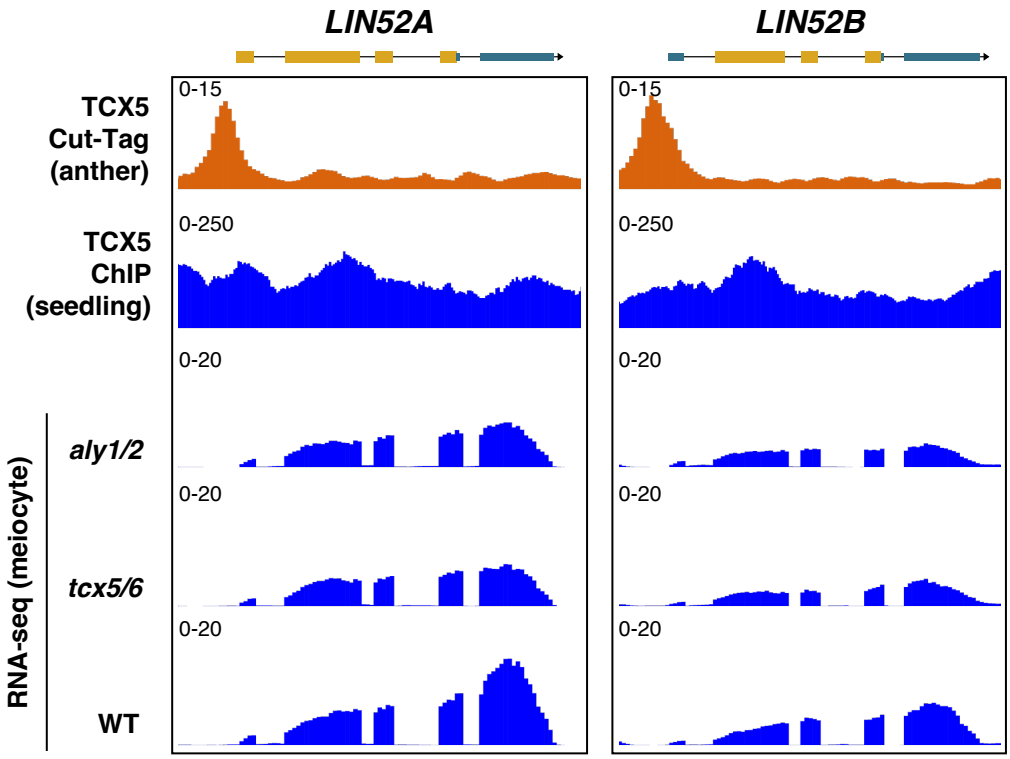
Supplementary Figure 2.6. Expression profiles of *ALY2, TCX5, TCX6* in male meiocytes.

Genome browser visualization depicting *ALY2, TCX5, TCX6* transcript abundance (blue tracks) from RNA-seq analyses performed on WT, *aly1/2*, and *tcx5/6* meiocytes, overlaid with CUT&Tag data indicating GFP-TCX5 binding profiles in anther tissue (dark orange track).



Supplementary Figure 2.7. GFP-LIN37A and LIN37B-GFP expression and localization pattern in anthers at specific meiotic stages.

Representative confocal images of **(A)** GFP-LIN37A and **(B)** LIN37B-GFP at anthers during distinct meiotic stages. Bright field/fluorescence overlays are provided in the second row for context. Scale bars, 10 μm**.**



Supplementary Figure 2.8. Expression profiles of LIN52A and LIN52B in male meiocytes and TCX5 binding on their promoters in anther and seedlings.

Genome browser visualization showing *LIN52A* and *LIN52B* transcript abundance (blue tracks) from RNA-seq analyses of WT, *aly1/2*, and *tcx5/6* meiocytes. GFP-TCX5 CUT&Tag binding profiles in anther tissue (dark orange track) are overlaid with ChIP-seq data for TCX5-FLAG in seedlings (blue track; data reanalyzed from Ning *et. al* 2020).

Supplementary Table 2.1. Differential transcription levels of DREAM complex components, associated cell cycle regulators, plant-specific DREAM components and TCX5 binding to their promoter regions in somatic and reproductive tissues.

Differential expression (log_2FC, *padj*) of core DREAM complex genes in *aly1/2* and *tcx5/6* male meiocytes versus WT; TCX5 target status (+/–/NA) from anther CUT&Tag; differential expression (log_2FC, *padj*) in *tcx5/6* seedlings versus WT (*Ning et al., 2020*); TCX5 target status (+/–/NA) from seedling ChIP (*Ning et al., 2020*). "NA" indicates data not available.

	Gene ID	Name	Seedling data (*Ning et al. 2020*)			Male meiocytes and anthers (This study)				
			tcx5/6		TCX5 ChIP	*aly1/2*		*tcx5/6*		TCX5 C&T
			log2FC	*padj*		log2FC	*padj*	log2FC	padj	
Core MuvB components	AT5G27610	ALY1	2.7065	4.6247E-75	+	-3.7063	0.15601667	1.7271	5.29E-17	+
	AT3G05380	ALY2	1.0110	1.8512E-18	+	-7.3484	8.987E-104	1.0370	2.37E-12	+
	AT3G21430	ALY3	0.5103	1.6825E-05	-	0.0349	0.95198935	0.3623	0.05930403	-
	AT4G29000	TCX5	-0.9808	8.3222E-06	+	0.7086	0.00214916	-0.4777	0.09329362	+
	AT2G20110	TCX6	2.2686	5.4041E-32	+	1.5058	1.5566E-16	0.4116	0.36288955	+
	AT1G04930	LIN37A	0.8185	0.01458289	+	0.6957	0.00032612	0.9707	5.04E-07	+
	AT2G32840	LIN37B	0.4243	0.12928802	+	0.4248	0.48478061	0.7570	0.05596831	-
	AT2G45250	LIN52A	NA	NA	-	NA	NA	NA	NA	+
	AT4G38280	LIN52B	NA	NA	-	NA	NA	NA	NA	+
	AT5G65120	MSI1	1.1672	2.1294E-07	+	0.3277	0.18179794	0.8374	0.00000172	+

	Gene ID	Name	Seedling data (*Ning et al. 2020*)		TCX5 ChIP	Male meiocytes and anthers (This study)				TCX5 C&T
			tcx5/6			*aly1/2*		*tcx5/6*		
			log2FC	*padj*		log2FC	*padj*	log2FC	padj	
Associated cell-cycle regulators	AT3G12280	RBR1	0.6523	1.4637E-11	+	0.1687	0.56148344	0.3412	0.0713844	+
	AT4G32730	MYB3R1	0.6001	2.6831E-07	+	0.5181	0.00305796	0.5602	0.00165141	+
	AT3G09370	MYB3R3	0.3284	0.2891163	+	0.4292	0.15042958	0.5299	0.04388857	+
	AT5G11510	MYB3R4	1.2356	8.426E-23	+	0.5384	0.03369291	1.1161	5.64E-10	+
	AT5G02320	MYB3R5	0.6728	0.05255186	+	0.4280	0.22269214	0.2384	0.454929	-
	AT2G36010	E2FA	1.5548	4.4834E-18	+	0.4925	0.11173878	0.6942	0.00378522	+
	AT5G22220	E2FB	1.0468	2.8651E-07	+	0.3678	0.28095349	0.7677	0.00331485	-
	AT1G47870	E2FC	1.6907	4.0733E-30	+	-0.0101	0.99002251	0.3032	0.24515648	+
	AT3G48160	E2FE (DEL1)	0.9471	0.00012199	+	0.8382	0.00586893	1.1457	0.0000521	-
	AT5G02470	DPA	0.3287	0.30609952	+	0.3278	0.1905406	0.5306	0.01763898	+
	AT5G03415	DPB	-0.0442	0.91737267	+	0.1019	0.81554183	0.2684	0.33489414	-
Plant-specific components	AT5G10110	FLIC	1.0941	2.2786E-08	+	0.4785	0.07135366	0.8369	0.0000605	+
	AT5G65120	FLAC	1.1672	2.1294E-07	+	0.3277	0.18179794	0.8374	0.00000172	+
	AT2G40630	BTE1	0.3768	0.06084218	+	0.7671	0.01979566	0.9633	0.00155493	-
	AT5G05240	BTL1	1.4310	2.9247E-17	+	1.2264	5.914E-10	1.5625	9.32E-15	-

	Gene ID	Name	Seedling data (*Ning et al. 2020*)		TCX5 ChIP	Male meiocytes and anthers (This study)				TCX5 C&T
			tcx5/6			*aly1/2*		*tcx5/6*		
			log2FC	*padj*		log2FC	*padj*	log2FC	padj	
DREAM associated factors	AT5G14960	E2FD (DEL2)	0.7650	0.03651336	+	0.8542	0.00672355	1.5987	3.87E-10	-
	AT3G01330	E2FF(DEL3)	2.4101	2.5255E-39	+	0.4389	0.13526393	1.2390	1.58E-09	+
	AT5G25790	TCX7	1.9154	5.0494E-08	+	1.2026	3.6099E-06	0.8272	0.00044758	+
	AT3G16160	TCX8	1.9611	0.00497328	+	0.3531	0.54029496	0.4285	0.38786199	-
	AT3G22760	SOL1	1.0865	2.7858E-16	+	1.3473	0.0032507	2.8027	4.12E-24	-
	AT4G14770	SOL2	0.6757	7.7718E-10	+	0.5569	0.11439845	1.0508	0.0000315	-
	AT3G22780	TSO1	0.2449	0.0789202	+	0.0866	0.86858439	0.3019	0.1499291	-

CHAPTER III. An outlook to regulation of meiosis by the DREAM complex through DNA methylation

1. INTRODUCTION

DNA methylation, by modulating chromatin structure and regulating DNA accesibility, plays a pivotal role in controlling gene expression, silencing transposable elements (TEs), and thereby ensures proper plant development. Comparative analyses of DNA methylomes between Arabidopsis male germ cells and somatic tissues have revealed dynamic methylation changes during germline development. Specifically, male meiocytes, microspores, and sperm exhibit elevated CHG and reduced CHH methylation levels relative to somatic tissues, suggesting enhanced CMT3 and diminished CMT2 activity (Hsieh *et al.*, 2016; Walker *et al.*, 2018). These dynamic changes in methylation may contribute to the regulation of the meiotic transcriptome.

In seedlings, the DREAM complex transcriptionally represses several genes involved in DNA methylation maintenance, including *MET1*, *CMT3*, *DDM1*, *KYP*, and *VIMs*. Loss of DREAM function leads to upregulation of these genes, resulting in a genome-wide increase in CHG methylation and, to a lesser extent, CG methylation (Ning *et al.*, 2020). Interestingly, combining DREAM mutants with *ddm1* or *cmt3* mutants partially rescues developmental defects, indicating that these phenotypes are at least partially caused by transcriptional deregulation resulting from altered DNA methylation.

In this chapter, I investigate whether DNA methylation maintenance genes are also regulated by the DREAM complex in male meiocytes, and whether such regulation influences the meiotic defects observed in the absence of the DREAM components ALY1/2 and TCX5/6.

2. RESULTS

As previously reported, the DREAM complex represses DNA methylation maintenance genes in seedlings, and mutants of its core components exhibit genome-wide CHG hypermethylation (Ning *et al.*, 2020). To investigate whether these genes are similarly dysregulated in male meiocytes of *aly1/2* and *tcx5/6* mutants, I analyzed RNA-seq data. Consistent with RNA-seq data from seedlings (Ning *et al.*, 2020), *MET1*, *CMT3*, *DDM1*, *VIM1/2/3/4*, and *KYP/SUVH4* were upregulated in *tcx5/6* male meiocytes. In contrast, only *DDM1* and *VIM1/2/4* transcription levels were upregulated in *aly1/2* compared to WT, while the expression of other genes remained unchanged (Table 3.1). Although TCX5 binds the promoters of all differentially expressed DNA methylation maintenance genes in seedlings (Ning *et al.*, 2020), CUT&Tag data from anthers revealed enrichment only at the *CMT3* promoter (Table 3.1, and Figure 3.1A). This suggests that, in reproductive tissue, the regulation of DNA methylation maintenance genes may occur indirectly of TCX5 binding.

To determine whether the upregulation of DNA methylation maintenance genes contributes to meiotic defects, I combined the *cmt3* mutant, a direct TCX5 target in anthers, with *aly1/2* and *tcx5/6* mutants and examined chromosome dynamics during meiosis via acid spreads in respective triple homozygous mutants. The *cmt3* single mutant, which displays loss of CHG methylation and reduced H3K9me2 without affecting CG or CHH methylation (Bartee, Malagnac and Bender, 2001; Underwood *et al.*, 2018), exhibits normal CO formation, chromosome segregation and meiotic progression, like WT (Figure 3.1C, upper row).

Surprisingly, the *aly1/2 cmt3* triple mutant showed a restoration of CO formation to WT level, with an average bivalent number of 5.0 compared to 3.8 in *aly1/2* mutants (Figure 3.1 B, C). Additionally, chromosome entanglement at metaphase I was reduced to 2%, from 23% in *aly1/2* (n = 107 and n = 65, respectively), and meiotic stages appeared indistinguishable from wild-type. Similarly, *tcx5/6 cmt3* mutants exhibited partial restoration of CO formation, with the bivalent number increasing from 3.3 to 4.6 (Figure 3.1 B, C). Chromosome entanglement decreased from 15% in *tcx5/6* to 7% in the *tcx5/6 cmt3* combination (n = 53 and n = 55, respectively). These results

suggest that *CMT3* loss mitigates the recombination defects in both mutant backgrounds without inducing aberrant chromosome interactions.

Notably, *tcx5/6 cmt3* mutants still displayed chromosome segregation defects not observed in *aly1/2 cmt3* (Figure 3.1C, middle and bottom row). At interkinesis and metaphase II, uneven chromosome distribution (e.g., four and six chromosomes at opposite poles, Figure 3.1C, bottom row) was evident, and micronuclei were present at the tetrad stage. These findings indicate that while *cmt3* mutation can rescue recombination defects, it is insufficient to fully restore meiotic integrity in *tcx5/6* mutants.

These results demonstrate that the DREAM complex modulates the expression of DNA methylation maintenance genes in male meiocytes, with *CMT3* playing a critical role in mediating the meiotic defects observed in *aly1/2* and *tcx5/6* mutants.

Table 3.1. Differential transcription levels of DNA methylation maintenance genes.

Differential expression (log_2FC, *padj*) of DNA methylation maintenance genes in *aly1/2* and *tcx5/6* male meiocytes versus WT; GFP-TCX5 enrichment in promoter region (– : not targeted, + : TCX5 target) in anthers obtained from CUT&Tag data. log_2FC: log_2 (Fold-change), *padj*: adjusted *p*-value.

Gene ID	Gene Name	*aly1/2*		*tcx5/6*		TCX5 CUT&Tag
		log2FC	*padj*	log2FC	*padj*	
AT5G49160	MET1/DMT1	0.1009	0.8821	**0.6132**	**0.0185**	-
AT1G69770	CMT3	0.3811	0.1611	**1.2865**	**<0.0001**	+
AT5G66750	**DDM1**	**0.6487**	**0.0155**	**0.8294**	**0.0007**	-
AT1G57820	**ORTH2/VIM1**	**0.5174**	**0.0197**	**0.9590**	**<0.0001**	-
AT1G66050	**ORTH5/VIM2**	**1.0966**	**0.0139**	**1.3887**	**0.0001**	-
AT5G39550	ORTH1/VIM3	0.3349	0.3634	**0.6304**	**0.0101**	-
AT1G66040	**ORTH4/VIM4**	**3.3017**	**0.0000**	**4.2383**	**<0.0001**	-
AT1G57800	ORTH3/VIM5	1.4400	1.0000	-3.2202	1.0000	-
AT5G13960	SUVH4 (KYP)	0.3089	0.3808	**0.7159**	**0.0013**	-
AT2G35160	SUVH5	-0.2330	0.4214	-0.0577	0.8781	-
AT2G22740	SUVH6	-0.1002	0.8777	-0.1285	0.7633	-

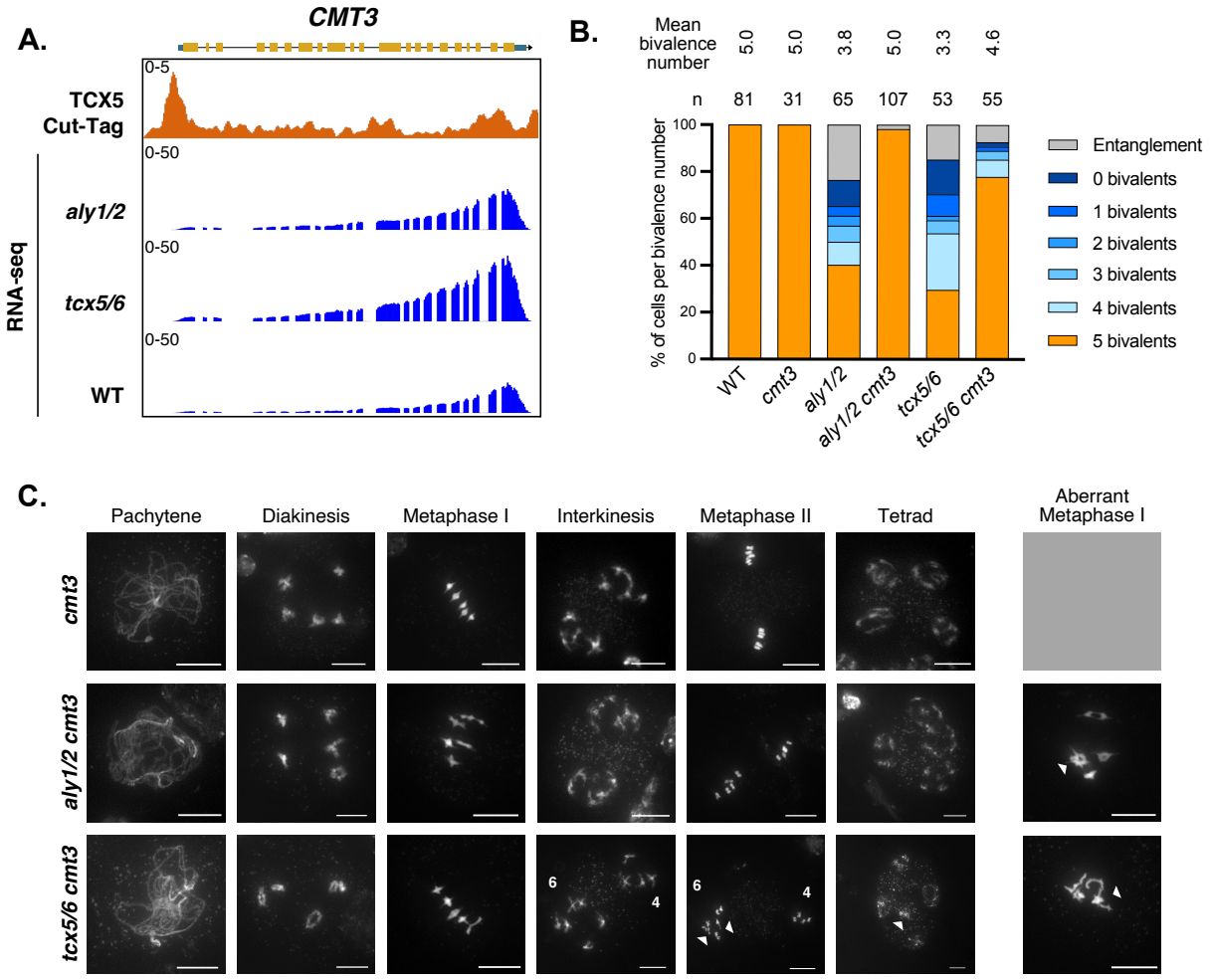


Figure 3.1. Loss of *CMT3* in DREAM mutant background mostly recovers CO loss phenotype.

(A) Genome browser view showing *CMT3* transcript abundance (blue tracks) from RNA-seq analyses of WT, *aly1/2*, and *tcx5/6* meiocytes, overlaid with CUT&Tag data illustrating GFP-TCX5 binding profiles in anther tissue (dark orange track). **(B)** Quantification of bivalent numbers per cell at metaphase I, along with the frequency of chromosome entanglement, across WT, *cmt3*, *aly1/2*, *aly1/2 cmt3*, *tcx5/6*, and *tcx5/6 cmt3* genotypes. Bars indicate the distribution of bivalents per cell and the proportion of cells exhibiting chromosome entanglement. The total number of metaphase I cells analyzed (*n*) and their respective average bivalent numbers are provided above each column. **(C)** Representative images of chromosomes captured at distinct meiotic stages: pachytene, diakinesis, metaphase I, interkinesis, metaphase II, tetrad and aberrant metaphase I in *cmt3* (top row), *aly1/2 cmt3* (middle row), and *tcx5/6 cmt3* (bottom row) mutants. White arrow heads indicates chromosome entanglement at metaphase I (aberrant), chromosome fragmentation at methaphase II,and micronuclei at tetrad stage. Scale bars,10 μm.

3. DISCUSSION

The regulatory roles of DNA and histone methylation in shaping the meiotic transcriptome have only recently begun to be elucidated (Choi *et al.*, 2018; Gaysinskaya *et al.*, 2018; Walker *et al.*, 2018; de la Fuente *et al.*, 2021; C. Wang *et al.*, 2022). Transcriptomic and methylome profiling of isolated male meiocytes in *Arabidopsis* has revealed that DNA methylation levels influence the transcription of many meiotic genes. For instance, RNA-seq data indicate that POL2A and SUVH2 jointly repress a subset of genes in male meiocytes, several of which share features associated with meiotic DSB sites (Wang *et al.*, 2022). Furthermore, in *ibm1* mutants, ectopic accumulation of H3K9me2 and increased gene body CHG methylation lead to synapsis defects, chromosome entanglement, and reduced COs. These meiotic abnormalities are rescued by additional mutations in *SUVH4/KYP* or *CMT3* (Saze *et al.*, 2008; Inagaki *et al.*, 2017; C. He *et al.*, 2022; Cheng, 2022).

Beyond transcriptional control, DNA methylation also affects CO distribution along chromosomes (Melamed-Bessudo and Levy, 2012; Yelina *et al.*, 2015; Choi *et al.*, 2018; Underwood *et al.*, 2018; Zhao *et al.*, 2021). Inhibition of either the CHG maintenance pathway—mediated by CMT3 or H3K9 methylation— leads to a modest but significant increase in CO formation in pericentromeric regions, coupled with a reduction in COs along chromosome arms (Choi *et al.*, 2018; Underwood *et al.*, 2018). Additionally, DNA hypermethylation has been associated with defects in meiotic progression. For example, CHH hypermethylation of TEs in AUXIN RESISTANT 1 (AXR1) mutants correlates with CO-depleted regions (Christophorou *et al.*, 2020).

Given the importance of DNA methylation roles in meiosis, I examined whether DREAM complex mutants, known to exhibit genome-wide hypermethylation in seedlings (Ning *et al.*, 2020), show transcriptional misregulation of DNA methylation maintenance genes in male meiocytes. RNA-seq analyses confirmed that *tcx5/6* mutants upregulate multiple same set of DNA methylation maintenance genes previously found de-regulated in seedlings (Ning *et al.*, 2020), including *CMT3*, *MET1*, *DDM1*, *VIM1/2/3/4*, and *SUVH4/KYP*. In contrast, *aly1/2* mutants showed a more restricted effect, with upregulation limited to *VIM1/2/4* and *DDM1* (Table 3.1).

To evaluate the functional relevance of this misregulation, I combined the *cmt3* mutation, a direct target of TCX5 (Figure 3.1A), with *aly1/2* and *tcx5/6* backgrounds. Strikingly, *cmt3* completely rescued the meiotic defects in *aly1/2*, restoring wild-type-like CO formation and meiotic progression. However, in the *tcx5/6* background, *cmt3* only partially rescued defects: while CO frequency was largely restored, *tcx5/6 cmt3* meiocytes still exhibited unbalanced chromosome segregation during meiosis II and micronuclei formation at the tetrad stage (Figure 3.1B,C). This suggests that *tcx5/6* mutants cause broader misregulation of DNA methylation maintenance genes than *aly1/2*, potentially leading to stronger hypermethylation and more severe meiotic defects.

Interestingly, TCX5 appears to bind only the *CMT3* promoter in reproductive tissues, indicating that its regulation of other methylation genes may be indirect. However, since CUT&Tag data were generated from whole anthers, where meiocytes constitute only a fraction of the cells, it remains possible that TCX5 directly binds additional targets specifically in meiocytes but was undetectable due to cellular dilution.

The observation that *tcx5/6 cmt3* largely rescues meiosis I defects, such as CO loss, but not meiosis II abnormalities provides a valuable opportunity to dissect gene networks governing distinct meiotic stages. Comparative transcriptomic analyses between *tcx5/6* and *tcx5/6 cmt3* could identify transcriptional changes underlying meiosis II-specific defects. Likewise, comparing their methylomes would clarify whether and how DNA methylation shapes these transcriptional dynamics in meiocytes. Future bisulfite sequencing and RNA-seq analyses in these mutant backgrounds will help determine the extent to which meiotic gene regulation is methylation-dependent and distinguish genes involved in CO formation from those required for chromosome segregation in later meiotic stages.

All together, these findings underscore a critical role for DREAM-mediated repression of DNA methylation maintenance genes in ensuring proper meiotic progression. While loss of *CMT3* can fully restore meiotic integrity in *aly1/2* mutants, its partial rescue in *tcx5/6* suggests that TCX5/6 has broader regulatory functions beyond *CMT3*. This

work highlights how differential misregulation of DNA methylation pathways can selectively disrupt early (meiosis I) and late (meiosis II) meiotic events and emphasizes the need to further explore the epigenetic regulation of meiotic gene expression.

4. MATERIALS & METHODS

4.1. Plant materials and growth conditions

Arabidopsis thaliana accession Columbia (Col-0) was used as the WT reference in all experiments. All mutant lines employed in this study were in the Col-0 background. T-DNA insertion lines included *tcx5-1* (SALK_047165), *tcx6-1* (GK-453H07), *aly1-1* (SALK_073108), *aly2-2* (SALK_118765C), *cmt3-11* (SALK_148381), obtained from the SALK and GABI-KAT T-DNA collections. Plants were cultivated in controlled growth chambers under long-day conditions (16 h light at 21°C / 8 h dark at 18°C) with 60% relative humidity.

4.2. Genotyping

Genotyping was performed as described in Chapter II 24.3. Primer sequences used for the identification of specific mutant alleles are listed in Appendix Table 1.

4.3. Cell spreads

Meiotic chromosome spreads were prepared using the acid spread technique, as described in Chapter I. Detailed protocols for sample preparation, fixation, and DAPI staining are provided in Methods section of Chapter I.

4.4. Transcriptome and CUT&Tag data anlaysis

Differentially expressed genes in *aly1/2* and *tcx5/6* male meiocytes relative to WT were analyzed in Chapter I, as detailed in Methods section. TCX5 target genes in anthers were identified using CUT&Tag. Sample preparation, library construction, and data processing for the CUT&Tag experiment were performed as described in the Chapter I Methods. In the present chapter, I highlighted transcriptional changes and TCX5 binding profiles of selected genes involved in DNA methylation maintenance. RNA-seq and CUT&Tag data were visualized using JBrowse (Version 2.13.1).

4.5. Statistical analysis

All statistical analyses and data visualizations were performed using GraphPad Prism 10 (Version 10.4.2). To quantify the percentage of cells with a given number of bivalents, chromosome entanglement, or fragmentation within a genotype, the fraction of total analyzed cells was calculated. Comparisons of bivalent numbers between genotypes were conducted using one-way ANOVA followed by Dunnett's T3 multiple comparisons test.

APPENDIX

Appendix Table 1. Primer pairs used for genotyping each insertion line are listed.

T-DNA line	Primer Name	Primer sequence (5´→ 3´)
aly1-1 (SALK_073108*)*	*aly1-1* LP	AATTTGGGATTTGTGGATTCC
	aly1-1 RP	CCACCTGAGTTTTCACACAGG
aly2-2 (SALK_118765C)	*aly2-2* LP	TTTTGGAAGCTCACTCGATTG
	aly2-2 RP	GGGAGAGATAAATACGCCTGG
tcx5-1 (SALK_047165)	tcx5-1 LP	TGGATTTTTCGAGCTGATTTG
	tcx5-1 RP	CAGAGTTGCTTCCACAGCTTC
tcx6-1 (GK-453H07)	tcx6-1 LP	AACCATTAACATTGTGTCCCGTTC
	tcx6-1 RP	CAGAGTTGCTTCCACAGCTTC
lin37a-2 (SALK_057175)	lin37a-2 LP	CACGTCCAACAACTCACATTG
	lin37a-2 RP	TCCCCCAATAAAGAAAAATGG
lin37b-3 (SALK_103139C)	lin37b-3 LP	TCTCCGGTGACACAACCTAAC
	lin37b-3 RP	CCCTCGGTTATTCTAACCTGC
fancm-1	fancm LP	CAGAGACATAATGAACGCATTAAG
	fancm RP	CACCAATAGATGTTGCGACAAT
recq4a-4 (GABI_203C07)	recq4a-4 LP	TATATATAGAATCGCCGGGGG
	recq4a-4 RP	ATCCCAATCAGTTTTGTTCCC
recq4b-2 (SALK_011357)	recq4b-2 LP	ACTTCAGAAAGTTGCTCTGCG
	recq4b-2 RP	CTGCTTCAGAACACCAAGACC
mus81-2 (SALK_107515)	mus81-2 LP	TGGTGAAATCTAGCAACCCAG
	mus81-2 RP	AATTTTCCACAAACCCTTTGG
cmt3-11 (SALK_148381)	cmt3-11 LP	TGCACTAGCTTCAGAAGTTTAAGG
	cmt3-11 RP	ATAAGAGAAGGAGCTGCTGCC
SALK lines T-DNA border primer	LBb1.3	ATTTTGCCGATTTCGGAAC
GABI lines T-DNA border primer	GK-RB-o3144	GTGGATTGATGTGATATCTCC

REFERENCES

Andersen, S.U. *et al.* (2007) 'The conserved cysteine-rich domain of a tesmin/TSO1-like protein binds zinc in vitro and TSO1 is required for both male and female fertility in Arabidopsis thaliana', *Journal of Experimental Botany*, 58(13), pp. 3657–3670. Available at: https://doi.org/10.1093/jxb/erm215.

Armstrong, S.J. *et al.* (2002) 'Asy1, a protein required for meiotic chromosome synapsis, localizes to axis-associated chromatin in Arabidopsis and Brassica', *Journal of Cell Science*, 115(18), pp. 3645–3655. Available at: https://doi.org/10.1242/jcs.00048.

Armstrong, S.J. and Jones, G.H. (2003) 'Meiotic cytology and chromosome behaviour in wild-type Arabidopsis thaliana', *Journal of Experimental Botany*, 54(380), pp. 1–10. Available at: https://doi.org/10.1093/jxb/erg034.

Asthana, A. *et al.* (2022) 'The MuvB complex binds and stabilizes nucleosomes downstream of the transcription start site of cell-cycle dependent genes', *Nature Communications*, 13(1), p. 526. Available at: https://doi.org/10.1038/s41467-022-28094-1.

Azumi, Y. *et al.* (2002) 'Homolog interaction during meiotic prophase I in Arabidopsis requires the SOLO DANCERS gene encoding a novel cyclin-like protein', *The EMBO Journal*, 21(12), pp. 3081–3095. Available at: https://doi.org/10.1093/emboj/cdf285.

Barakate, A. *et al.* (2021) 'Barley Anther and Meiocyte Transcriptome Dynamics in Meiotic Prophase I', *Frontiers in Plant Science*, 11(January), pp. 1–24. Available at: https://doi.org/10.3389/fpls.2020.619404.

Barra, L. *et al.* (2021) 'Meiocyte Isolation by INTACT and Meiotic Transcriptome Analysis in Arabidopsis', *Frontiers in Plant Science*, 12(March), pp. 1–15. Available at: https://doi.org/10.3389/fpls.2021.638051.

Bartee, L., Malagnac, F. and Bender, J. (2001) 'Arabidopsis cmt3 chromomethylase mutations block non-CG methylation and silencing of an endogenous gene', *Genes & Development*, 15(14), pp. 1753–1758. Available at: https://doi.org/10.1101/gad.905701.

Baudat, F. and de Massy, B. (2007) 'Regulating double-stranded DNA break repair towards crossover or non-crossover during mammalian meiosis', *Chromosome Research*, 15(5), pp. 565–577. Available at: https://doi.org/10.1007/s10577-007-1140-3.

Beall, E.L. *et al.* (2002) 'Role for a Drosophila Myb-containing protein complex in site-specific DNA replication', *Nature*, 420(6917), pp. 833–837. Available at: https://doi.org/10.1038/nature01228.

Beall, E.L. *et al.* (2007) 'Discovery of tMAC: A Drosophila testis-specific meiotic arrest complex paralogous to Myb-Muv B', *Genes and Development*, 21(8), pp. 904–919. Available at: https://doi.org/10.1101/gad.1516607.

Beattie, G.S. (2016) *Chromatin structure and gene expression : from the TMAC complex to the dREAM complex*.

Bhatt, A.M. *et al.* (2004) 'Gene structure and molecular analysis of Arabidopsis thaliana ALWAYS EARLY homologs', *Gene*, 336(2), pp. 219–229. Available at: https://doi.org/10.1016/j.gene.2004.03.033.

Bishop, D.K. and Zickler, D. (2004) 'Early Decision: Meiotic Crossover Interference prior to Stable Strand Exchange and Synapsis', *Cell*, 117(1), pp. 9–15. Available at: https://doi.org/10.1016/S0092-8674(04)00297-1.

Blanchard, D.P. *et al.* (2014) 'Chromatin reader L(3)mbt requires the Myb-MuvB/DREAM transcriptional regulatory complex for chromosomal recruitment', *Proceedings of the National Academy of Sciences of the United States of America*, 111(40), pp. E4234–E4243. Available at: https://doi.org/10.1073/pnas.1416321111.

Bleuyard, J.-Y. and White, C.I. (2004) 'The Arabidopsis homologue of Xrcc3 plays an essential role in meiosis', *The EMBO Journal*, 23(2), pp. 439–449. Available at: https://doi.org/10.1038/sj.emboj.7600055.

Börner, G.V., Kleckner, N. and Hunter, N. (2004) 'Crossover/noncrossover differentiation, synaptonemal complex formation, and regulatory surveillance at the leptotene/zygotene transition of meiosis', *Cell*, 117(1), pp. 29–45. Available at: https://doi.org/10.1016/s0092-8674(04)00292-2.

Bouveret, R. *et al.* (2006) 'Regulation of flowering time by Arabidopsis MSI1', *Development (Cambridge, England)*, 133(9), pp. 1693–1702. Available at: https://doi.org/10.1242/dev.02340.

Brar, G.A. and Amon, A. (2008) 'Emerging roles for centromeres in meiosis I chromosome segregation.', *Nature reviews. Genetics*, 9(12), pp. 899–910. Available at: https://doi.org/10.1038/nrg2454.

Brown, M.S. and Bishop, D.K. (2015) 'DNA Strand Exchange and RecA Homologs in Meiosis', *Cold Spring Harbor Perspectives in Biology*, 7(1), p. a016659. Available at: https://doi.org/10.1101/cshperspect.a016659.

Bujarrabal-Dueso, A. *et al.* (2023) 'The DREAM complex functions as conserved master regulator of somatic DNA-repair capacities', *Nature Structural & Molecular Biology*, 30(4), pp. 475–488. Available at: https://doi.org/10.1038/s41594-023-00942-8.

Bulankova, P. *et al.* (2010) 'Meiotic progression in Arabidopsis is governed by complex regulatory interactions between SMG7, TDM1, and the meiosis I-specific cyclin TAM', *Plant Cell*, 22(11), pp. 3791–3803. Available at: https://doi.org/10.1105/tpc.110.078378.

Bulankova, P. *et al.* (2013) 'Identification of Arabidopsis Meiotic Cyclins Reveals Functional Diversification among Plant Cyclin Genes', *PLoS Genetics*, 9(5). Available at: https://doi.org/10.1371/journal.pgen.1003508.

Caniçais, C. *et al.* (2025) 'Transcriptomic analysis and epigenetic regulators in human oocytes at different stages of oocyte meiotic maturation', *Developmental Biology*, 519, pp. 55–64. Available at: https://doi.org/10.1016/j.ydbio.2024.12.004.

Capilla-Pérez, L. *et al.* (2021) 'The synaptonemal complex imposes crossover interference and heterochiasmy in Arabidopsis', *Proceedings of the National Academy of Sciences of the United States of America*, 118(12), pp. 1–11. Available at: https://doi.org/10.1073/pnas.2023613118.

Chelysheva, L. *et al.* (2007) 'Zip4/Spo22 is required for class I CO formation but not for synapsis completion in Arabidopsis thaliana', *PLoS Genetics*, 3(5), pp. 802–813. Available at: https://doi.org/10.1371/journal.pgen.0030083.

Chelysheva, L. *et al.* (2012) 'The Arabidopsis HEI10 is a new ZMM protein related to Zip3', *PLoS Genetics*, 8(7). Available at: https://doi.org/10.1371/journal.pgen.1002799.

Chen, C. *et al.* (2005) 'The Arabidopsis ROCK-N-ROLLERS gene encodes a homolog of the yeast ATP-dependent DNA helicase MER3 and is required for normal meiotic crossover formation', *The Plant Journal*, 43(3), pp. 321–334. Available at: https://doi.org/10.1111/j.1365-313X.2005.02461.x.

Chen, C. *et al.* (2010) 'Meiosis-specific gene discovery in plants: RNA-Seq applied to isolated Arabidopsis male meiocytes', *BMC Plant Biology*, 10(1), p. 280. Available at: https://doi.org/10.1186/1471-2229-10-280.

Chen, H. *et al.* (2021) 'RAD51 supports DMC1 by inhibiting the SMC5/6 complex during meiosis', *The Plant Cell*, 33(8), pp. 2869–2882. Available at: https://doi.org/10.1093/plcell/koab136.

Chen, Y. *et al.* (2018) 'Single-cell RNA-seq uncovers dynamic processes and critical regulators in mouse spermatogenesis', *Cell Research*, 28(9), pp. 879–896. Available at: https://doi.org/10.1038/s41422-018-0074-y.

Cheng, J. (2022) 'H3K9 demethylases IBM1 and JMJ27 are required for male meiosis in Arabidopsis thaliana Jinping', *New Phytologist*, 44(8), pp. 1–29. Available at: https://doi.org/10.1088/1751-8113/44/8/085201.

Cheng, M.H. *et al.* (2017) 'The Drosophila LIN54 homolog Mip120 controls two aspects of oogenesis', *Biology Open*, 6(7), pp. 967–977. Available at: https://doi.org/10.1242/bio.025825.

Choi, K. *et al.* (2018) 'Nucleosomes and DNA methylation shape meiotic DSB frequency in Arabidopsis thaliana transposons and gene regulatory regions', *Genome Research*, 28(4), pp. 532–546. Available at: https://doi.org/10.1101/gr.225599.117.

Chowdary, K.V.S.K.A., Saini, R. and Singh, A.K. (2023) 'Epigenetic regulation during meiosis and crossover', *Physiology and Molecular Biology of Plants*, 29(12), pp. 1945–1958. Available at: https://doi.org/10.1007/s12298-023-01390-w.

Christophorou, N. *et al.* (2020) 'AXR1 affects DNA methylation independently of its role in regulating meiotic crossover localization', *PLoS Genetics*, 16(6), pp. 1–23. Available at: https://doi.org/10.1371/journal.pgen.1008894.

Cifuentes, M. *et al.* (2016) 'TDM1 Regulation Determines the Number of Meiotic Divisions', *PLoS Genetics*, 12(2), pp. 1–22. Available at: https://doi.org/10.1371/journal.pgen.1005856.

Cloud, V. *et al.* (2012) 'Rad51 is an accessory factor for Dmc1-mediated joint molecule formation during meiosis', *Science (New York, N.Y.)*, 337(6099), pp. 1222–1225. Available at: https://doi.org/10.1126/science.1219379.

Crismani, W. *et al.* (2012) 'FANCM Limits Meiotic Crossovers', *Science*, 336(6088), pp. 1588–1590. Available at: https://doi.org/10.1126/science.1220381.

Cromer, L. *et al.* (2012) 'OSD1 promotes meiotic progression via APC/C inhibition and forms a regulatory network with TDM and CYCA1;2/TAM', *PLoS Genetics*, 8(7). Available at: https://doi.org/10.1371/journal.pgen.1002865.

da Cruz, I. *et al.* (2016) 'Transcriptome analysis of highly purified mouse spermatogenic cell populations: gene expression signatures switch from meiotic-to postmeiotic-related processes at pachytene stage', *BMC Genomics*, 17(1), p. 294. Available at: https://doi.org/10.1186/s12864-016-2618-1.

De Jaeger-Braet, J. *et al.* (2022) 'Heat stress reveals a specialized variant of the pachytene checkpoint in meiosis of Arabidopsis thaliana', *The Plant Cell*, 34(1), pp. 433–454. Available at: https://doi.org/10.1093/plcell/koab257.

De Storme, N. and Geelen, D. (2013) 'Cytokinesis in plant male meiosis', *Plant Signaling & Behavior*, 8(3), p. e23394. Available at: https://doi.org/10.4161/psb.23394.

Dissmeyer, N. *et al.* (2007) 'T-Loop Phosphorylation of Arabidopsis CDKA;1 Is Required for Its Function and Can Be Partially Substituted by an Aspartate Residue', *The Plant Cell*, 19(3), pp. 972–985. Available at: https://doi.org/10.1105/tpc.107.050401.

Doggett, K. *et al.* (2011a) 'Wake-up-call, a lin-52 paralogue, and Always early, a lin-9 homologue physically interact, but have opposing functions in regulating testis-specific gene expression', *Developmental Biology*, 355(2–2), pp. 381–393. Available at: https://doi.org/10.1016/j.ydbio.2011.04.030.

Doggett, K. *et al.* (2011b) 'Wake-up-call, a lin-52 paralogue, and Always early, a lin-9 homologue physically interact, but have opposing functions in regulating testis-specific gene expression', *Developmental Biology*, 355(2), pp. 381–393. Available at: https://doi.org/10.1016/j.ydbio.2011.04.030.

Du, J. *et al.* (2012) 'Dual Binding of Chromomethylase Domains to H3K9me2-Containing Nucleosomes Directs DNA Methylation in Plants', *Cell*, 151(1), pp. 167–180. Available at: https://doi.org/10.1016/j.cell.2012.07.034.

Du, J. *et al.* (2015) 'DNA methylation pathways and their crosstalk with histone methylation', *Nature Reviews Molecular Cell Biology*, 16(9), pp. 519–532. Available at: https://doi.org/10.1038/nrm4043.

Dukowic-Schulze, S. *et al.* (2014) 'Comparative Transcriptomics of Early Meiosis in Arabidopsis and Maize', *Journal of Genetics and Genomics* [Preprint]. Available at: https://doi.org/10.1016/j.jgg.2013.11.007.

Dukowic-Schulze, S. and Chen, C. (2014) 'The meiotic transcriptome architecture of plants', *Frontiers in Plant Science*, 5(JUN), pp. 1–16. Available at: https://doi.org/10.3389/fpls.2014.00220.

Emmenecker, C. *et al.* (2024) 'FIGL1 attenuates meiotic interhomolog repair and is counteracted by RAD51 paralog XRCC2 and chromosome axis protein ASY1 during meiosis'. Available at: https://doi.org/10.1101/2024.04.25.591231.

Erdmann, R.M. and Picard, C.L. (2020) 'RNA-directed DNA Methylation', *PLOS Genetics*, 16(10), p. e1009034. Available at: https://doi.org/10.1371/journal.pgen.1009034.

d'Erfurth, I. *et al.* (2010) 'The cyclin-A CYCA1;2/TAM is required for the meiosis I to meiosis II transition and cooperates with OSD1 for the prophase to first meiotic division transition', *PLoS genetics*, 6(6), p. e1000989. Available at: https://doi.org/10.1371/journal.pgen.1000989.

Esterlechner, J. *et al.* (2013) 'LIN9, a Subunit of the DREAM Complex, Regulates Mitotic Gene Expression and Proliferation of Embryonic Stem Cells', *PLOS ONE*, 8(5), p. e62882. Available at: https://doi.org/10.1371/journal.pone.0062882.

Evans, E. *et al.* (2014) 'Riding the Spermatogenic Wave: Profiling Gene Expression Within Neonatal Germ and Sertoli Cells During a Synchronized Initial Wave of Spermatogenesis in Mice1', *Biology of Reproduction*, 90(5), pp. 108, 1–12. Available at: https://doi.org/10.1095/biolreprod.114.118034.

Ferdous, M. *et al.* (2012) 'Inter-Homolog Crossing-Over and Synapsis in Arabidopsis Meiosis Are Dependent on the Chromosome Axis Protein AtASY3', *PLoS Genetics*, 8(2), p. e1002507. Available at: https://doi.org/10.1371/journal.pgen.1002507.

Fischer, M., Grossmann, P., *et al.* (2016) 'Integration of TP53, DREAM, MMB-FOXM1 and RB-E2F target gene analyses identifies cell cycle gene regulatory networks', *Nucleic Acids Research*, 44(13), pp. 6070–6086. Available at: https://doi.org/10.1093/nar/gkw523.

Fischer, M., Quaas, M., *et al.* (2016) 'The p53-p21-DREAM-CDE/CHR pathway regulates G2/M cell cycle genes', *Nucleic Acids Research*, 44(1), pp. 164–174. Available at: https://doi.org/10.1093/nar/gkv927.

Fischer, M. *et al.* (2022) 'Coordinating gene expression during the cell cycle', *Trends in Biochemical Sciences*, 47(12), pp. 1009–1022. Available at: https://doi.org/10.1016/j.tibs.2022.06.007.

Fischer, M. and DeCaprio, J.A. (2015) 'Does Arabidopsis thaliana DREAM of cell cycle control?', *The EMBO Journal*, 34(15), pp. 1987–1989. Available at: https://doi.org/10.15252/embj.201592196.

Fischer, M. and Müller, G.A. (2017) 'Cell cycle transcription control: DREAM/MuvB and RB-E2F complexes', *Critical Reviews in Biochemistry and Molecular Biology*, 52(6), pp. 638–662. Available at: https://doi.org/10.1080/10409238.2017.1360836.

Flores Sanchez, M.A. (2024) 'Generation of meiosis-specific proximity labeling constructs and localization analysis of interactors of the DREAM complex in *Arabidopsis thaliana* male', M.Sc thesis, Universität Hamburg, unpublished.

France, M.G. *et al.* (2021) 'ZYP1 is required for obligate cross-over formation and cross-over interference in Arabidopsis', *Proceedings of the National Academy of Sciences of the United States of America*, 118(14), pp. 1–11. Available at: https://doi.org/10.1073/pnas.2021671118.

de la Fuente, R. *et al.* (2021) 'Epigenetic dysregulation of mammalian male meiosis caused by interference of recombination and synapsis', *Cells*, 10(9), pp. 1–24. Available at: https://doi.org/10.3390/cells10092311.

Gallo, D. *et al.* (2022) 'CCNE1 amplification is synthetic lethal with PKMYT1 kinase inhibition', *Nature*, 604(7907), pp. 749–756. Available at: https://doi.org/10.1038/s41586-022-04638-9.

Gao, J., Qin, Y. and Schimenti, J.C. (2024) 'Gene regulation during meiosis', *Trends in Genetics*, 40(4), pp. 326–336. Available at: https://doi.org/10.1016/j.tig.2023.12.006.

Gaysinskaya, V. *et al.* (2018) 'Transient reduction of DNA methylation at the onset of meiosis in male mice', *Epigenetics and Chromatin*, 11(1), p. 15. Available at: https://doi.org/10.1186/s13072-018-0186-0.

Georlette, D. *et al.* (2007) 'Genomic profiling and expression studies reveal both positive and negative activities for the Drosophila Myb–MuvB/dREAM complex in proliferating cells', *Genes & Development*, 21(22), pp. 2880–2896. Available at: https://doi.org/10.1101/gad.1600107.

Girard, C. *et al.* (2014) 'FANCM-associated proteins MHF1 and MHF2, but not the other Fanconi anemia factors, limit meiotic crossovers', *Nucleic Acids Research*, 42(14), pp. 9087–9095. Available at: https://doi.org/10.1093/nar/gku614.

Girard, C. *et al.* (2015) 'AAA-ATPase FIDGETIN-LIKE 1 and Helicase FANCM Antagonize Meiotic Crossovers by Distinct Mechanisms', *PLOS Genetics*. Edited by M. Lichten, 11(7), p. e1005369. Available at: https://doi.org/10.1371/journal.pgen.1005369.

Goetsch, P.D. and Strome, S. (2022) 'DREAM interrupted: severing LIN-35-MuvB association in *Caenorhabditis elegans* impairs DREAM function but not its chromatin localization', *Genetics*. Edited by C. Kaplan, 221(3), p. iyac073. Available at: https://doi.org/10.1093/genetics/iyac073.

Gorbsky, G.J. (2015) 'The spindle checkpoint and chromosome segregation in meiosis', *The FEBS journal*, 282(13), pp. 2471–2487. Available at: https://doi.org/10.1111/febs.13166.

Gosh, A. (2024) '*aMP: Deep learning framework to characterize meiosis progression timeline in tetraploid Arabidopsis thaliana*', PhD thesis, Universität Hamburg (unpublished).

Grelon, M. *et al.* (2001) 'AtSPO11-1 is necessary for efficient meiotic recombination in plants', *The EMBO Journal*, 20(3), pp. 589–600. Available at: https://doi.org/10.1093/emboj/20.3.589.

Grelon, M. *et al.* (2003) 'The Arabidopsis MEI1 gene encodes a protein with five BRCT domains that is involved in meiosis-specific DNA repair events independent of SPO11-induced DSBs', *The Plant Journal: For Cell and Molecular Biology*, 35(4), pp. 465–475. Available at: https://doi.org/10.1046/j.1365-313x.2003.01820.x.

Guiley, K.Z. *et al.* (2015) 'Structural mechanisms of DREAM complex assembly and regulation', *Genes and Development*, 29(9), pp. 961–974. Available at: https://doi.org/10.1101/gad.257568.114.

Guo, J. *et al.* (2018) 'The adult human testis transcriptional cell atlas', *Cell Research*, 28(12), pp. 1141–1157. Available at: https://doi.org/10.1038/s41422-018-0099-2.

Haga, N. *et al.* (2011) 'Mutations in MYB3R1 and MYB3R4 cause pleiotropic developmental defects and preferential down-regulation of multiple G2/M-specific genes in Arabidopsis', *Plant Physiology*, 157(2), pp. 706–717. Available at: https://doi.org/10.1104/pp.111.180836.

Harrison, M.M. *et al.* (2006) 'Some C. elegans class B synthetic multivulva proteins encode a conserved LIN-35 Rb-containing complex distinct from a NuRD-like complex', *Proceedings of the National Academy of Sciences*, 103(45), pp. 16782–16787. Available at: https://doi.org/10.1073/pnas.0608461103.

Hartung, F. *et al.* (2008) 'Topoisomerase 3α and RMI1 Suppress Somatic Crossovers and Are Essential for Resolution of Meiotic Recombination Intermediates in Arabidopsis thaliana', *PLOS Genetics*, 4(12), p. e1000285. Available at: https://doi.org/10.1371/journal.pgen.1000285.

Hartung, F., Suer, S. and Puchta, H. (2007) 'Two closely related RecQ helicases have antagonistic roles in homologous recombination and DNA repair in Arabidopsis thaliana', *Proceedings of the National Academy of Sciences*, 104(47), pp. 18836–18841. Available at: https://doi.org/10.1073/pnas.0705998104.

Hansen, B. (2022) ‘Cloning of genomic reporter constructs to analyze the expression and localization of ALWAYS EARLY 3 in meiotic tissue of *Arabidopsis*’, B.Sc thesis, Universität Hamburg, unpublished.

Hauser, B.A. *et al.* (2000) ‘TSO1 is a novel protein that modulates cytokinesis and cell expansion in Arabidopsis’, *Development*, 127(10), pp. 2219–2226.

He, C. *et al.* (2022) ‘Molecular Plant Histone demethylase IBM1-mediated meiocyte gene expression ensures meiotic chromosome synapsis and recombination’, *PLoS Genet*, pp. 1–30. Available at: https://doi.org/10.1371/journal.pgen.1010041.

He, L. *et al.* (2022) ‘DNA methylation-free Arabidopsis reveals crucial roles of DNA methylation in regulating gene expression and development’, *Nature Communications*, 13(1), pp. 1–16. Available at: https://doi.org/10.1038/s41467-022-28940-2.

Hennig, L. *et al.* (2003) ‘Arabidopsis MSI1 is required for epigenetic maintenance of reproductive development’, *Development (Cambridge, England)*, 130(12), pp. 2555–2565. Available at: https://doi.org/10.1242/dev.00470.

Hesse, S. *et al.* (2019) ‘Ultrastructure and dynamics of synaptonemal complex components during meiotic pairing and synapsis of standard (A) and accessory (B) rye chromosomes’, *Frontiers in Plant Science*, 10(June), pp. 1–20. Available at: https://doi.org/10.3389/fpls.2019.00773.

Higgins, J.D. *et al.* (2005) ‘The Arabidopsis synaptonemal complex protein ZYP1 is required for chromosome synapsis and normal fidelity of crossing over’, *Genes & Development*, 19(20), pp. 2488–2500. Available at: https://doi.org/10.1101/gad.354705.

Higgins, J.D., Vignard, J., *et al.* (2008) ‘AtMSH5 partners AtMSH4 in the class I meiotic crossover pathway in Arabidopsis thaliana, but is not required for synapsis’, *The Plant Journal*, 55(1), pp. 28–39. Available at: https://doi.org/10.1111/j.1365-313X.2008.03470.x.

Higgins, J.D., Buckling, E.F., *et al.* (2008) ‘Expression and functional analysis of AtMUS81 in Arabidopsis meiosis reveals a role in the second pathway of crossing-over’, *The Plant Journal*, 54(1), pp. 152–162. Available at: https://doi.org/10.1111/j.1365-313X.2008.03403.x.

Higgins, J.D. *et al.* (2011) ‘The RecQ helicase AtRECQ4A is required to remove inter-chromosomal telomeric connections that arise during meiotic recombination in Arabidopsis’, *The Plant Journal*, 65(3), pp. 492–502. Available at: https://doi.org/10.1111/j.1365-313X.2010.04438.x.

Hinch, A.G. *et al.* (2020) ‘The Configuration of RPA, RAD51, and DMC1 Binding in Meiosis Reveals the Nature of Critical Recombination Intermediates’, *Molecular Cell*, 79(4), p. 689. Available at: https://doi.org/10.1016/j.molcel.2020.06.015.

Hoareau, M. *et al.* (2024) 'DREAM a little dREAM of DRM: Model organisms and conservation of DREAM-like complexes', *BioEssays*, 46(2), p. 2300125. Available at: https://doi.org/10.1002/bies.202300125.

Holm, P.B. and Rasmussen, S.W. (1980) 'Chromosome pairing, recombination nodules and chiasma formation in diploid Bombyx males', *Carlsberg Research Communications*, 45(6), pp. 483–548. Available at: https://doi.org/10.1007/BF02932921.

Hsieh, P.H. *et al.* (2016) 'Arabidopsis male sexual lineage exhibits more robust maintenance of CG methylation than somatic tissues', *Proceedings of the National Academy of Sciences of the United States of America*, 113(52), pp. 15132–15137. Available at: https://doi.org/10.1073/pnas.1619074114.

Huang, J. *et al.* (2019) 'Meiocyte-Specific and AtSPO11-1–Dependent Small RNAs and Their Association with Meiotic Gene Expression and Recombination', *The Plant Cell*, 31(2), pp. 444–464. Available at: https://doi.org/10.1105/tpc.18.00511.

Hwang, Y.-J. and Kim, M.J. (2025) 'Emerging Role of the DREAM Complex in Cancer and Therapeutic Opportunities', *International Journal of Molecular Sciences*, 26(1), p. 322. Available at: https://doi.org/10.3390/ijms26010322.

Inagaki, S. *et al.* (2017) 'Gene-body chromatin modification dynamics mediate epigenome differentiation in Arabidopsis', *The EMBO Journal*, 36(8), pp. 970–980. Available at: https://doi.org/10.15252/embj.201694983.

Ines, O.D. *et al.* (2012) 'Differing Requirements for RAD51 and DMC1 in Meiotic Pairing of Centromeres and Chromosome Arms in Arabidopsis thaliana', *PLOS Genetics*, 8(4), p. e1002636. Available at: https://doi.org/10.1371/journal.pgen.1002636.

Ines, O.D. *et al.* (2013) 'Meiotic Recombination in Arabidopsis Is Catalysed by DMC1, with RAD51 Playing a Supporting Role', *PLOS Genetics*, 9(9), p. e1003787. Available at: https://doi.org/10.1371/journal.pgen.1003787.

Jan, S.Z. *et al.* (2017) 'Unraveling transcriptome dynamics in human spermatogenesis', *Development*, 144(20), pp. 3659–3673. Available at: https://doi.org/10.1242/dev.152413.

Jiang, J. *et al.* (2007) 'Tombola, a tesmin/TSO1-family protein, regulates transciptional activation in the Drosophila male germline and physically interacts with always early', *Development*, 134(8), pp. 1549–1559. Available at: https://doi.org/10.1242/dev.000521.

Jiang, J. and White-Cooper, H. (2003) 'Transcriptional activation in Drosophila spermatogenesis involves the mutually dependent function of aly and a novel meiotic arrest gene cookie monster', *Development*, 130(3), pp. 563–573. Available at: https://doi.org/10.1242/dev.00246.

Jiang, Y. *et al.* (2023) 'The coordinated regulation of early meiotic stages is dominated by non-coding RNAs and stage-specific transcription in wheat', *The Plant Journal*, 114(1), pp. 209–224. Available at: https://doi.org/10.1111/tpj.16125.

Jing, J. *et al.* (2025) 'Maximizing meiotic crossover rates reveals the map of Crossover Potential', *Nature Communications*, 16(1), p. 5306. Available at: https://doi.org/10.1038/s41467-025-60663-y.

Kankel, M.W. *et al.* (2003) 'Arabidopsis MET1 cytosine methyltransferase mutants', *Genetics*, 163(3), pp. 1109–1122.

Kaur, H., GN, K. and Lichten, M. (2019) 'Unresolved Recombination Intermediates Cause a RAD9-Dependent Cell Cycle Arrest in Saccharomyces cerevisiae', *Genetics*, 213(3), pp. 805–818. Available at: https://doi.org/10.1534/genetics.119.302632.

Keeney, S., Giroux, C.N. and Kleckner, N. (1997) 'Meiosis-Specific DNA Double-Strand Breaks Are Catalyzed by Spo11, a Member of a Widely Conserved Protein Family', *Cell*, 88(3), pp. 375–384. Available at: https://doi.org/10.1016/S0092-8674(00)81876-0.

Kim Guisbert, K.S. *et al.* (2012) 'Meiosis-induced alterations in transcript architecture and noncoding RNA expression in S. cerevisiae', *RNA*, 18(6), pp. 1142–1153. Available at: https://doi.org/10.1261/rna.030510.111.

Kirik, A. *et al.* (2006) 'The Chromatin Assembly Factor Subunit FASCIATA1 Is Involved in Homologous Recombination in Plants', *The Plant Cell*, 18(10), pp. 2431–2442. Available at: https://doi.org/10.1105/tpc.106.045088.

Kobayashi, K., Suzuki, T., Iwata, E., Magyar, Z., *et al.* (2015) 'MYB3Rs, plant homologs of Myb oncoproteins, control cell cycle-regulated transcription and form DREAM-like complexes', *Transcription*, 6(5), pp. 106–111. Available at: https://doi.org/10.1080/21541264.2015.1109746.

Kobayashi, K., Suzuki, Toshiya, Iwata, E., Nakamichi, N., *et al.* (2015) 'Transcriptional repression by MYB3R proteins regulates plant organ growth', *The EMBO Journal*, 34(15), pp. 1992–2007. Available at: https://doi.org/10.15252/embj.201490899.

Koliopoulos, M.G. *et al.* (2022) 'Structure of a nucleosome-bound MuvB transcription factor complex reveals DNA remodelling', *Nature Communications*, 13(1), p. 5075. Available at: https://doi.org/10.1038/s41467-022-32798-9.

Komaki, S. and Schnittger, A. (2017) 'The Spindle Assembly Checkpoint in Arabidopsis Is Rapidly Shut Off during Severe Stress', *Developmental Cell*, 43(2), pp. 172-185.e5. Available at: https://doi.org/10.1016/j.devcel.2017.09.017.

Korenjak, M. *et al.* (2004) 'Native E2F/RBF Complexes Contain Myb-Interacting Proteins and Repress Transcription of Developmentally Controlled E2F Target

Genes', *Cell*, 119(2), pp. 181–193. Available at: https://doi.org/10.1016/j.cell.2004.09.034.

Kudron, M. *et al.* (2013) 'Tissue-specific direct targets of Caenorhabditis elegans Rb/E2F dictate distinct somatic and germline programs', *Genome Biology*, 14(1). Available at: https://doi.org/10.1186/gb-2013-14-1-r5.

Kumar, R. *et al.* (2019) 'Antagonism between BRCA2 and FIGL1 regulates homologous recombination', *Nucleic Acids Research*, 47(10), pp. 5170–5180. Available at: https://doi.org/10.1093/nar/gkz225.

Kurzbauer, M.-T. *et al.* (2012) 'The recombinases DMC1 and RAD51 are functionally and spatially separated during meiosis in Arabidopsis', *The Plant Cell*, 24(5), pp. 2058–2070. Available at: https://doi.org/10.1105/tpc.112.098459.

Kurzbauer, M.T. *et al.* (2018) 'Arabidopsis thaliana FANCD2 promotes meiotic crossover formation', *Plant Cell*, 30(2), pp. 415–428. Available at: https://doi.org/10.1105/tpc.17.00745.

Laktionov, P. *et al.* (2014) 'Transcription factor Comr acts as a direct activator in the genetic program controlling spermatogenesis in D. melanogaster', *Molecular Biology*, 48. Available at: https://doi.org/10.1134/S0026893314010087.

Laktionov, P.P. *et al.* (2018) 'Genome-wide analysis of gene regulation mechanisms during Drosophila spermatogenesis', *Epigenetics and Chromatin*, 11(1), pp. 1–15. Available at: https://doi.org/10.1186/s13072-018-0183-3.

Lamarche, B.J., Orazio, N.I. and Weitzman, M.D. (2010) 'The MRN complex in double-strand break repair and telomere maintenance', *FEBS Letters*, 584(17), pp. 3682–3695. Available at: https://doi.org/10.1016/j.febslet.2010.07.029.

Lambing, C. *et al.* (2020) 'ASY1 acts as a dosage-dependent antagonist of telomere-led recombination and mediates crossover interference in Arabidopsis', *Proceedings of the National Academy of Sciences of the United States of America*, 117(24), pp. 13647–13658. Available at: https://doi.org/10.1073/pnas.1921055117.

Lang, L. *et al.* (2021) 'The DREAM complex represses growth in response to DNA damage in Arabidopsis', *Life Science Alliance*, 4(12), p. e202101141. Available at: https://doi.org/10.26508/lsa.202101141.

Lang, L. *et al.* (2023) 'The two plant-specific DREAM components FLIC and FLAC repress floral transition in Arabidopsis'. bioRxiv, p. 2023.08.07.552284. Available at: https://doi.org/10.1101/2023.08.07.552284.

Latorre, I. *et al.* (2015) 'The DREAM complex promotes gene body H2A.Z for target repression', *Genes and Development*, 29(5), pp. 495–500. Available at: https://doi.org/10.1101/gad.255810.114.

Law, J.A. and Jacobsen, S.E. (2010) 'Establishing, maintaining and modifying DNA methylation patterns in plants and animals', *Nature Reviews Genetics*, 11(3), pp. 204–220. Available at: https://doi.org/10.1038/nrg2719.

Lee, S.C. *et al.* (2023) 'Chromatin remodeling of histone H3 variants by DDM1 underlies epigenetic inheritance of DNA methylation', *Cell*, 186(19), pp. 4100-4116.e15. Available at: https://doi.org/10.1016/j.cell.2023.08.001.

Lewis, P.W. *et al.* (2004) 'Identification of a Drosophila Myb-E2F2/RBF transcriptional repressor complex', *Genes and Development*, 18(23), pp. 2929–2940. Available at: https://doi.org/10.1101/gad.1255204.

Li, J. *et al.* (2015) 'The plant-specific protein FEHLSTART controls male meiotic entry, initializing meiotic synchronization in Arabidopsis', *Plant Journal*, 84(4), pp. 659–671. Available at: https://doi.org/10.1111/tpj.13026.

Li, W. *et al.* (2004) 'The Arabidopsis AtRAD51 gene is dispensable for vegetative development but required for meiosis', *Proceedings of the National Academy of Sciences of the United States of America*, 101(29), pp. 10596–10601. Available at: https://doi.org/10.1073/pnas.0404110101.

Li, X. *et al.* (2021) 'Regulation of interference-sensitive crossover distribution ensures crossover assurance in *Arabidopsis*', *Proceedings of the National Academy of Sciences*, 118(47), p. e2107543118. Available at: https://doi.org/10.1073/pnas.2107543118.

Lindroth, A.M. *et al.* (2001) 'Requirement of CHROMOMETHYLASE3 for maintenance of CpXpG methylation', *Science (New York, N.Y.)*, 292(5524), pp. 2077–2080. Available at: https://doi.org/10.1126/science.1059745.

Litovchick, L. *et al.* (2007) 'Evolutionarily Conserved Multisubunit RBL2/p130 and E2F4 Protein Complex Represses Human Cell Cycle-Dependent Genes in Quiescence', *Molecular Cell*, 26(4), pp. 539–551. Available at: https://doi.org/10.1016/j.molcel.2007.04.015.

Litovchick, L. *et al.* (2011) 'DYRK1A protein kinase promotes quiescence and senescence through DREAM complex assembly', *Genes and Development*, 25(8), pp. 801–813. Available at: https://doi.org/10.1101/gad.2034211.

Lloyd, A. (2022) 'Crossover patterning in plants.', *Plant reproduction* [Preprint], (0123456789). Available at: https://doi.org/10.1007/s00497-022-00445-4.

Lu, P. *et al.* (2014) 'Arabidopsis PTD Is Required for Type I Crossover Formation and Affects Recombination Frequency in Two Different Chromosomal Regions', *Journal of Genetics and Genomics*, 41(3), pp. 165–175. Available at: https://doi.org/10.1016/j.jgg.2014.02.001.

Ma, H. (2006) 'A Molecular Portrait of Arabidopsis Meiosis', *The Arabidopsis Book*, 4, p. e0095. Available at: https://doi.org/10.1199/tab.0095.

Macaisne, N., Vignard, J. and Mercier, R. (2011) 'SHOC1 and PTD form an XPF–ERCC1-like complex that is required for formation of class I crossovers', *Journal of Cell Science*, 124(16), pp. 2687–2691. Available at: https://doi.org/10.1242/jcs.088229.

Magnard, J.-L. *et al.* (2001) 'The Arabidopsis Gene Tardy Asynchronous Meiosis Is Required for the Normal Pace and Synchrony of Cell Division during Male Meiosis', *Plant Physiology*, 127(3), pp. 1157–1166.

Magyar, Z. *et al.* (2012) 'Arabidopsis E2FA stimulates proliferation and endocycle separately through RBR-bound and RBR-free complexes', *EMBO Journal*, 31(6), pp. 1480–1493. Available at: https://doi.org/10.1038/emboj.2012.13.

Magyar, Z., Bögre, L. and Ito, M. (2016) 'DREAMs make plant cells to cycle or to become quiescent', *Current Opinion in Plant Biology*, 34, pp. 100–106. Available at: https://doi.org/10.1016/j.pbi.2016.10.002.

Malumbres, M. and Barbacid, M. (2009) 'Cell cycle, CDKs and cancer: a changing paradigm', *Nature Reviews Cancer*, 9(3), pp. 153–166. Available at: https://doi.org/10.1038/nrc2602.

Marceau, A.H. *et al.* (2016) 'Structural basis for LIN54 recognition of CHR elements in cell cycle-regulated promoters', *Nature Communications*, 7. Available at: https://doi.org/10.1038/ncomms12301.

Marceau, A.H. *et al.* (2019) 'An order-to-disorder structural switch activates the FoxM1 transcription factor', *eLife*. Edited by L.E. Kay, C. Wolberger, and L.E. Kay, 8, p. e46131. Available at: https://doi.org/10.7554/eLife.46131.

Marston, A.L. and Wassmann, K. (2017) 'Multiple Duties for Spindle Assembly Checkpoint Kinases in Meiosis', *Frontiers in Cell and Developmental Biology*, 5. Available at: https://doi.org/10.3389/fcell.2017.00109.

Mata, J. *et al.* (2002) 'The transcriptional program of meiosis and sporulation in fission yeast', *Nature Genetics*, 32(1), pp. 143–147. Available at: https://doi.org/10.1038/ng951.

Matzke, M.A. and Mosher, R.A. (2014) 'RNA-directed DNA methylation: an epigenetic pathway of increasing complexity'. Available at: https://doi.org/10.1038/nrg3683.

Mazina, O.M. *et al.* (2004) 'Saccharomyces cerevisiae Mer3 Helicase Stimulates 3′–5′ Heteroduplex Extension by Rad51: Implications for Crossover Control in Meiotic Recombination', *Cell*, 117(1), pp. 47–56. Available at: https://doi.org/10.1016/S0092-8674(04)00294-6.

Melamed-Bessudo, C. and Levy, A.A. (2012) 'Deficiency in DNA methylation increases meiotic crossover rates in euchromatic but not in heterochromatic regions in Arabidopsis', *Proceedings of the National Academy of Sciences of the United States of America*, 109(16). Available at: https://doi.org/10.1073/pnas.1120742109.

Mercier, R. *et al.* (2005) 'Two Meiotic Crossover Classes Cohabit in Arabidopsis: One Is Dependent on MER3,whereas the Other One Is Not', *Current Biology*, 15(8), pp. 692–701. Available at: https://doi.org/10.1016/j.cub.2005.02.056.

Mercier, R. *et al.* (2015) 'The Molecular Biology of Meiosis in Plants', *Annual Review of Plant Biology*, 66(1), pp. 297–327. Available at: https://doi.org/10.1146/annurev-arplant-050213-035923.

Miller, M.P. *et al.* (2012) 'Meiosis I chromosome segregation is established through regulation of microtubule–kinetochore interactions', *eLife*. Edited by M. Botchan, 1, p. e00117. Available at: https://doi.org/10.7554/eLife.00117.

Morgan, C. *et al.* (2021) 'Diffusion-mediated HEI10 coarsening can explain meiotic crossover positioning in Arabidopsis', *Nature Communications*, 12(1). Available at: https://doi.org/10.1038/s41467-021-24827-w.

Müller, G.A. *et al.* (2016) 'Timing of transcription during the cell cycle: Protein complexes binding to E2F, E2F/CLE, CDE/CHR, or CHR promoter elements define early and late cell cycle gene expression', *Oncotarget*, 8(58), pp. 97736–97748. Available at: https://doi.org/10.18632/oncotarget.10888.

Müller, G.A. and Engeland, K. (2010) 'The central role of CDE/CHR promoter elements in the regulation of cell cycle-dependent gene transcription', *The FEBS Journal*, 277(4), pp. 877–893. Available at: https://doi.org/10.1111/j.1742-4658.2009.07508.x.

Nakagawa, T. *et al.* (2007) 'Improved gateway binary vectors: High-performance vectors for creation of fusion constructs in transgenic analysis of plants', *Bioscience, Biotechnology and Biochemistry*, 71(8), pp. 2095–2100. Available at: https://doi.org/10.1271/bbb.70216.

Nandanan, K.G. *et al.* (2021) 'Regulation of Msh4-Msh5 association with meiotic chromosomes in budding yeast', *Genetics*, 219(2), p. iyab102. Available at: https://doi.org/10.1093/genetics/iyab102.

Nelms, B. and Walbot, V. (2019) 'Defining the developmental program leading to meiosis in maize', *Science*, 364(6435), pp. 52–56. Available at: https://doi.org/10.1126/science.aav6428.

Nibau, C. *et al.* (2020) 'CDKG1 Is Required for Meiotic and Somatic Recombination Intermediate Processing in Arabidopsis', *The Plant Cell*, 32(4), pp. 1308–1322. Available at: https://doi.org/10.1105/tpc.19.00942.

Ning, Y.Q. *et al.* (2020) 'DREAM complex suppresses DNA methylation maintenance genes and precludes DNA hypermethylation', *Nature Plants*, 4. Available at: https://doi.org/10.1038/s41477-020-0710-7.

Nonomura, K.-I. *et al.* (2011) 'A novel RNA-recognition-motif protein is required for premeiotic G1/S-phase transition in rice (Oryza sativa L.)', *PLoS genetics*, 7(1), p. e1001265. Available at: https://doi.org/10.1371/journal.pgen.1001265.

Oji, A. *et al.* (2020) 'TESMIN, METALLOTHIONEIN-LIKE 5, is required for spermatogenesis in mice†.', *Biology of reproduction*, pp. 1–27. Available at: https://doi.org/10.1093/biolre/ioaa002.

Osman, K. *et al.* (2011) 'Pathways to meiotic recombination in *Arabidopsis thaliana*', *New Phytologist*, 190(3), pp. 523–544. Available at: https://doi.org/10.1111/j.1469-8137.2011.03665.x.

Oura, S. *et al.* (2022) 'Proximity-dependent biotin labeling in testicular germ cells identified TESMIN-associated proteins', *Scientific Reports*, 12(1), p. 22198. Available at: https://doi.org/10.1038/s41598-022-26501-7.

Peterson, R., Slovin, J.P. and Chen, C. (2010) 'A Simplified Method for Differential Staining of Aborted and Non-Aborted Pollen Grains', *International Journal of Plant Biology*, 1(2), p. e13. Available at: https://doi.org/10.4081/pb.2010.e13.

Pilkinton, M., Sandoval, R. and Colamonici, O.R. (2007) 'Mammalian Mip/LIN-9 interacts with either the p107, p130/E2F4 repressor complex or B-Myb in a cell cycle-phase-dependent context distinct from the Drosophila dREAM complex', *Oncogene*, 26(54), pp. 7535–7543. Available at: https://doi.org/10.1038/sj.onc.1210562.

Prusicki, M.A. *et al.* (2019) 'Live cell imaging of meiosis in Arabidopsis thaliana', *eLife*, 8. Available at: https://doi.org/10.7554/eLife.42834.

Rechtsteiner, A. *et al.* (2019) 'Repression of Germline Genes in Caenorhabditis elegans Somatic Tissues by H3K9 Dimethylation of Their Promoters', *Genetics*, 212(1), pp. 125–140. Available at: https://doi.org/10.1534/genetics.118.301878.

Ren, Y. *et al.* (2019) 'OsSHOC1 and OsPTD1 are essential for crossover formation during rice meiosis', *The Plant Journal*, 98(2), pp. 315–328. Available at: https://doi.org/10.1111/tpj.14214.

Ross, K.J., Fransz, P. and Jones, G.H. (1996) 'A light microscopic atlas of meiosis in Arabidopsis thaliana', *Chromosome Research*, 4(7), pp. 507–516. Available at: https://doi.org/10.1007/BF02261778.

Rovani, M.K. *et al.* (2012) 'The dREAM/Myb–MuvB complex and Grim are key regulators of the programmed death of neural precursor cells at the *Drosophila* posterior wing margin', *Developmental Biology*, 372(1), pp. 88–102. Available at: https://doi.org/10.1016/j.ydbio.2012.08.022.

Sadasivam, S. and DeCaprio, J.A. (2013) 'The DREAM complex: Master coordinator of cell cycle-dependent gene expression', *Nature Reviews Cancer*, 13(8), pp. 585–595. Available at: https://doi.org/10.1038/nrc3556.

Šamanić, I. *et al.* (2013) 'Evidence for Distinct Functions of MRE11 in Arabidopsis Meiosis', *PLoS ONE*, 8(10), p. e78760. Available at: https://doi.org/10.1371/journal.pone.0078760.

Sanchez-Moran, E. *et al.* (2007) 'ASY1 mediates AtDMC1-dependent interhomolog recombination during meiosis in Arabidopsis', *Genes & Development*, 21(17), pp. 2220–2233. Available at: https://doi.org/10.1101/gad.439007.

Sánchez-Rebato, M.H., Schubert, V. and White, C.I. (2024) 'Meiotic double-strand break repair DNA synthesis tracts in Arabidopsis thaliana', *PLOS Genetics*, 20(7), p. e1011197. Available at: https://doi.org/10.1371/journal.pgen.1011197.

Saze, H. *et al.* (2008) 'Control of Genic DNA Methylation by a jmjC Domain-Containing Protein in Arabidopsis thaliana', *Science*, 319(5862), pp. 462–465. Available at: https://doi.org/10.1126/science.1150987.

Saze, H., Scheid, O.M. and Paszkowski, J. (2003) 'Maintenance of CpG methylation is essential for epigenetic inheritance during plant gametogenesis', *Nature Genetics*, 34(1), pp. 65–69. Available at: https://doi.org/10.1038/ng1138.

Schade, A.E. *et al.* (2019) 'Cyclin D-CDK4 relieves cooperative repression of proliferation and cell cycle gene expression by DREAM and RB.', *Oncogene*, 38(25), pp. 4962–4976. Available at: https://doi.org/10.1016/j.gde.2016.03.011.

Schmit, F., Cremer, S. and Gaubatz, S. (2009) 'LIN54 is an essential core subunit of the DREAM/LINC complex that binds to the cdc2 promoter in a sequence-specific manner', *FEBS Journal*, 276(19), pp. 5703–5716. Available at: https://doi.org/10.1111/j.1742-4658.2009.07261.x.

Schröpfer, S. *et al.* (2014) 'Defining the roles of the N-terminal region and the helicase activity of RECQ4A in DNA repair and homologous recombination in Arabidopsis', *Nucleic Acids Research*, 42(3), pp. 1684–1697. Available at: https://doi.org/10.1093/nar/gkt1004.

Séguéla-Arnaud, M. *et al.* (2015a) 'Multiple mechanisms limit meiotic crossovers: TOP3α and two BLM homologs antagonize crossovers in parallel to FANCM', *Proceedings of the National Academy of Sciences of the United States of America*, 112(15), pp. 4713–4718. Available at: https://doi.org/10.1073/pnas.1423107112.

Séguéla-Arnaud, M. *et al.* (2015b) 'Multiple mechanisms limit meiotic crossovers: TOP3α and two BLM homologs antagonize crossovers in parallel to FANCM', *Proceedings of the National Academy of Sciences*, 112(15), pp. 4713–4718. Available at: https://doi.org/10.1073/pnas.1423107112.

Séguéla-Arnaud, M. *et al.* (2017) 'RMI1 and TOP3α limit meiotic CO formation through their C-terminal domains', *Nucleic Acids Research*, 45(4), pp. 1860–1871. Available at: https://doi.org/10.1093/nar/gkw1210.

Serra, H. *et al.* (2017) 'Massive crossover elevation via combination of HEI10 and recq4a recq4b during Arabidopsis meiosis'. bioRxiv, p. 159764. Available at: https://doi.org/10.1101/159764.

Shook, M.S. and Richards, E.J. (2014) 'VIM proteins regulate transcription exclusively through the MET1 cytosine methylation pathway', *Epigenetics*, 9(7), pp. 980–986. Available at: https://doi.org/10.4161/epi.28906.

Sim, C.K. *et al.* (2012) 'Epigenetic regulation of olfactory receptor gene expression by the Myb–MuvB/dREAM complex', *Genes & Development*, 26(22), pp. 2483–2498. Available at: https://doi.org/10.1101/gad.201665.112.

Sims, J., Schlögelhofer, P. and Kurzbauer, M.T. (2021) 'From Microscopy to Nanoscopy: Defining an Arabidopsis thaliana Meiotic Atlas at the Nanometer Scale', *Frontiers in Plant Science*, 12(May). Available at: https://doi.org/10.3389/fpls.2021.672914.

Sofroni, K. *et al.* (2020) 'CDKD-dependent activation of CDKA;1 controls microtubule dynamics and cytokinesis during meiosis', *Journal of Cell Biology*, 219(8), p. e201907016. Available at: https://doi.org/10.1083/jcb.201907016.

Song, J.Y. *et al.* (2000) 'Regulation of meristem organization and cell division by TSO1, an Arabidopsis gene with cysteine-rich repeats', *Development*, 127(10), pp. 2207–2217.

Stroud, H. *et al.* (2013) 'Comprehensive analysis of silencing mutants reveals complex regulation of the Arabidopsis methylome', *Cell*, 152(1–2), pp. 352–364. Available at: https://doi.org/10.1016/j.cell.2012.10.054.

Stroud, H. *et al.* (2014) 'Non-CG methylation patterns shape the epigenetic landscape in Arabidopsis', *Nature Structural & Molecular Biology*, 21(1), pp. 64–72. Available at: https://doi.org/10.1038/nsmb.2735.

Su, Y. *et al.* (2024) 'Transcriptomic analysis of the spatiotemporal axis of oogenesis and fertilization in C. elegans', *Frontiers in Cell and Developmental Biology*, 12. Available at: https://doi.org/10.3389/fcell.2024.1436975.

Tabuchi, T.M. *et al.* (2011) 'Chromosome-biased binding and gene regulation by the caenorhabditis elegans DRM complex', *PLoS Genetics*, 7(5), p. 1002074. Available at: https://doi.org/10.1371/journal.pgen.1002074.

Tabuchi, T.M. *et al.* (2013) 'Opposing Activities of DRM and MES-4 Tune Gene Expression and X-Chromosome Repression in Caenorhabditis elegans Germ Cells', *G3: Genes|Genomes|Genetics*, 4(1), pp. 143–153. Available at: https://doi.org/10.1534/g3.113.007849.

Takahashi, N. *et al.* (2019) 'A regulatory module controlling stress-induced cell cycle arrest in Arabidopsis', *eLife*, 8, p. e43944. Available at: https://doi.org/10.7554/eLife.43944.

Tang, S. *et al.* (2015) 'Pervasive and essential roles of the Top3-Rmi1 decatenase orchestrate recombination and facilitate chromosome segregation in meiosis', *Molecular Cell*, 57(4), pp. 607–621. Available at: https://doi.org/10.1016/j.molcel.2015.01.021.

Tzur, Y.B. *et al.* (2018) 'Spatiotemporal Gene Expression Analysis of the Caenorhabditis elegans Germline Uncovers a Syncytial Expression Switch', *Genetics*, 210(2), pp. 587–605. Available at: https://doi.org/10.1534/genetics.118.301315.

Uanschou, C. *et al.* (2007) 'A novel plant gene essential for meiosis is related to the human CtIP and the yeast COM1/SAE2 gene', *The EMBO Journal*, 26(24), pp. 5061–5070. Available at: https://doi.org/10.1038/sj.emboj.7601913.

Underwood, C.J. *et al.* (2018) 'Epigenetic activation of meiotic recombination near Arabidopsis thaliana centromeres via loss of H3K9me2 and non-CG DNA methylation', *Genome Research*, 28(4), pp. 519–531. Available at: https://doi.org/10.1101/gr.227116.117.

Vershon, A.K. and Pierce, M. (2000) 'Transcriptional regulation of meiosis in yeast', *Current Opinion in Cell Biology* [Preprint]. Available at: https://doi.org/10.1016/S0955-0674(00)00104-6.

Vrielynck, N. *et al.* (2016) 'A DNA topoisomerase VI-like complex initiates meiotic recombination', *Science (New York, N.Y.)*, 351(6276), pp. 939–943. Available at: https://doi.org/10.1126/science.aad5196.

Walker, J. *et al.* (2018) 'Sexual-lineage-specific DNA methylation regulates meiosis in Arabidopsis', *Nature Genetics*, 50(1), pp. 130–137. Available at: https://doi.org/10.1038/s41588-017-0008-5.

Walston, H., Iness, A.N. and Litovchick, L. (2021) 'DREAM On: Cell Cycle Control in Development and Disease', *Annual Review of Genetics*, 55(1), pp. 309–329. Available at: https://doi.org/10.1146/annurev-genet-071819-103836.

Wang, C. *et al.* (2022) 'DNA polymerase epsilon interacts with SUVH2/9 to repress the expression of genes associated with meiotic DSB hotspot in *Arabidopsis*', *Proceedings of the National Academy of Sciences*, 119(41), p. e2208441119. Available at: https://doi.org/10.1073/pnas.2208441119.

Wang, K. *et al.* (2011) 'PAIR3, an axis-associated protein, is essential for the recruitment of recombination elements onto meiotic chromosomes in rice', *Molecular Biology of the Cell*, 22(1), pp. 12–19. Available at: https://doi.org/10.1091/mbc.e10-08-0667.

Wang, M. *et al.* (2018) 'Single-Cell RNA Sequencing Analysis Reveals Sequential Cell Fate Transition during Human Spermatogenesis', *Cell Stem Cell*, 23(4), pp. 599-614.e4. Available at: https://doi.org/10.1016/j.stem.2018.08.007.

Wang, T. *et al.* (2023) 'HEI10 is subject to phase separation and mediates RPA1a degradation during meiotic interference-sensitive crossover formation', *Proceedings of the National Academy of Sciences*, 120(52), p. e2310542120. Available at: https://doi.org/10.1073/pnas.2310542120.

Wang, W. *et al.* (2018) 'Arabidopsis TSO1 and MYB3R1 form a regulatory module to coordinate cell proliferation with differentiation in shoot and root', *Proceedings of the National Academy of Sciences of the United States of America*, 115(13), pp. E3045–E3054. Available at: https://doi.org/10.1073/pnas.1715903115.

Wang, Y. *et al.* (2004) 'Progression through Meiosis I and Meiosis II in Arabidopsis Anthers Is Regulated by an A-Type Cyclin Predominately Expressed in Prophase I', *Plant Physiology*, 136(4), pp. 4127–4135. Available at: https://doi.org/10.1104/pp.104.051201.

Wang, Y. *et al.* (2022) 'The Arabidopsis DREAM complex antagonizes WDR5A to modulate histone H3K4me2/3 deposition for a subset of genome repression', *Proceedings of the National Academy of Sciences*, 119(27), p. e2206075119. Available at: https://doi.org/10.1073/pnas.2206075119.

Watanabe, Y. (2012) 'Geometry and force behind kinetochore orientation: lessons from meiosis', *Nature Reviews. Molecular Cell Biology*, 13(6), pp. 370–382. Available at: https://doi.org/10.1038/nrm3349.

Werwein, E. *et al.* (2019) 'Activation of the oncogenic transcription factor B-Myb via multisite phosphorylation and prolyl cis/trans isomerization', *Nucleic Acids Research*, 47(1), pp. 103–121. Available at: https://doi.org/10.1093/nar/gky935.

White-Cooper, H. *et al.* (2000) 'Transcription of meiotic cell cycle and terminal differentiation genes depends on a conserved chromatin associated protein, whose nuclear localisation is regulated', *Development*, 127(24), pp. 5463–5473.

Wijnker, E. and Schnittger, A. (2013) 'Control of the meiotic cell division program in plants', *Plant Reproduction*, 26(3), pp. 143–158. Available at: https://doi.org/10.1007/s00497-013-0223-x.

Woo, H.R. *et al.* (2007) 'VIM1, a methylcytosine-binding protein required for centromeric heterochromatinization', *Genes & Development*, 21(3), pp. 267–277. Available at: https://doi.org/10.1101/gad.1512007.

Xu, Y. *et al.* (2022) 'MSI1 and HDA6 function interdependently to control flowering time via chromatin modifications', *The Plant Journal*, 109(4), pp. 831–843. Available at: https://doi.org/10.1111/tpj.15596.

Yang, C. *et al.* (2019) 'The Arabidopsis Cdk1/Cdk2 homolog CDKA ;1 controls chromosome axis assembly during plant meiosis', *The EMBO Journal*, (December), pp. 1–19. Available at: https://doi.org/10.15252/embj.2019101625.

Yang, C. *et al.* (2020) 'State changes of the HORMA protein ASY1 are mediated by an interplay between its closure motif and PCH2', *Nucleic Acids Research*, 48(20), pp. 11521–11535. Available at: https://doi.org/10.1093/nar/gkaa527.

Yang, H. *et al.* (2011) 'The transcriptome landscape of Arabidopsis male meiocytes from high-throughput sequencing: The complexity and evolution of the meiotic

process', *Plant Journal*, 65(4), pp. 503–516. Available at: https://doi.org/10.1111/j.1365-313X.2010.04439.x.

Yelina, N.E. *et al.* (2012) 'Epigenetic Remodeling of Meiotic Crossover Frequency in Arabidopsis thaliana DNA Methyltransferase Mutants', *PLoS Genetics*, 8(8), p. e1002844. Available at: https://doi.org/10.1371/journal.pgen.1002844.

Yelina, N.E. *et al.* (2015) 'DNA methylation epigenetically silences crossover hot spots and controls chromosomal domains of meiotic recombination in Arabidopsis', *Genes and Development*, 29(20), pp. 2183–2202. Available at: https://doi.org/10.1101/gad.270876.115.

Zemach, A. *et al.* (2013) 'The Arabidopsis nucleosome remodeler DDM1 allows DNA methyltransferases to access H1-containing heterochromatin', *Cell*, 153(1), pp. 193–205. Available at: https://doi.org/10.1016/j.cell.2013.02.033.

Zhang, X. *et al.* (2006) 'Agrobacterium-mediated transformation of Arabidopsis thaliana using the floral dip method', *Nature Protocols*, 1(2), pp. 641–646. Available at: https://doi.org/10.1038/nprot.2006.97.

Zhang, X. *et al.* (2021) 'Nuclear translocation of MTL5 from cytoplasm requires its direct interaction with LIN9 and is essential for male meiosis and fertility', *PLOS Genetics*, 17(8), p. e1009753. Available at: https://doi.org/10.1371/journal.pgen.1009753.

Zhang, Y.-R. *et al.* (2024) 'The landscape of transcriptional profiles in human oocytes with different chromatin configurations', *Journal of Ovarian Research*, 17(1), p. 99. Available at: https://doi.org/10.1186/s13048-024-01431-2.

Zhao, M. *et al.* (2021) 'The mop1 mutation affects the recombination landscape in maize.', *Proceedings of the National Academy of Sciences of the United States of America*, 118(7), pp. 1–8. Available at: https://doi.org/10.1073/pnas.2009475118.

Zheng, T. *et al.* (2014) 'CDKG1 protein kinase is essential for synapsis and male meiosis at high ambient temperature in Arabidopsis thaliana', *Proceedings of the National Academy of Sciences of the United States of America*, 111(6), pp. 2182–2187. Available at: https://doi.org/10.1073/pnas.1318460111.

Zickler, D. and Kleckner, N. (2015) 'Recombination, Pairing, and Synapsis of Homologs during Meiosis', *Cold Spring Harbor Laboratory Press*, p. 1,2.

ACKNOWLEDGEMENT

First and foremost, I would like to express my deepest gratitude to Prof. Dr. Arp Schnittger for supervising me on this wild and wonderful journey. Thank you for giving me the opportunity to work on such an exciting (and yes, slightly risky!) project. Thank you for your support from the very beginning. Many times I walked into your office, eager to share a new result—sometimes small, sometimes surprising—you met my excitement with your own. You made sure I had everything I needed to grow, not just the project. Whether it was learning a new technique, getting access to resources, or just needing a boost after a failed experiment, you were there. Working on the DREAM has truly been a dream, and I'll be forever grateful for your guidance and belief in me.

I also want to thank Dr. Magdalena Weingartner for kindly agreeing to be my second examiner. But beyond that, you were my very first supervisor during my master's. I still build on the things you taught me back then. I hope you enjoy the read.

A special shoutout goes to Dr. Maren Heese, Dr. Joke De Jaeger Braet, Dr. Franziska Böwer, and Dr. Lucas Lang for your thoughtful feedback and critical reading of parts of this thesis. Your comments definitely made it better—and I'm truly thankful for your time, insight, and encouragement.

It's also been an honor to be part of the Pro Exzellenzia-Plus project which supported me financially and personally. The workshops, mentoring, and community spirit offered a space for female academics to grow beyond professional boundaries, and left a lasting mark on me.

This work would not have been possible without the crucial scientific and financial support of Prof. Dr. Moussa Benhamed. I'm especially grateful for the time spent working alongside Dr. David Latrasse. Our attempts to make CUT&Tag work on meiocytes and anthers were both challenging and surprisingly fun. Both David and Moussa treated this project as their own and made me feel part of the lab. I learned so much from our discussions and hands-on troubleshooting (and occasionally, despair!).

My sincere thanks to Xing Ma, your expertise with CUT&Tag and RNA-seq was indispensable, and working with you was always smooth and reassuring. To the entire ChromD team: thank you for making my time in Paris feel like home. Science, coffee, and daily doses of French pâtisserie… what more could one want? I'll carry the memories—and the sugar—with me for a long time.

Heartfelt thanks to Maren Heese, a wonderful discussion partner who was always curious about my project and full of thoughtful questions. I also truly appreciated our many chats about life, science, and everything in between. You were there in more ways than one, and it meant a lot.

To my fellow DREAMer Lucas, from the moment we started sharing this project, your generosity, insight, and dry humor made even the tangled parts of DREAM a joy to unravel and and turned my time in the lab into something genuinely enjoyable.

Many thanks to Franzi — From our "Fraaanzi, I have a question" days to sharing the Schmidt-Chnasit lab during lockdown, I really appreciated the solidarity, the rooftop drinks, and the occasional venting sessions that kept us both sane.

Lab breaks wouldn't have been the same without Kostas—your wit and warmth turned even the shortest moments into real conversations. I'll always treasure the laughs, honest talks, and little adventures we shared.

A heartful of thank you to Joke**,** for being by my side—not just at the bench, but through many things in between.You somehow always knew how to bring a little light in. Your presence and gentle encouragement made more of a difference than you probably realize.

I am grateful to our wonderful TAs—Maren K., Dagmar, and Katja—for their invaluable support in the lab; to Susanne for making our lunch conversations entertaining and engaging in a different way every time; and to Maren R. for helping with all the bureaucratic work and making everything run more smoothly.

Special thanks to Lev and Bingyan, for your companionship and the shared ups and downs, motivating and supporting each other along the way.

XX

To my students Lovis and Mateo—it was a real pleasure working with you. Your curiosity and questions brought fresh energy to the project, and I truly enjoyed our time together at the lab.

Big thanks to all past and present members of the Schnittger lab—Ankit, Bingyan, Chao, Dagmar, Fany, Franzi, Jay, Joke, Katja, Kostas, Kosti, Lev, Lucas, Maren K., Maren R., Maria, Mariana, Marti, Max, Misato, Oscar, Reinhold, Rümeysa, Seiji, Susanne, Yingqi and Yuki. It's been a joy sharing the lab, the laughs, the coffee breaks, and the science with you. Thanks for the support, the good vibes, and all the little things that made this journey a lot more fun.

Beyond the lab, I was lucky to be surrounded by people who contributed so much to my well-being. A special thanks to my dear Hamburgarian friends—Elif Turhan, Elit İşcan, Ezgi Yurtsever, Kübra Gümüşay, and Seda Kacak—for bringing light, laughter, and warmth to life in Hamburg.

I am thankful to my family for their support, encouragement, and for believing in me throughout this journey. To my sister, thank you for visiting often and being close, even from afar. And to my parents, thank you for trusting me, for standing behind my decisions, and for always encouraging me to follow my own path.

Some of the most unexpectedly joyful memories came from visits to Paris. Şeyma Gümüş and Mehmet Büyükgümüş, thank you for making my Paris visits so full of laughter, great memories, and a sense of home. I'm so glad those trips brought us closer—it was one of the sweetest surprises along the way.

Life and academia have been far more meaningful with Ebru Ecem Tavacıoğlu by my side. I feel so lucky for your nourishing and encouraging friendship—for our foodie talks, unique conversations, and treasured Thursday meetings.

I am grateful to Zeynep Karagöz and Murat Sarıhan—thank you for your steady friendship and support. And to Zeynep, for showing up even in the hardest moments, and somehow always making things feel a little lighter, a little easier—just by being you.

To my dear friend Heja Netirk— watching you grow and glow into your voice as an artist and as a person has been inspiring. I am grateful for the joy, depth, and ease you bring into my life.

To Arda Çiltepe— I feel fortunate to have seen all that you're creating—both in your work and in the beautiful life you're building. Thank you for always being there, for our laughter-filled, sometimes deep, but always comforting conversations. My heartfelt thanks also go to Julia Tielke and Kaya Tielke, for bringing a sense of serenity and warmth into my life.

A special shoutout goes to Beyza Türkoğulları—these past years would not have been nearly as cheerful, real, calm, or fun without you. I'm especially grateful for our Alster walks and terrace talks, which opened my heart and mind, and helped me find strength, resilience, and trust in myself. Thank you for always looking up at the sky for the beautiful clouds and sunsets and for making sure I noticed them too. Thank you for pointing out the beautiful things in life and gently reminding me to hold onto them. Living just three minutes away from you was one of life's greatest gifts. Let's always keep that "three-minute walking distance" kind of comfort between us, no matter where life takes us.

To Ayşe Büşra Koca and Ayşe Berre Anlaş—thank you for being my home, my anchor, and my chosen family, helping me become more of who I am meant to be.You are the home I've always longed for, the kind that stays with me across distances, woven into who I am. I love you both, and the beautiful families you've built with such care and warmth. I feel profoundly lucky to be part of your journeys—and I look forward to continuing to grow, love, and embrace life together, wherever we may be.

This journey has been difficult to put into words. Along the way, I found a room of my own—a space to grow, both as a scientist and as a person. I embraced the challenges, and I loved how they changed me. I feel incredibly lucky to have been surrounded by such inspiring, amazing people. Without their presence and support, none of this would have been possible. But I also want to recognize the part of myself that kept going. The part that found strength and resilience, again and again, even when life threw unexpected surprises my way. It wasn't a straight path—there were many ups

and downs, difficult days intertwined with lighter ones. With time, I learned to recognize that beauty often lives next to the hard moments and sometimes right inside them. Perhaps that's a more honest way of seeing life. And now, here I am— still in awe of how many wonderful things unfolded along the way and deeply grateful for all that this journey has brought me and all that it has shaped me into. It was more than I ever could have anticipated.

"Verily, with every difficulty there is relief."

DECLERATION OF OATH

Eidesstattliche Versicherung:

Hiermit versichere ich an Eides statt, die vorliegende Dissertationsschrift selbst verfasst und keine anderen als die angegebenen Hilfsmittel und Quellen benutzt zu haben. Sofern im Zuge der Erstellung der vorliegenden Dissertationsschrift generative Künstliche Intelligenz (gKI) basierte elektronische Hilfsmittel verwendet wurden, versichere ich, dass meine eigene Leistung im Vordergrund stand und dass eine vollständige Dokumentation aller verwendeten Hilfsmittel gemäß der Guten wissenschaftlichen Praxis vorliegt. Ich trage die Verantwortung für eventuell durch die gKI generierte fehlerhafte oder verzerrte Inhalte, fehlerhafte Referenzen, Verstöße gegen das Datenschutz- und Urheberrecht oder Plagiate.

Affidavit:

I hereby declare and affirm that this doctoral dissertation is my own work and that I have not used any aids and sources other than those indicated. If electronic resources based on generative artificial intelligence (gAI) were used in the course of writing this dissertation, I confirm that my own work was the main and value-adding contribution and that complete documentation of all resources used is available in accordance with good scientific practice. I am responsible for any erroneous or distorted content, incorrect references, violations of data protection and copyright law or plagiarism that may have been generated by the gAI.



Hamburg, den Unterschrift